



Defence Research and
Development Canada

Recherche et développement
pour la défense Canada



Initial investigation on the aerodynamic performance of flapping wings for nano air vehicles

*F. Lesage
N. Hamel
DRDC Valcartier*

*X. Huang
W. Yuan
M. Khalid
Institute for Aerospace Research, NRC*

*P. Zdunich
Advanced Subsonics, Inc.*

Defence R&D Canada – Valcartier

Technical Memorandum

DRDC Valcartier TM 2007-550

February 2008

Canada

Initial investigation on the aerodynamic performance of flapping wings for nano air vehicles

F. Lesage
N. Hamel
DRDC Valcartier

X. Huang
W. Yuan
M. Khalid
Institute for Aerospace Research, NRC

P. Zdunich
Advanced Subsonics, Inc.

Defence R&D Canada Valcartier

Technical Memorandum

DRDC Valcartier TM 2007-550

February 2008

Author

Francois Lesage

Approved by

Alexandre Jouan
Head, Precision Weapons Section

Approved for release by

Christian Carrier
Chief Scientist

© Her Majesty the Queen as represented by the Minister of National Defence, 2008

© Sa majesté la reine, représentée par le ministre de la Défense nationale, 2008

Abstract

A four-year project was approved with the purpose of increasing our understanding of the issues concerning the flight of very small air vehicles using flapping wings. This technical memorandum presents the progress made during the first year of the project. The potential impact of this technology on military operations and R&D is first described. The project plan, as revised during the first year, is presented. It combines the development of an ability to capture detailed flow physics using both a highly accurate Computational Fluid Dynamics (CFD) solution and a tailored experimental facility with an engineering-type method. The general characteristics of the target Nano Air Vehicle (NAV) to be studied, such as size, mass and wing motion, were established based on system considerations. Standard test cases in 2D and 3D for simulation and experimentation were set up by applying simplifications and scaling arguments to the target NAV. CFD simulations were initiated with the standard two-dimensional test case previously defined. The in-house INSflow code and the commercially-available Fluent code were both used to solve this unsteady incompressible flow. Motion rigs in 2D and in 3D for the NRC-IAR water tunnel were designed and are being fabricated. A micro-PIV method was also developed. The required equipment, mainly a high-frequency laser, was purchased. The system is being implemented.

Résumé

Un projet de quatre ans a été approuvé et a pour but d'accroître notre compréhension des enjeux du vol de très petits véhicules aériens (nanodrones) utilisant des ailes battantes. On présente dans ce mémorandum technique les progrès faits pendant la première année du projet. On décrit d'abord l'impact potentiel de cette technologie sur les opérations militaires et sur la R et D. On présente ensuite le plan du projet tel que révisé pendant la première année. Celui-ci combine le développement d'une habilité à capturer la physique détaillée de l'écoulement utilisant la grande précision d'une solution de calcul de fluide numérique (CFD) et une installation expérimentale sur mesure, avec une méthode de type engineering. On a établi les caractéristiques du nanodrone ciblé pour l'étude, telles que ses dimensions, sa masse et le mouvement des ses ailes, en se basant sur des considérations de systèmes. On a créé des cas tests standard en 2D et 3D pour la simulation et l'expérimentation en appliquant des simplifications et des lois d'échelle au véhicule ciblé. On a entrepris des simulations de CFD avec le cas test en 2D défini précédemment. On a utilisé le code maison INSflow et le code commercial Fluent pour résoudre cet écoulement incompressible instationnaire. On a conçu le dispositif de mouvement en 2D et 3D du tunnel hydrodynamique du CNRC-IAR et celui-ci est en fabrication. On a aussi développé une méthode de micro-PIV. On a acheté l'équipement requis, principalement un laser haute fréquence. On est à implanter le système.

This page intentionally left blank.

Executive summary

The development and acquisition of a new class of military system known as Nano Air Vehicle (NAV) is possible in the not so distant future as a result of technological progress in a number of areas such as aerodynamics, micro-electronics, sensors, micro-electromechanical systems (MEMS) and micro-manufacturing. A NAV, according to DARPA's definition, will be smaller than 7.5 cm and will weigh less than 10 grams. The potential of NAVs opens up new possibilities in the formulation of military strategies with respect to information superiority in urban operations. It is expected that their main attributes will be low cost, low weight, little to no logistical footprint, mission versatility, covertness and precision. Their distinctive flight envelope will include hovering, perching and other high-agility manoeuvres. The real mission niche for these insect-size aircraft may well be in the indoor setting where there is currently no reconnaissance asset available for military use. There is strong evidence that for very small craft, flapping-wing performance is superior to other options due to dynamic effects that create much higher average lift at low Reynolds numbers.

A four-year project was approved with the purpose of increasing our understanding of the issues concerning the flight of very small air vehicles using flapping wings. A research team was formed with experts from DRDC Valcartier (aerodynamics and the military context), NRC-IAR (experimental and numerical low Reynolds number aerodynamics), and Advanced Subsonics (design and fabrication of flapping wing vehicles). Although progress in many technology areas will be required before a practical insect-size aircraft can be built, this project focuses on the efficient generation of forces through flapping motion. To limit the scope of the project, many research fields that are crucial to insect-size aircraft development, such as energy sources, morphing structures, advanced guidance navigation and control, payload, and communication, are not investigated in this project.

This technical memorandum presents the progress made during the first year of the project. The potential impact of this technology on military operations and R&D is first described. The project plan, as revised by the team during the first year, is presented. It combines the development of an ability to capture detailed flow physics using a highly accurate Computational Fluid Dynamics (CFD) solution and a tailored experimental facility with an engineering-type method (vortex-lattice method). The general characteristics of the target NAV to be studied, such as size, mass and wing motion, were established based on system considerations. Standard test cases in 2D and 3D for simulation and experimentation were set up by applying simplifications and scaling arguments to the target NAV. CFD simulations were initiated with the standard two-dimensional test case defined by the team. The in-house INSflow code and the commercially-available Fluent code were both used to solve this unsteady incompressible flow. Motion rigs in 2D and in 3D for the IAR water tunnel were designed and are being fabricated. A micro-PIV method was also developed. The required equipment, mainly a high-frequency laser, was purchased. The system is being implemented.

Lesage, F., Hamel, N., Huang, X., Yuan, W., Khalid, M., Zdunich, P. 2008. Initial investigation on the aerodynamic performance of flapping wings for nano air vehicles. DRDC Valcartier TM 2007-550. Defence R&D Canada Valcartier.

Sommaire

Le développement et l'acquisition d'une nouvelle classe de système militaire du nom de « nanodrone » sera possible dans un avenir rapproché grâce aux progrès technologiques dans plusieurs domaines tels que l'aérodynamique, la micro-électronique, les capteurs, les systèmes micro-électromécaniques (MEMS) and la microfabrication. Un nanodrone, selon la définition de DARPA, sera plus petit que 7,5 cm et pèsera moins de 10 g. Le potentiel des nanodrones ouvre la voie à de nouvelles possibilités dans la formulation de stratégies militaires par rapport à la maîtrise de l'information en opérations urbaines. On s'attend à ce que leurs attributs principaux soient coût et poids faibles, empreinte logistique faible ou nulle, polyvalence pour la mission, faible signature visuelle et auditive, et précision. Leur enveloppe de vol distincte comprend le vol stationnaire, l'action de se percher, et d'autres manœuvres de haute agilité. La niche réelle pour la mission de ces véhicules de la taille d'un insecte est fort probablement dans l'environnement intérieur où il n'existe présentement aucun véhicule de reconnaissance d'usage militaire. Il y a une forte probabilité que pour les véhicules de très petite taille, la performance des ailes battantes soit supérieure à celle des autres options à cause d'effets dynamiques qui créent une portance moyenne plus grande à ces faibles nombres de Reynolds.

Un projet de quatre ans a été approuvé et a pour but d'accroître notre compréhension des enjeux du vol de très petits véhicules aériens utilisant des ailes battantes. On a formé une équipe de recherche avec des experts de RDRC Valcartier (aérodynamique et le contexte militaire), du CNRC- IRA (aérodynamique expérimentale et numérique à faible nombre de Reynolds), et d'Advanced Subsonics (conception et fabrication de véhicule à ailes battantes). Même si des progrès dans plusieurs domaines technologiques sont nécessaires pour un véhicule complet de la taille d'un insecte, ce projet se concentre sur la génération efficace de forces par le mouvement battant des ailes. Plusieurs domaines de recherche, cruciaux au développement de ces véhicules tels que les sources d'énergie, le morphage de structures, le guidage-navigation-contrôle avancé, la charge utile et les communications, ne font pas partie du projet dans le but d'en limiter l'étendu.

On présente dans ce memorandum technique les progrès faits pendant la première année du projet. On décrit d'abord l'impact potentiel de cette technologie sur les opérations militaires et sur la R et D. On présente ensuite le plan du projet tel que révisé par l'équipe de projet pendant la première année. Celui-ci combine le développement d'une habilité à capturer la physique détaillée de l'écoulement utilisant la grande précision d'une solution de calcul de fluide numérique (CFD) et une installation expérimentale sur mesure, avec une méthode de type "engineering". On a établi les caractéristiques du nanodrone ciblé pour l'étude, telles que ses dimensions, sa masse et le mouvement des ses ailes, en se basant sur des considérations de systèmes. On a créé des cas tests standard en 2D et 3D pour la simulation et l'expérimentation en appliquant des simplifications et des lois d'échelle au véhicule ciblé. On a entrepris des simulations de CFD avec le cas test en 2D défini par l'équipe. On a utilisé le code maison INSflow et le code commercial Fluent pour résoudre cet écoulement incompressible instationnaire. On a conçu le dispositif de mouvement en 2D et 3D du tunnel hydrodynamique de IRA et celui-ci est en fabrication. On a aussi développé une méthode de micro-PIV. On a

acheté l'équipement requis, principalement un laser hautes fréquences. On est à implanter le système.

Lesage, F., Hamel, N., Huang, X., Yuan, W., Khalid, M., Zdunich, P. 2008. Initial Investigation on the Aerodynamic Performance of Flapping Wings for Nano Air Vehicles. DRDC TM 2007-550. RDDC Valcartier.

This page intentionally left blank.

Table of contents

Abstract/Résumé.....	i
Executive summary	iii
Sommaire.....	iv
Table of contents	vii
List of figures	x
List of Tables.....	x
1. Introduction	1
2. Potential impact on military operations and R&D program.....	4
2.1 Military operations	4
2.2 R&D program	4
3. Project plan.....	6
3.1 Navier-Stokes simulation of low-Reynolds-number insect-like wings in complex unsteady motions	8
3.1.1 Simple traditional airfoils	8
3.1.2 Steady rigid insect-like wing	8
3.1.3 Unsteady rigid insect-like wing.....	8
3.1.4 Unsteady elastic insect-like wing	9
3.2 Experimental study	9
3.2.1 Design and application of a 2D rig for standard 2D test case	9
3.2.2 Mini-scale surface and off-surface visualization.....	9
3.2.3 Single wing three-degree-of-freedom motion system	10
3.2.4 Multiple wing 3-DOF rig.....	10
3.2.5 Parametric study of motion and geometry including aero-elastic wing model. 10	
3.2.6 Stability and controllability study	10
3.3 Vortex lattice modeling	10

3.3.1	Convert existing 2D unsteady aerodynamic model to 3D.....	11
3.3.2	Model calibration using CFD and experimental data.....	11
3.3.3	Wings performance investigation.....	11
3.3.4	Identification of optimal performance points for sample vehicle criteria and flight modes.....	11
3.4	System considerations for directions to aerodynamic studies.....	11
3.4.1	Definition of four candidate missions	12
3.4.2	System components and entire-vehicle parameters.....	12
3.4.3	Directions to other activities.....	12
4.	Progress in first year.....	13
4.1	System considerations	13
4.1.1	Pitfalls and opportunities.....	13
4.1.2	NAV characteristics	14
4.1.3	Dimensionless parameters for NAV.....	17
4.1.3.1	Reynolds number	17
4.1.3.2	Reduced frequency	18
4.1.3.3	Flap amplitude to chord ratio.....	19
4.1.4	Definition of standard test cases.....	19
4.1.4.1	Two-dimensional test case.....	19
4.1.4.2	Three-dimensional test case.....	23
4.2	Navier-Stokes simulation with Fluent.....	25
4.3	Navier-Stokes simulations with INSFlow	26
4.4	Water tunnel experiment	28
4.5	Vortex-lattice modelling.....	29
5.	Conclusions	30
6.	References	32
	Annex 1 – Small scale flapping flight: pitfalls and opportunities – July 2006.....	35
	Annex 2 - Highlights of systems considerations for flapping-wing NAV – April 2007	74
	Annex 3 – CFD 2007 Conference paper; June 2007	86
	Annex 4 – CASI Aerodynamics Symposium 2007 conference paper; April 2007	111

Annex 5 – ICAS 2006 conference paper; September 2006	112
Annex 6 – Experimental research on flapping wing aerodynamics; April 2007	126
List of symbols/abbreviations/acronyms/initialisms	143
Distribution list	145

List of figures

Figure 1: Representative NAV. Wings flap about vertical axis at body. Wings passively twist about the leading edge. Based on Mentor.	16
Figure 2: Description of airfoil flapping showing pitching and plunging	21
Figure 3: Schematic of the flat plate airfoil.	23
Figure 4: Schematic of the 3D test case as viewed along the axis of freestream velocity.....	24
Figure 5: Vorticity magnitude contour for the flat plate airfoil.....	26
Figure 6: Spanwise vorticity over the flapping NACA 0005 airfoil during the downstroke period with pitching axis $x_0/c=0.5$ at $Re=1.2\times 10^4$	27
Figure 7: Design of two-dimensional rig in water tunnel.....	28

List of tables

Table 1. Project schedule.....	7
Table 2. Dimensions of representative NAV.....	16
Table 3. Notional mass breakdown for the conceptual NAV	16
Table 4. Calculated parameters of representative NAV	19
Table 5. Two-dimensional test case summary.....	22
Table 6. Three-dimensional test case summary.....	24

1. Introduction

The development and acquisition of a new class of military system known as Nano Air Vehicle (NAV) is possible in the not so distant future as a result of technological progress in a number of areas such as aerodynamics, micro-electronics, sensors, micro-electromechanical systems (MEMS) and micro-manufacturing. A NAV, according to DARPA's definition [1], will be smaller than 7.5 cm and will weigh less than 10 grams. The potential of NAVs opens up new possibilities in the formulation of military strategies with respect to information superiority in urban operations. It is expected that their main attributes will be low cost, low weight, little to no logistical footprint, mission versatility, endurance, low visibility, covertness and precision. Their distinctive flight envelope will include hovering, perching, and other high-agility manoeuvres in order to perform their missions. The real mission niche for these insect-size aircraft may well be in the indoor setting where there is currently no reconnaissance asset available for military use. Fixed-wing solutions are immediately discounted because they require either high forward speed or large wings. The alternative is a method of creating circulation over the wings in the absence of fuselage translation. This movement can be a circular motion as in a rotorcraft or it can be a reciprocating motion as in a flapping wing. There is strong evidence that for very small craft (less than 5 cm), flapping-wing performance is superior to rotors due to dynamic effects that create much higher average lift at low Reynolds numbers.

A four-year project, called Aero-NAV, was approved with the purpose of increasing our understanding of the issues concerning the flight of very small air vehicles using flapping wings. A research team was formed with experts from DRDC Valcartier (aerodynamics and the military context), NRC-IAR (experimental and numerical low Reynolds number aerodynamics), and Advanced Subsonics (design and fabrication of flapping-wing vehicles). The project focuses on the development of modelling and experimental capabilities and investigations as to the appropriate sizes and performance parameters with some considerations of system integration. Although progress in many technology areas will be required before a practical insect-size aircraft can be built, this project focuses on the efficient generation of forces through flapping motion. In order to limit the scope of the project, many research fields that are crucial to insect-size aircraft development, such as energy sources, morphing structures, advanced guidance navigation and control, payload, and communication, are not part of the current investigation. It is recognized that progress in these areas is essential for a viable insect-size aircraft system.

Even though there has been considerable analysis of bird and insect flight mechanisms, no machine at the size level of a hummingbird has been demonstrated. There is more to designing insect-size vehicles than just scaling down the dimensions of UAVs. The aerodynamics of an insect-scale aircraft in the low Reynolds number regime differs significantly from the aerodynamics of mini vehicles, such as UAVs [2]. There has been considerable analysis of the mechanisms of bird and insect flight [3-5], providing insight into the design of small scale flapping-wing aircraft [6-8]. Insect flight has been successful in nature for millions of years and relies on unsteady aerodynamics to produce high lift coefficients and excellent maneuverability. Insects fly by oscillating (plunging) and rotating (pitching) their wings through large angles, while sweeping them forwards and backwards.

The dramatic lift-boosting unsteady aerodynamic phenomena that are exploited by insect flapping wings are however not yet fully understood. The main likely aerodynamic phenomena occurring in insect-like flapping are: 1) bound leading edge vortex, persisting during each half-cycle and shed at the end of it; 2) effects of wing pitching, plunging and sweeping present all the time; and 3) wing interaction with its own convected wake, due to its forward-backward sweeping. It has also been qualitatively found that insects achieve their high flight performance using active flow control.

The aerodynamic performance of insects has motivated the development of aerodynamically scaled flapping mechanisms [9-11]. These devices allowed progress in gathering experimental data on insect aerodynamics, but were generally too bulky for NAVs. Although the mechanism was completed, there are still significant uncertainties in the modelling and understanding of the relevant aerodynamics. The technical difficulties relate to the complex unsteady motion required to produce high lift and the effects of flow at low Reynolds number.

The aerodynamic modelling and experimental evaluation of flapping wings at a low Reynolds number (Re) have identified several key areas of interest. Researchers [10, 12, 13] have described the importance of the leading-edge vortex (LEV) that is formed by small flapping wings and its effects in stall-delay during the flapping cycle, yielding very high lift coefficients for this Re regime. The ability of birds and insects to expertly regulate the movement of the LEV on lifting wings gives them fine control during flight at very low speeds. Others [14] have investigated both experimentally and computationally, the performance of flapping wings at low Re numbers and concluded that a more complete understanding of dynamic stall performance is required. Elsewhere cameras installed on birds have monitored their behaviour in flight. Interesting phenomena related to feathers on different section of the wing are seen to provide the fine control and agility associated with birdflight.

A 2D time-stepping vortex-lattice model capable of analyzing LEV shedding and determining the aerodynamic forces generated and power consumed by the wings has been developed [15]. The beneficial interference between wings such as the clap-fling effect was studied [16, 17] and experimentally shown to be effective for high disc-loading conditions [18]. Experimentally, two approaches for flapping-wing evaluation have been attempted by measurement of forces [19-21], and flow visualization studies [21-23]. The main Computational Fluid Dynamics (CFD) approaches needed for predicting unsteady flows at low Reynolds numbers in incompressible regimes are summarized in [24]. In related studies, researchers have developed and validated a time-marching aeroelastic model of a large-scale flapping wing [25].

Although flapping-wing products may be purchased in hobby stores and university teams may fabricate aero models with flapping wings, the insect-size aircraft for military applications still has a long way to go. DARPA has just launched their Phase I NAV program, which is focused on developing a system that will have the power, navigation, communications and mechanisms needed to provide lift, thrust, and hover capabilities [1].

The design and analysis capability within the scientific community has progressed to a point where it can handle simple cases such as pure-plunge of airfoil. The understanding of the issues for the full 3-D motion representative of insect wing beat kinematics appears now to be

within reach and is the objective of this project. This is an essential step towards engineering realization of the functionality of insect flight.

This on-going project combines an ability to capture the relevant detailed flow physics using a highly accurate CFD solution and a tailored experimental facility with an engineering-type method refined with the higher-accuracy CFD and experimental results. This combination of three different approaches provides different views of the problem and its solutions and mitigates risk. A significant outcome should be quantitative relations between the LEV behaviour and wing geometry and motion variables for the purpose of the conceptual design of a flapping-wing NAV.

This technical memorandum presents the progress made during the first year of the project, which started in April 2006. It describes the potential impact of this technology on military operations and R&D, the four-year project plan, and the progress accomplished during the first year.

This project is funded in part by Beaver Works 42gg11 (first year) and in part by Technology Investment Fund 12pz12 (following three years).

2. Potential impact on military operations and R&D program

2.1 Military operations

It is expected that future conflicts will see an increased use of complex terrain by enemies, particularly in urban environments, for dispersion and exploitation of close combat opportunities to offset Western military superiority. In these urban environments, adversaries will attempt to conceal themselves among the general population, and will employ adaptive and unconventional operational methods that include asymmetric attacks against weaknesses that present themselves. Operational success in the future security environment depends on highly developed sense capabilities to collect, process and disseminate information. The potential of nano-air vehicles, with their small size and hover capability, opens up new possibilities in the formulation of military strategies with respect to information superiority in urban operations. These vehicle systems will have attributes such as low cost, low weight, little to no logistical footprint, mission versatility, high agility at low speed for rapid manoeuvres in all directions, vertical take-off and landing (VTOL) for launch and touch-down with no special ground preparation, endurance, stealth, and precision. This technology will have a major impact by enhancing intelligence event horizon, providing greater field of vision while risking less. The real mission niche for small flapping-wing aircraft may well be indoors where there is no existing reconnaissance asset available for area surveillance.

The 2005 Defence Policy Statement entails the most significant changes to Canada's military in fifteen years. One key component of this transformation is the enhancement and expansion of the two special operations forces (JTF-2 and JNBCD). This project will contribute to master the technologies that will make insects-size aircraft operational systems for military applications. These systems should have a strong impact on the counter-terrorism missions carried out by JTF-2 and on the detection, sampling and identification of hazards and threats carried out by JNBCD.

The project relates to one key element of the Army strategy: to transform into a medium-weight, information-age army which is to remain an agile, lethal, and survivable force through continuous modernization. It also relates to Horizon 3 targets of National Defence Strategic Capability Investment Plan:

- Power projection tailored to the operational (theater) situation with an inherently mobile force
- Seamless situational awareness at all levels of command and control

2.2 R&D program

Recently, DARPA began its nano air vehicle (NAV) program with a 7.5 cm limit on maximum dimension and 10 g weight limit (including a 2g payload) [1]. The US is investing considerable effort in bringing this idea to fruition. The Canadian expertise in the low-

Reynolds aerodynamics is currently at the forefront, but needs to progress quickly to maintain its edge and potential for international collaboration.

The project will contribute to several S&T challenges of the Defence S&T strategy: non-lethal weapons (7.1), enhanced weapons systems for complex environments, including urban operations (7.4), intelligent autonomous systems for operation in complex environments (5.1), new sensing technologies (3.3), and integrated platform modes and their applications (6.2).

For challenges 7.1 and 7.4, the technology acquired will allow for the replacement of humans in dangerous tasks and increase local situational awareness in urban environments. It will play a key role in the weapon delivery chain.

For challenge 5.1, the insect-size aircraft is a totally new class of autonomous vehicle that will allow early sensing and shaping of the battlespace prior to and during force deployment. They may play a significant role for military personnel who are involved in urban environments where the enemy exploits close combat opportunities to offset the effect of Western military superiority.

With respect to challenge 3.3 detection, tracking and classification functions are markedly simplified and improved when the sensor can be covertly transported to an ideal vantage point. The results of the insect-size aircraft research provides the means of moving the sensor to locations that are much closer to difficult targets than traditional fixed wing or rotor Micro Air Vehicles.

For challenge 6.2, there is a need to develop reliable CFD for complex configurations and extreme flows. The CFD technology is improving, but there is no CFD code available that provides adequate understanding of the flow physics of the insect flight for future NAVs (very low Reynolds number unsteady flows).

3. Project plan

The project's approach is based on the expertise of IAR with low Reynolds number aerodynamics, and Advanced Subsonics with engineering models and systems. DRDC Valcartier brings in the knowledge of military context, an expertise in CFD and the coordination of the project. The combination of an ability to capture the detailed flow physics using a highly accurate CFD solution and a tailored experimental facility with an engineering-type method refined with higher accuracy CFD and experimental results will together form a complete flapping-wing air-vehicle research and development capability.

The main areas are:

(1) CFD solutions of unsteady low Reynolds number flows. A three-dimensional Reynolds-averaged Navier-Stokes code (INSFlow) will be extended to complex geometry flows and to direct simulations of flows in laminar regime. A parametric analysis will be performed with variations of Reynolds number and motion patterns; the Chimera moving mesh techniques will enable modeling of flows past wings and components executing defined plunge/pitch/flapping motions. This approach coupled with the application of Large Eddy or Direct Numerical Simulation should provide the resolution of grid scale transients to capture the leading edge vortex accurately. In parallel, the commercial Fluent code will be exploited to solve the complex three-dimensional motion.

(2) low Reynolds number experimentation on flapping-wing aerodynamics in a water tunnel. A motion rig and a micro-PIV method will be developed and tested on a reference insect-type wing undergoing a reference flapping motion. Based on understanding of the physics gained, the wing geometry and the motions will be varied and optimized and the stability and controllability will be assessed;

(3) the development and validation of an engineering-type model (vortex-lattice model) for flapping-wing vehicle design. With the model, a variety of prescribed wing shapes and flapping patterns will be investigated to identify relationships and suitable candidate wings and flapping patterns to be used in an experimental program;
and

(4) candidate missions will be identified, and estimates of the performance of other NAV system components will be made in order to constrain the aerodynamic research efforts to concentrate on the most useful performance parameter range.

The project schedule is provided in Table 1 and further details in the following subsections.

Table 1. Project schedule

	Year 1				Year 2				Year 3				Year 4			
Navier-Stokes simulation of low-Reynolds-number insect-like wings in complex unsteady motions																
Simple traditional airfoils																
Steady rigid insect-like wing																
Unsteady rigid insect-like wing																
Unsteady elastic insect-like wing																
Experimental study																
Design and application of a 2D rig for standard 2D test case																
Mini-scale surface and off-surface visualization																
Single wing three-degree-of-freedom motion system																
Multiple wing 3-DOF rig																
Parametric study of motion and geometry including aero-elastic wing model																
Stability and controllability study																
Vortex lattice modelling																
Convert existing 2D unsteady aerodynamic model to 3D																
Model calibration using CFD and experimental data																
Wings performance investigation																
Identification of optimal performance points for sample vehicle and flight modes																
System considerations for directions to aerodynamic studies																
Definition of four candidate missions																
System components and entire-vehicle parameters																
Directions to other activities																

3.1 Navier-Stokes simulation of low-Reynolds-number insect-like wings in complex unsteady motions

A three-dimensional code (INSFlow) specifically developed by IAR for low Reynolds number incompressible flows will be extended to complex geometry flows. The implementation of an overlapping scheme coupled with the existing dynamics topology will be considered to allow the code to handle arbitrary moving boundaries. As the insect-like flapping flight is operated at low Reynolds numbers, it is expectedly feasible to perform genuine Large Eddy Simulation (LES). Physical modelling parameters of the numerical schemes will be calibrated using experimental data obtained in the water tunnel. It is expected that capturing the leading edge separation for low Reynolds number flows past insect-like wings will be possible. Recent experience with LES on low Reynolds number airfoil flows indicated that the grid resolution on the suction surface has a dominant effect on the results and is the key to success. A parametric analysis will be performed with variations of Reynolds number and motion patterns. In parallel, the commercial Fluent code will be exploited to solve the complex three-dimensional motion.

3.1.1 Simple traditional airfoils

The current extension of the INSFlow CFD code to equip with capabilities for complex geometries at arbitrary angles of attack will be completed (the leading edge of the NAV flapping wing may be forwards and backwards during each wingbeat cycle).

The existing multi-block structure in the INSFlow code will be extended and overlapping technique will be implemented.

The implementation by simulations of the 2D standard test cases will be calibrated using both INSFlow (NACA0005 only) and Fluent (NACA0012 of Anderson and standard test cases (NACA0005 and flat plate)).

3.1.2 Steady rigid insect-like wing

The flow around rigid insect-like wings in steady case will be simulated.

The INSFlow code, if needed, will be equipped with some unstructured code features handling any collapsing of the points on the root and tip of the wing more precisely.

Calculations of flows past a stationary 3D wing (standard 3D wing as defined by the team) will be performed.

3.1.3 Unsteady rigid insect-like wing

A parametric study on the effects of the unsteady kinematics of insect-like flapping wings will be carried out.

First, a calculation of the unsteady flow past the 3D flapping wing (plunging and pitching standard 3D case) will be carried out.

Then, the flow patterns, amplitude and frequency of the pitching, plunging and yawing motions will be changed and laminar or LES-based calculations will be performed.

3.1.4 Unsteady elastic insect-like wing

A calculation with elastic deformations of an insect-like wing used in the last section will be performed by combining dynamics mesh and overlapping technique.

3.2 Experimental study

The unique experimental facilities being developed by IAR will be exploited. IAR's water and glycerine tunnels allow low Reynolds number flows around wings to be measured by adjusting the size of the model and appropriately scaling the density and viscosity of the fluid. A three-degree-of-freedom rig with independently controlled step motors being developed will allow the representation of insect wing motions based on Fourier analysis of actual insect flights. The boundary layer behaviour on flapping-wing surfaces which is fundamentally important to the aerodynamic forces acting on the wing will be measured using mini-scale PIV (particle image velocimetry) technology. This will be done by first developing an optical system capable of focusing on an extremely small area (~ 1 mm in diameter) adjacent to the surface with the resolution of no more than $50\text{ }\mu\text{m}$; then by the identification of the proper seeding material and seeding method for boundary layer study; and finally by modifying the existing software to compensate for the reflection and refraction problems associated with the test. The flow physics will be analyzed for baseline flapping patterns and wing designs, for an optimum flapping design and finally for an elastic model, either one mode or multi-modes.

3.2.1 Design and application of a 2D rig for standard 2D test case

A 2-D rig capable of pitching and plunging a 2-D airfoil will be fabricated. It will include load cells to measure lift and drag (ideally). Two models (NACA005 and 5% thickness flat plate) will be built.

The rig will be used to test the two airfoils with only one motion (standard 2D test case). Force and PIV measurements will be obtained.

3.2.2 Mini-scale surface and off-surface visualization

An optical system capable of focusing on an extremely small area (1 mm) adjacent to the surface with a resolution better than $50\text{ }\mu\text{m}$ will be developed.

The proper seeding material and seeding method for boundary layer study will be identified.

The existing software to compensate for the reflection and refraction problems associated with the test will be modified.

3.2.3 Single wing three-degree-of-freedom motion system

The existing rig will be modified to remove backlash. A rigid 3D wing model (designed by the project team) will be fabricated and will be connected to the rig through a five-component balance.

The 3-DOF motions will be independently controlled by three step motors. Appropriate motions will be imparted based on analysis of insects or birds hover motions described by Fourier series.

The forces and flowfield in the boundary layer, sub-layer, and wake will be measured and analysed for the standard 3D test case defined by the team using the single wing.

3.2.4 Multiple wing 3-DOF rig

A 4-wing rig for 3-DOF will be designed and built.

The forces and flowfield in the boundary layer, sub-layer, and wake will be measured and analysed for the standard 3D test case defined by the team using the multiple wing rig.

3.2.5 Parametric study of motion and geometry including aero-elastic wing model.

Motions and flow visualization results will be studied for different wing geometries; an optimum flapping design will be identified.

Based on the previous results, an elastic model, either one or multi-modes, will be designed, fabricated and tested.

3.2.6 Stability and controllability study

As the aerodynamic forces will be measured by the five-component balance, the stability will be tested and improved based on the flight requirements.

3.3 Vortex lattice modeling

As a result of previous work on the DARPA Micro Air-Vehicle and Micro-Adaptive Flow Control programs, Advanced Subsonics has a unique vortex-lattice model (VLM) that solves the basic problem of modeling vortex shedding from both the leading and trailing edges of a flapping wing of arbitrary thin cross-sectional shape. The VLM is an engineering-type model where the variables are fewer and easily manipulated compared to CFD, and can yield design rules. The two-dimensional model will be converted to a three-dimensional model and aeroelasticity will be built into it. This model will be used for a systematic parametric study

with variables like pitch amplitude, flapping angle, phase angles between motions, and most importantly, the influence of multiple wings on each other. A variety of prescribed wing shapes and flapping patterns based on biomimetics, including those studied by CFD and experiments, will be investigated with the model to identify relationships and suitable candidate wings and flapping patterns. The model will be verified through experiments so that it may be used as a design tool in the development of flapping-wing NAVs.

3.3.1 Convert existing 2D unsteady aerodynamic model to 3D.

The unique vortex-lattice model of Advanced Subsonics will be converted to a three-dimensional model in order to capture the effects of a) variation of airspeed with span wise position, b) span wise flow, c) the influence of multiple wings on each other

The mathematical layout that 3D-model will use will be established, including frames of reference to be used and lattice shapes to be allowed.

The overall 3D-model flowchart will be established.

The 3D-model will be completed.

3.3.2 Model calibration using CFD and experimental data

Simple methods for implementation of external data to improve model accuracy will be identified and implemented.

3.3.3 Wings performance investigation

The performance for rigid wing will be predicted. A variety of prescribed wing shapes and flapping patterns will be investigated in order to identify relationships and to identify suitable candidate wings and flapping patterns to be used to verify this model experimentally.

3.3.4 Identification of optimal performance points for sample vehicle criteria and flight modes.

The model will be used to investigate optimum performance that may be expected using flapping wings. The result of this task will be the development of rules regarding flapping-wing flight performance.

3.4 System considerations for directions to aerodynamic studies

Early on and throughout the project, system considerations will provide guidance to the aerodynamic investigations as to the appropriate sizes and performance parameters on which to concentrate through considerations of system integration requirements, and mission performance.

3.4.1 Definition of four candidate missions

Up to four candidate missions for which a small-scale flapping-wing vehicle may be the best-performing technology will be defined, and the performance metrics for those missions will be determined.

Mission niches that are not addressed by existing assets will be identified. With consideration of distances involved, navigational requirements, communications and payload requirements, and other critical mission factors, such as noise emission, the approximate flight performance desirables to conduct such missions will be outlined.

3.4.2 System components and entire-vehicle parameters

Likely candidate system components for NAVs now and in the future, will be investigated and these will be used to estimate entire-vehicle parameters.

Present state-of-the-art technologies suitable to flapping-wing NAV will be identified, and their performance into near-future (<10 years) will be extrapolated. The study will include energy sources, materials, micro-control actuation methods, and communications.

A picture of what a complete vehicle system must look like will be generated, including size and weight, for various missions.

3.4.3 Directions to other activities

Directions to the other activities of the project will be provided to ensure that the investigations are consistent with likely future vehicles.

Guidance to the instructional aero-model development, experimental tool development, and detailed CFD model development will be provided to focus efforts to flapping-wing performance parameters that are consistent with the real anticipated mission conditions.

Proposals for wing designs and motions to be investigated in simulation and experiment will be provided. Methods for generating deformed wing shapes as a function of motion (aerodynamic loads and inertia) will be investigated and such shape estimates will be provided.

4. Progress in first year

The System Consideration is introduced first, although it is last in the project plan, since it drives what is done in the other areas of the project.

4.1 System considerations

4.1.1 Pitfalls and opportunities

The approach used by Advanced Subsonics for their successful contribution to two DARPA programs was reviewed (Annex 1). In the first program, called the micro air vehicle (MAV) program, engineering research was undertaken on small scale flapping wings that were suitable for hover and forward flight. “Rules and Tools” pertaining to small hovering flapping wing vehicle design were developed. This work included development of specialized wings and wing actuation methods for small, hovering MAV (< 6 inch max dimension, 150 g maximum). They designed and tested aeroelastically tailored wings suited to single degree of freedom actuation; they conducted wind tunnel tests to acquire flapping wing forces and moments; they developed and applied a time-marching model of 2-D unsteady aerodynamic flow about thin wings. In the second DARPA project, which was a one year follow-on project within the Micro Adaptive Flow Control program, they used their rules and tools to develop a stable, untethered flying vehicle in less than a year (called Mentor); they created a simulation for control system development and vehicle layout; they developed a lightweight on-board PID controller; they developed and flew two different vehicles (internal combustion and battery powered). The Mentor vehicle was the world’s first hovering flapping-wing aircraft and first flew stably and freely under operator control in March of 2002. This work was done in collaboration with SRI of Menlo Park, California, who developed electro-active polymer muscles for the purposes of driving the flapping wings. SRI also contributed the dynamic simulation engine for the project.

Based on their previous experience, Advanced Subsonics identified some possible pitfalls from a design point of view:

Shotgun approach: A very large test matrix with many parameters is inefficient and historically an ineffective way to develop wings; CFD and experiment must run some identical cases and the earlier the better.

Inconsistent metrics: The performance parameters that pertain to flapping-wing vehicles differ substantially from those of steady aerodynamics. For example, it is difficult to identify the airfoil lift to drag ratio given that under flight conditions the wing does not produce drag, but instead produces thrust. Moreover, in an aeroelastic wing whose shape changes through a flapping cycle, there is no single characteristic airfoil shape as a reference. Of greater importance are the overall system performance metrics, such as the power consumption during hovering flight and the forward-flight performance (both speed and power consumption).

Resonance: Resonance in the wings can not be exploited for efficiency; effective flapping-wing systems are highly damped (that is they put all available energy into the flow; damping is the useful work); resonant aero-mechanical systems such as bridges, power lines, and stop signs extract energy from the flow; flapping wings impart energy to the flow. Any energy that is stored as ‘resonance’ is not going into the flow and therefore not helping you fly.

On the opportunity side, the following aspects were identified:

CFD model: The development of an accurate 3D CFD model of low Re wings operating in proximity to one another and its verification with experimental results. Collaboration between the accurate Navier-Stokes CFD solution and fast running engineering model will likely be a very useful tool to rapidly converge on optimums in the problem space. CFD and experiments must test the exact same case for calibration and the earlier this is done the better. The results should focus on critical variables. The test cases should reflect realistic wing loading and flapping frequency.

Aeroelastic model: Eventually, an aeroelastic model should be integrated with the aerodynamic model for a comprehensive design tool.

4.1.2 NAV characteristics

In order to guide NAV development and to illustrate potential military uses for a nano air vehicle, four candidate missions were identified:

1. High speed ingress, hover at target, and return
2. Outdoor urban perch and stare
3. Indoor autonomous or assisted navigation of low speed and/or hovering flight
4. Outdoor hover outside a window

These missions are not addressed by existing assets. The approximate flight performance requirements necessary to conduct such missions were identified and are available in [26] and in Annex 1. The characteristics of some existing small flight vehicles were reviewed and are given in [26].

In order to achieve these missions, desirable NAV characteristics were investigated. The characteristics below were examined and the results are presented in Annex 1 and in [26]:

- Noise emission
- Perching and releasing
- Power requirements (hover and forward flight)
- Aerodynamic efficiency
- Hover efficiency (clap-fling phenomenon)
- Flapping wings compared to props and rotors
- Power sources (batteries, thermo electric generators, electromagnetic motors, ultrasonic motors, internal combustion, external combustion, fuel cells)

- Control actuator requirements and force generation
- Actuation methods (servos, shape memory alloys, piezoelectric actuators)
- Notional concepts and weight estimates

A target nano air vehicle for the purpose of the project was defined based on the mission requirements, expected progress in complementary technologies, and the experience of Advanced Subsonics in working on the Mentor micro air vehicle (MAV). Like the Mentor, the target NAV flaps its wings in a three dimensional manner. That is, the wing is finite and the wing tips move farther and faster than the root of the wing. Figure 1 illustrates the notional NAV. The system would have the following geometrical characteristics:

- 4 wing “Double-Hummingbird” X-wing configuration developed for Mentor
- Capable of hover and fast translation flight
- Single degree of freedom root-flapping actuation
- Very thin flat wings
- Aeroelastic tailoring to give appropriate camber and span dependent twist

Table 2 lists a number of geometric properties of a reasonable NAV and Table 3 gives the mass breakdown for the vehicle.

The target NAV will exploit the clap-fling phenomenon [16, 17] in order to obtain improved thrust to power ratio (already verified to 40%) and very high thrust for limited disk area. The flapping mechanism will be by a single DOF actuation since the mechanism does not need to be overly complicated and therefore is light and robust.

System considerations [26] dictates a thrust to power of 16 g/W for the wings only; a Figure of Merit of 0.5 (a 50% conversion efficiency to thrust power); and an average of 0.6 W input at the wings to drive them.

The target NAV control will be using wings only. This should make the vehicle more maneuverable and less susceptible to changes in free stream velocity (descent or gusts). In order to keep the target NAV within 20 cm of prescribed path, the thrust needs to be altered only by 5% per wing, the control force must be achieved within about 0.1 to 0.2 seconds (8 to 16 flaps). This is based on gusts of nearly double the induced velocity. (Induced velocity being the mean wake velocity induced by the flapping wing set.)

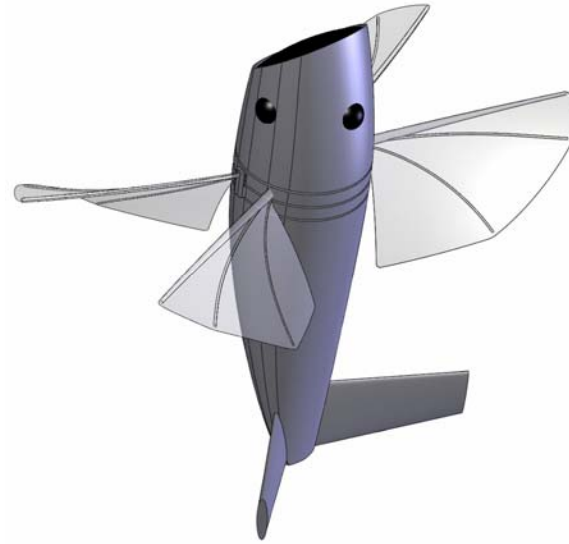


Figure 1: Representative NAV. Wings flap about vertical axis at body. Wings passively twist about the leading edge. Based on Mentor.

Table 2. Dimensions of representative NAV

mass (m)	10 g = 0.01 kg
weight (W) = thrust (T)	~0.1 N
span (b)	7.5 cm = 0.075 m
semi-span (b/2)	3.75 cm = 0.0375 m
chord (c)	0.019 m
frequency (f)	80 Hz (best estimate of req'd freq)
peak plunge amplitude angle (γ)	75 deg (= 1.31 rad)
disk area (A)	$= \pi r^2 = \pi(0.0375\text{m})^2 = 0.00442\text{m}^2$
disk loading (T/A)	23.9 N/m ²

Table 3. Notional mass breakdown for the conceptual NAV

Component	Mass
Battery/Power Source	5g
Payload	2g
Onboard electronics for navigation and communications	0.5g
Complete vehicle structure	1g
Wing flapping actuator	1.5g

4.1.3 Dimensionless parameters for NAV

Certain dimensionless parameters are defined for the purpose of constructing a test case that is suitable for all concerned and is analogous to the conditions expected on an actual NAV. These parameters are Reynolds number, reduced frequency, and the flap amplitude to chord ratio.

4.1.3.1 *Reynolds number*

In a fixed wing aircraft, definition of Reynolds number is straightforward as the wings are stationary with respect to the body-fixed frame of reference and the velocity term in the calculation is simply the freestream velocity (vehicle velocity). Now consider a flapping-wing vehicle in which the wing velocity may be a significant portion of the vehicle's overall velocity. In this case, the reference velocity is not obvious. Consider also a hovering flapping-wing vehicle. In this case would the wing's velocity be used, or would one use the velocity of the jet induced by the flapping wings or some combination of these? For these reasons, alternate formulations of Reynolds number that rely on the wing's speed rather than the vehicle's have been developed and are presented in the sections that follow. In the first case frequency appears explicitly and in the second, the RMS value of wing speed is used.

- Reynolds number based on frequency

Freytmuth [27] provides the following definition of Reynolds number based on the maximum value of wing flap velocity ($2\pi fH$).

$$Re_f = \frac{2\pi f H c}{\nu}$$

- Reynolds number based on RMS wing speed

An alternate formulation uses the RMS value of wing velocity and is defined here. Consider usual form for Reynolds number:

$$Re = \frac{Vc}{\nu}$$

Let us define the characteristic velocity as the RMS value of the wing's velocity:

$$V_{RMS} = \frac{V_{peak}}{\sqrt{2}} = \frac{(2\pi f H)}{\sqrt{2}}$$

This results in a definition of Reynolds number based on RMS velocity:

$$\text{Re}_{RMS} = \frac{Vc}{\nu} = \frac{(2\pi fH)c}{\sqrt{2}\nu}$$

- Calculation of Reynolds Number for target NAV

The representative NAV (dimensions given previously in Table 2) has wings that flap about an axis at the root of the wing. Therefore, the tip moves more and faster than portions of the wing that are closer to the root. In either of the definitions of Reynolds number discussed earlier, the value depends on the flapping amplitude (which in three dimensions may also vary with spanwise location). For this example, the location 75% from the root is arbitrarily chosen as representative of the main ‘working’ portion of the wing. Consider our sample NAV where the semispan is 3.75 cm. Using the formula for arc length, the flapping amplitude at the 75% span location is given as:

$$H = \frac{r\theta}{2} = \frac{(0.0375\text{m} * 0.75) \left(\frac{75\text{deg} \pi \text{ rad}}{180 \text{ deg}} \right)}{2} = 0.0184\text{m}$$

The flapping frequency is $f = 80\text{Hz}$ and the chord length is $c = 0.019\text{m}$. Using the Reynolds number definition based on frequency this gives a Reynolds number for the NAV of:

$$\text{Re}_f = \frac{2\pi H f c}{\nu} = \frac{2\pi(0.0184\text{m})(80\text{Hz})(0.019\text{m})}{1.51e-5\text{m}^2/\text{s}} = 11637 \approx 12000$$

4.1.3.2 Reduced frequency

The reduced frequency (k), is functionally equivalent to Strouhal number and is commonly defined as follows:

$$k = \frac{\omega c}{2V_\infty} = \frac{(2\pi f)c}{2V_\infty} = \frac{\pi f c}{V_\infty}$$

where ω is the circular frequency, c is the chord, f is the frequency in Hz and V_∞ is the freestream velocity.

In the case of a hover, which is of particular interest, the vehicle’s velocity (freestream velocity) is zero. Therefore for the hover case we instead estimate the velocity induced by the wings by using actuator disk theory [28] (momentum theory) and the values in Table 1:

$$V_{induced} = \sqrt{\frac{T}{2\rho A}} = \sqrt{\frac{0.1\text{N}}{2(1.225\text{ kg/m}^3)(0.00418\text{ m}^2)}} = 3.0\text{m/s}$$

Where the average induced velocity ($V_{induced}$) is a function of the thrust produced (T), the fluid density (ρ), and the disk area (A). Substituting the induced velocity for freestream velocity the reduced frequency for the NAV is:

$$k = \frac{\pi f c}{V_{\infty}} = \frac{\pi(80\text{Hz})(0.019\text{m})}{3\text{m/s}} = 1.6$$

4.1.3.3 Flap amplitude to chord ratio

The flap amplitude to chord ratio is simply the ratio H/c which is an important non-dimensional parameter that must be matched.

4.1.4 Definition of standard test cases

4.1.4.1 Two-dimensional test case

From the characteristics of the target vehicle, we may construct a test case that is functionally similar, but has properties well suited to the existing experimental facility and test rig as well as the existing CFD code and meshing method. A representative 2D flapping test-case was developed based on the representative NAV which, of course, undergoes 3D flapping. For this 2D case, a representative section of the 3D wing is chosen at 75% of span as measured from the root. In this way, the additional parameters listed in Table 4 are calculated.

Table 4. Calculated parameters of representative NAV

Radius at 75% span (r)	$r = 0.75*b/2 = 0.028 \text{ m}$
Arc length of path at 75% span (S)	$S = r\gamma = 0.028\text{m} * 1.31 \text{ rad} = 0.0368 \text{ m}$
Plunge amplitude at 75% of span (H)	$H = S/2 = 0.0184 \text{ m}$
Amplitude to chord ratio (H/c)	$H/c = 0.98$
Aspect ratio of single wing (AR)	$AR = b/(2c) = 0.0375 \text{ m}/0.019 \text{ m} = 2$

For two-dimensional flapping, a wing of infinite span (or simply an airfoil) undergoes only pitching and plunging. The position of the airfoil at any time is given by the linear superposition of the motion due to plunging and that due to pitching. These motions are periodic and differentiable functions. It is assumed that wings undergo simple harmonic motion in angle. In other words, the angular flapping motion of the wing from the root and the angular pitching motion of the wing from the leading edge are simple harmonic motions. For the test case being developed here, let us set the point about which the airfoil pitches as the leading edge (LE). This is not unreasonable given the way Mentor's wings operated and is consistent with a passively twisted wing of the type envisioned for an eventual flight vehicle. The position due to plunging is given by:

$$h(t) = H \sin(2\pi f t + \delta)$$

Where:

h is the linear plunge displacement of the point about which airfoil pitches (LE)
 H is the amplitude (peak value) of the point about which the airfoil pitches
 f is the flapping frequency
 t is the time
 δ is the phase angle (the angle by which pitching lags plunging)

Given that the phase angle between pitching and plunging is $\delta = \pi/2$ rad, at the initial condition ($t=0$), the airfoil is at zero degrees angle of attack. This should aid the computational solution in that for the initial time steps, the bound circulation is not instantaneously at a large or maximum value. It was found during the Mentor program, as well as by numerous researchers on larger scale flapping-wing vehicles [29, 30], that a phase angle of around $\pi/2$ rad (90 deg) produces optimal results. During the Mentor program, this phase angle was measured only approximately using high speed video. It may be the case that another phase angle, and indeed non-sinusoidal motion may provide some benefits for a Mentor-type wing. This phase angle serves as a well known starting point for the test case.

The airfoil's rotational position due to pitching is given by:

$$\theta(t) = (\theta_0 + \Theta \sin(2\pi ft))$$

Where:

θ is the rotational displacement (angle) of the airfoil
 θ_0 is the mean rotational position of the airfoil (for the test case this will be zero)
 Θ is the rotational amplitude (peak value)
 f is the flapping frequency
 t is the time

These pitching and plunging motions are illustrated in Figure 2.

The velocity of the wing is given by the time derivatives of position:

$$\frac{dh}{dt} = V_{plunge} = 2\pi f H \cos(2\pi ft + \delta)$$

$$\frac{d\theta}{dt} = \omega = 2\pi f \Theta \cos(2\pi ft)$$

To effectively capture in 2D what is happening in 3D, the flapping amplitude to chord ratio of the NAV wing at 75% of span must also be matched in the test case. At this location the flap amplitude to chord ratio is $H/c \sim 1$ (Table 4).

The following approximate data on IAR's experimental test rig was used:

$$c = 2\text{in} = 0.051\text{m}$$

frequency range = 0 – 2 Hz

Given these values as appropriate starting points, we calculated the necessary model size and flapping kinematics. The dimensionless parameters for the NAV developed previously are matched to produce a case suitable for the IAR's water tunnel facility.

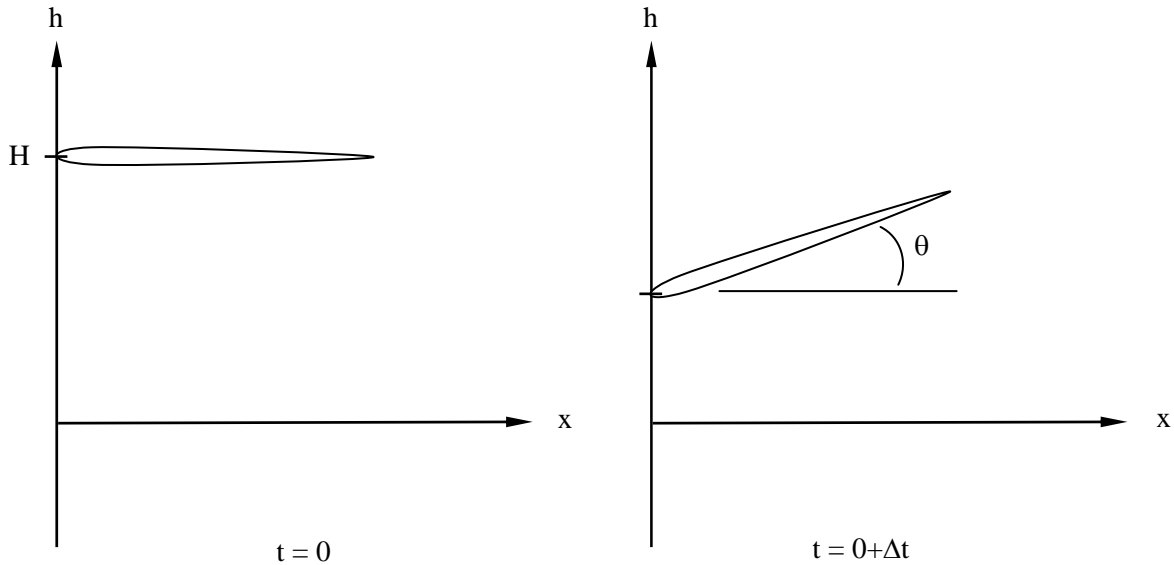


Figure 2: Description of airfoil flapping showing pitching and plunging

The maximum twist angle, θ , is set at 50 degrees from the axis of the freestream velocity. This is a good estimate of the twist angle encountered on the Mentor vehicle at the 75% span location.

The target NAV, with four wings acting in co-operation (clap-fling phenomenon), would produce substantially more thrust and thus more through-flow velocity than this test case. Because of this, it is suggested that a freestream velocity as specified below be imposed on the flow in order to match reduced frequency.

$$H = c = 0.0375\text{m}$$

$$f = \frac{\text{Re}_f \nu}{2\pi Hc} = \frac{(12000)(1.004e-6\text{m}^2/\text{s})}{2\pi(0.0375\text{m})(0.0375\text{m})} = 1.3\text{Hz}$$

$$k = \frac{\pi f c}{V_\infty} = 1.6$$

$$\Rightarrow V_\infty = \frac{\pi f c}{k} = \frac{\pi(1.3\text{Hz})(0.0375\text{m})}{1.6} = 0.1\text{m/s}$$

The airfoil should be as thin as possible to best approximate an actual NAV wing of the type used on the Mentor vehicle. Two different airfoils are identified for the test case: a symmetrical NACA 0005 airfoil section, and a flat plate with a thickness of 2mm (~5%). The leading and trailing edges are equilateral triangles as illustrated in Figure 3.

The plunging motion of the leading edge of the airfoil is therefore defined as follows:

$$h(t) = H \sin(2\pi f t + \delta)$$

$$h(t) = 0.0375\text{m} \sin(2\pi(1.3\text{Hz})t + \pi / 2\text{rad})$$

The pitching motion of the airfoil about the leading edge is described as:

$$\theta(t) = \theta_0 + \Theta \sin(2\pi f t)$$

$$\theta(t) = 0 + (0.87\text{rad}) \sin(2\pi(1.3\text{Hz})t)$$

Table 5 summarizes the values for the two-dimensional test case in water. It will be important for validation of methods that the CFD analysis run the exact same test as described in this section, utilizing the properties of water. The additional modeling of the actual NAV wing in air should also be easily accomplished.

Table 5. Two-dimensional test case summary

Variable	Symbol	Value
frequency	F	1.3 Hz
plunge amplitude	H	0.0375 m
twist amplitude	Θ	50 deg = 0.87 rad
airfoil chord	C	0.0375 m
airfoil max thickness	D	2 mm
freestream velocity	V_∞	0.1 m/s
kinematic viscosity of water	ν	1.004 e-6 m ² /s

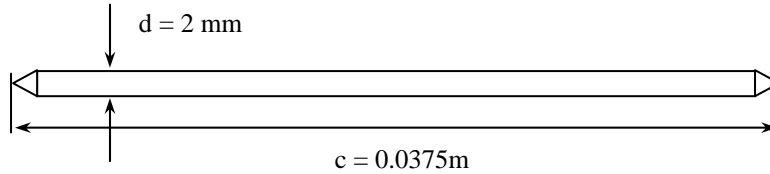


Figure 3: Schematic of the flat plate airfoil.

4.1.4.2 Three-dimensional test case

Because of the nature of the existing experimental test rig, a 3D test case that mimics the 2D case was developed. This is done by choosing the largest practicable aspect ratio to minimize tip effects. In other words, the chord length is set as $c=0.0375\text{m}$ and the span is as large as the facility and test rig allow ($b=0.4\text{ m}$). The root flapping angle is set so that at mid-span, the flap amplitude to chord ratio is equal to one ($H/c=1$). Note that the flap amplitude calculation at this location is based on the approximation that the curved path of the midpoint of the flapping wing is equal to $2H$ as described above in the 2D case. All local flow measurements, such as PIV measurements, are made in a plane near the mid-span point. To describe this root-flapping motion, a new variable, $\gamma(t)$, is introduced to describe the angular position of the wing from centre. The magnitude of this angle is termed Γ . The 3D case is shown schematically in Figure 4. The airfoil sections to be tested are the same as those in the 2D case.

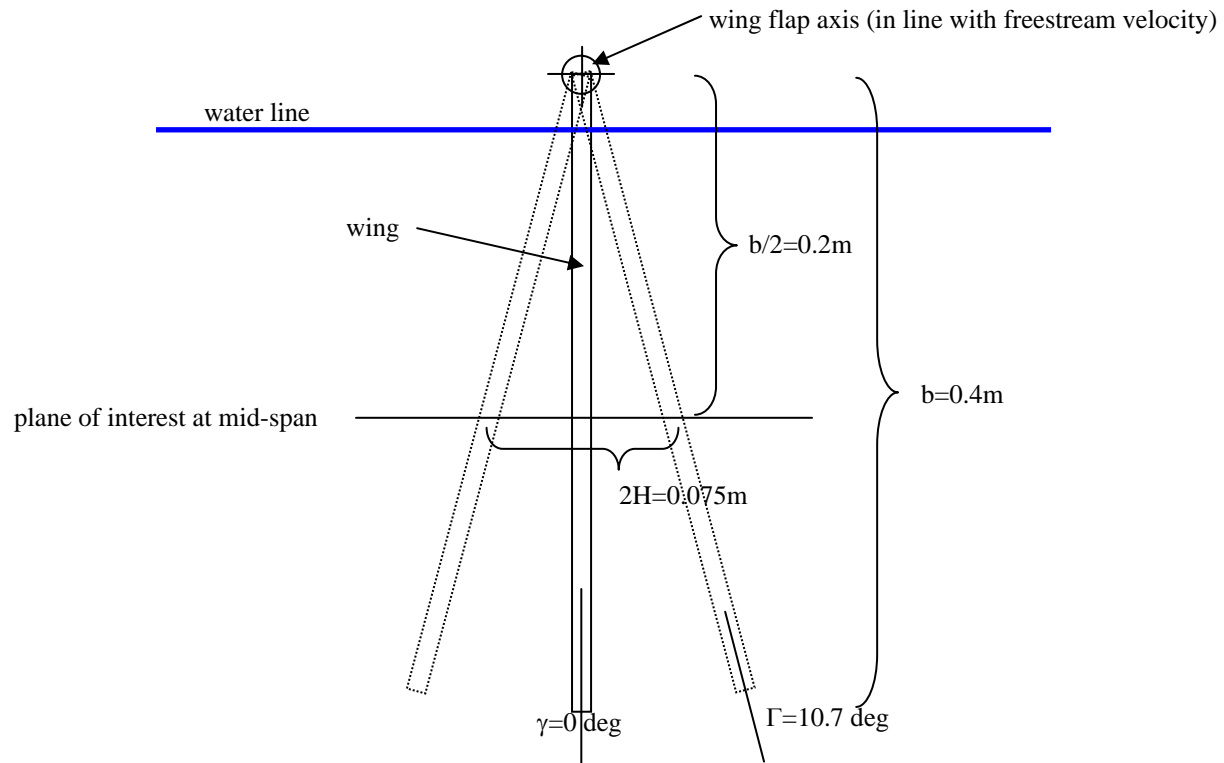


Figure 4: Schematic of the 3D test case as viewed along the axis of freestream velocity

Table 6. Three-dimensional test case summary

Variable	Symbol	Value
frequency	F	1.3 Hz
flap angle amplitude	Γ	10.7 deg = 0.19 rad
twist amplitude	Θ	50 deg = 0.87 rad
airfoil chord	C	0.0375 m
airfoil max thickness	D	2 mm
wing span	B	0.4 m
freestream velocity	V_{∞}	0.1 m/s
kinematic viscosity of water	ν	1.004 e-6 m ² /s

Using the values of Table 6, the 3D motion of the wing is defined below. The angular displacement of the leading edge of the airfoil due to flapping is defined as follows:

$$\gamma(t) = \Gamma \sin(2\pi f t + \delta)$$

$$\gamma(t) = (0.19\text{rad}) \sin(2\pi(1.3\text{Hz})t + \pi / 2\text{rad})$$

The pitching motion of the airfoil about the leading edge is described as:

$$\theta(t) = \theta_0 + \Theta \sin(2\pi f t)$$

$$\theta(t) = 0 + (0.87\text{rad}) \sin(2\pi(1.3\text{Hz})t)$$

4.2 Navier-Stokes simulation with Fluent

This study of the aerodynamics of flapping airfoil compares different viscous models available in Fluent. Two different nano-air vehicle (NAV) flapping-wing shapes were studied in 2-D, a flat plate and a NACA 0005. The motion defined in section 4.1.4.1 above was applied both. To simulate the airfoil motion, a completely structured grid was generated. The laminar, k- ω SST, DES with Spalart-Almaras and LES viscous models were compared quantitatively in terms of convergence speed and drag/propulsion force coefficient, and qualitatively, by comparing contour plots of vorticity magnitude.

This work, done at DRDC Valcartier, demonstrated that Fluent can simulate efficiently pitching and heaving airfoil. The technique was also verified against results found in the literature.

The force generated by the flapping airfoil did not vary significantly for one viscous model to the other. Also all the models predicted the same shape and strength of the leading edge vortex. This could be explained by the geometry of the thin airfoil. The flow detaches directly at the leading edge of the airfoil. Also, for all turbulence models the NACA 0005 airfoil gave superior propulsion forces than the flat plate for the same motion.

The laminar viscous model seems to be sufficient to estimate the forces generated by a plunging and pitching airfoil. On the other hand, to consider the vortices shed by the airfoil and interacting with the NAV airframe, the LES viscous model should be used (Fig. 5).

It was also demonstrated that the propulsion obtained by CFD is sufficient to permit to 10 gram NAV to hover.

A paper outlining this work was presented at the conference CFD 2007 in Toronto in June 2007 [31] and the paper can be found in Annex 3.

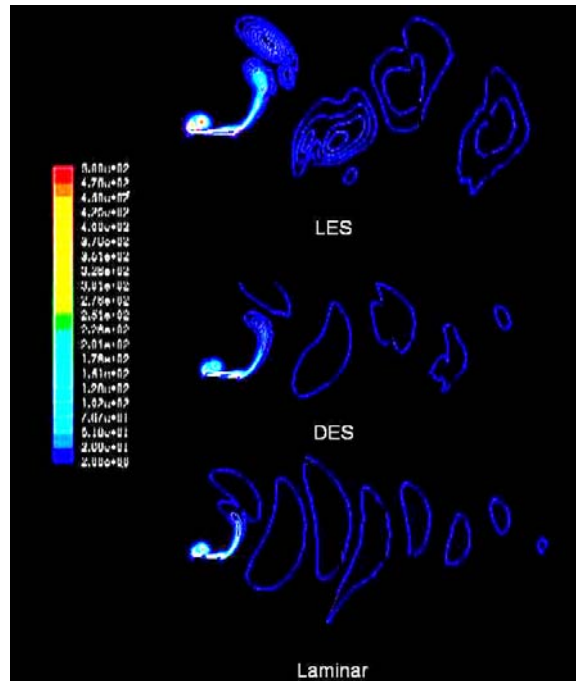


Figure 5: Vorticity magnitude contour for the flat plate airfoil

4.3 Navier-Stokes simulations with INSFlow

The in-house code INSflow [32] developed for computing three-dimensional (3D) unsteady incompressible flows was applied in the study. In the code, the integral form of the conservation law for mass and momentum was used. A fully implicit second-order temporal differencing scheme was used in the discretisation, which made the algorithm stable for large timesteps. The discretisation of the convective and diffusive fluxes was carried out in a co located variable arrangement using the finite-volume approach with a second-order accuracy in space. The coupling of the pressure and the velocity was handled using the SIMPLE algorithm [33]. The continuity equation was transformed into a pressure correction equation, which had the same general form as the discretized momentum equations. The use of the collocated variable arrangement on non-orthogonal grids required that the SIMPLE algorithm be modified slightly to dampen numerical oscillations. A pressure-velocity coupling method for complex geometries used by Ferziger and Perić [34] was implemented, where an additional pressure gradient term was subtracted from the velocity value at the surface of the control volume to prevent non-physical oscillations. To enable large-eddy simulation (LES) practices for complex geometry flows, the Smagorinsky [35] SGS model was implemented as a standard SGS model in the code.

The calculations were performed on moving grid configurations. The velocity of the grid movement was included in the governing equations [32], [36] in an inertial frame of reference. In order to avoid artificial mass sources generated by the grid velocity, as applied

by Demirdžić and Perić [37], a space conservation law was introduced to ensure a fully conservative property in the computations.

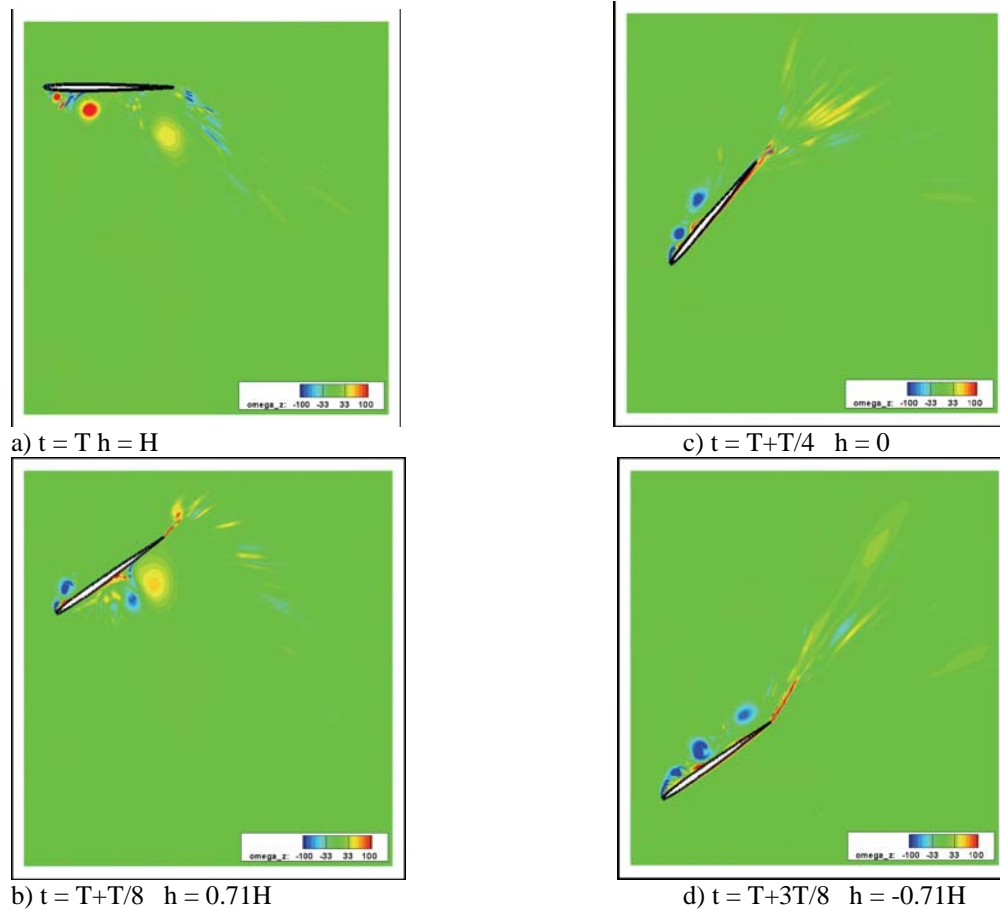


Figure 6: Spanwise vorticity over the flapping NACA 0005 airfoil during the downstroke period with pitching axis $x_0/c=0.5$ at $Re=1.2 \times 10^4$.

The preliminary simulations of plunging airfoils combined with a pitching motion about the airfoil leading edge (two-dimensional test case defined in 4.1.4.1) showed the leading-edge vortex formation and shedding process (Fig. 6). When the effective angle of attack approached the second maximum peaks, the leading-edge vortex formed and started shedding through the other half motion cycle. The largest thrust occurred when the leading-edge vortex was forming. However, the largest lift appeared when the effective angle of attack reached the second maximum followed by a flow hysteresis. It seems that the effect of the airfoil on the averaged lift/drag coefficients is limited. However, thin airfoil seems to be superior to thicker ones causing less drag and larger thrust coefficients. In addition, grid resolution affected the vortex shedding prediction and the pitching axis had clear influence on the integrated lift and thrust coefficients.

A paper outlining this work was presented at the conference CASI in Toronto in April 2007 [38] and the paper can be found in Annex 4.

4.4 Water tunnel experiment

Prior to the initiation of the project, a preliminary water tunnel experiment was conducted on an insect wing performing three degree-of-freedom motions [21] (Annex 5). For that experiment, a bi-fold five component strain-gauge balance has been developed to measure the aerodynamic behavior of insect's flapping wings. It has been found that at low to mid- range angles of attack, the normal force and pitching moment of the wing increase as the angle of attack increases. While at high angles of attack, the phase shift between the motion and the aerodynamic loads becomes obvious. The maximum normal force appears much ahead of the maximum angle of attack and decrease dramatically thereafter as the angle increases further. Introducing second and third degree-of-freedom motions could further increase the maximum normal force compared with one degree-of-freedom motion, indicating possible delayed stall caused by the additional motions.

During the first year of the project, two different rigs for the water tunnel were designed: one to produce a two-dimensional motion and the other to produce a three-dimensional motion (Annex 6). The micro PIV equipment required to measure flow vorticity in addition to velocity was identified. The current laser is only able to measure velocity fields. The selected equipment, a high frequency laser, was purchased.

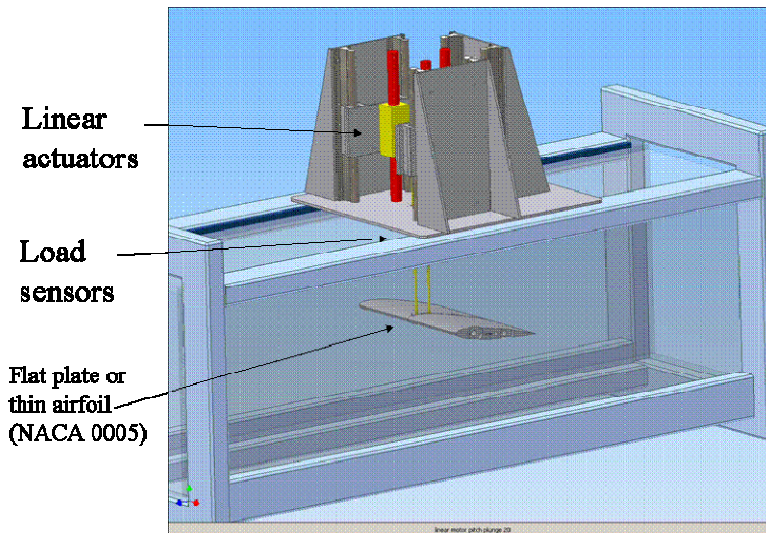


Figure 7: Design of two-dimensional rig in water tunnel

4.5 Vortex-lattice modelling

The vortex-lattice model (VLM) developed by Advanced Subsonics solves the basic problem of modeling vortex shedding from both the leading and trailing edges of a flapping wing of arbitrary thin cross-sectional shape. The VLM is an engineering-type model where the variables are fewer and easily manipulated compared to CFD, and can yield design rules. The characteristics of the existing 2D model are briefly given in Annex 2 and are detailed in [15]. The two-dimensional model will be converted to a three-dimensional model and if resources allow, aeroelasticity will be built into it.

The work on the engineering method just started at the end of the first year. Only the planning of the approach was done. The plan is in four steps.

In the first step, the original 2D model will be applied to the 2D test case and its results compared to the experimental results.

In the second step, the two-dimensional infinite vortices will be adapted to three-dimensional ring vortices. A high aspect ratio 3D wing will be used to mimic the 2D flow. The results will be compared to that of the previous model and to the experimental 2D results.

In the third step, a low aspect ratio wing will be modeled. Initially only plane flapping will be modeled. The simulation will be compared with experiments.

Finally, in the fourth step, root flapping will be added (as in the NAV concept) and two reflection planes will be added to model 4 wing clap-fling design.

5. Conclusions

A four-year project was approved with the purpose of increasing our understanding of the issues concerning the flight of very small air vehicles using flapping wings. The project focuses on the development of modelling and experimental capabilities, and investigations as to the appropriate sizes and performance parameters with some consideration of system integration. Although progress in many technology areas will be required before a practical insect-size aircraft can be built, this project focuses on the efficient generation of forces through flapping motion. To limit the scope of the project, many research fields that are crucial to insect-size aircraft development, such as energy sources, morphing structures, advanced guidance navigation and control, payload, and communication, are not investigated in this project. It is recognized that progress in these areas is essential for a viable insect-size aircraft system.

This technical memorandum presented the progress made during the first year of the project, which started in April 2006.

The potential impact of this technology on military operations and R&D was described. The potential of NAVs, with their small size and hover capability, opens up new possibilities in the formulation of military strategies with respect to information superiority in urban operations.

The project plan, as revised by the team during the first year, was presented. It combines the development of an ability to capture detailed flow physics using a highly accurate CFD solution and a tailored experimental facility with an engineering-type method. This combination of three different approaches supported by system considerations provides different views of the problem and its solutions, and mitigates risk. A significant outcome should be quantitative relations between the leading-edge vortex behaviour and wing geometry and motion variables for the purpose of the conceptual design of a flapping-wing NAV.

The general characteristics of the target NAV to be studied, such as size, mass and wing motion, were established based on system considerations. Some missions for the NAV were identified, the current and future technologies for the NAV components were examined, and the characteristics of existing very small air vehicles were looked at. Standard test cases in 2D and 3D for simulation and experimentation were set up by applying simplifications and scaling arguments to the target NAV.

Computational Fluid Dynamics simulations were initiated with the standard 2D test case defined by the team. The in-house INSflow code and the commercially-available Fluent code were both used to solve this unsteady incompressible flow. The challenges included the complex and large-amplitude motion involving both pitch and plunge schedules, and the capture of the leading edge vortex, which required high grid resolution and accurate models. Results from both INSflow and DRDC show favourable comparisons and are awaiting further experimental data for validation.

The low Reynolds number experimentation on flapping-wing aerodynamics will be carried out in the IAR water tunnel. Motion rigs in 2D and in 3D were designed and are being fabricated. A micro-PIV method was also developed. The required equipment, mainly a high-frequency laser, was purchased, and the system is being implemented.

The work on the engineering method (vortex-lattice method in three dimensions) just started at the end of the first year. Only the planning of the approach was done.

The project progressed very well during the first year and is on schedule.

6. References

1. BAA 06-06, Proposer Information Pamphlet (PIP) for Defense Advanced Research Projects Agency (DARPA), Defense Sciences Office (DSO) Nano Air Vehicle (NAV) Program, 2005
2. Ellington, C.P., "The Novel Aerodynamics of Insect Flight: Applications to Micro-Air Vehicles," *The Journal of Experimental Biology*, 202, 3439-3448, 1999
3. Carpentier, J., "Le vol animal et l'aéronautique", *Revue scientifique et technique de la défense*, no. 47, DGA, 2000
4. Sane, S.P., "The aerodynamics of insect flight", *The Journal of Experimental Biology*, 206, 4191-4208, 2003
5. Lehmann, F.-O., "The mechanisms of lift enhancement in insect flight", *Naturwissenschaften*, 2004, 91:101-122
6. Dickinson, M., "Solving the Mystery of Insect Flight," *Scientific American*, June 2001
7. Ellington, C.P., "Unsteady Aerodynamics of Insect Flight," *Biological Fluid Dynamics* (ed. C.P. Ellington and T.J. Pedley), *Symp. Soc. Exp. Biol.* 49, 109-129.
8. Woods, M.I., Henderson, J.F., and Lock, G.D., "Energy Requirement for the Flight of Micro Air Vehicles," *The Aeronautical Journal*, March 135-149, 2001.
9. van den Berg, C. and Ellington, C. P., 1997, *Series B, Biological Science*, 352/1531, pp. 317-328 and pp. 329-340
10. Dickinson et al., "Wing Rotation and the Aerodynamic Basis of Insect Flight", *Science*, pp. 1954-1960, 1999
11. Zbikowski, R., "Introduction to Flapping Wing MAVs", VKI lecture series RTO/AVT-104, 2003
12. Yuan, W. et al., "An Investigation of Low-Reynolds-number Flows past Airfoils", 23rd AIAA Applied Aerodynamics Conference, June 2005, Toronto, Canada
13. Liu, H., "Leading-Edge Vortices of Flapping and Rotary Wings at Low Reynolds Number", *Progress in Astronautics and Aeronautics Series*, V-195, pp. 34-43, 2001
14. Jones et al., "Experimental and Computational Investigation of Flapping-Wing Propulsion for Micro-Air Vehicles", *Progress in Astronautics and Aeronautics Series*, V-195, pp. 421-445, 2001
15. Zdunich, P., "A Discrete Vortex Model of Unsteady Separated Flow About a Thin Airfoil For Application to Hovering Flapping-Wing Flight", *UTIAS M.A.Sc. Thesis*, 2002

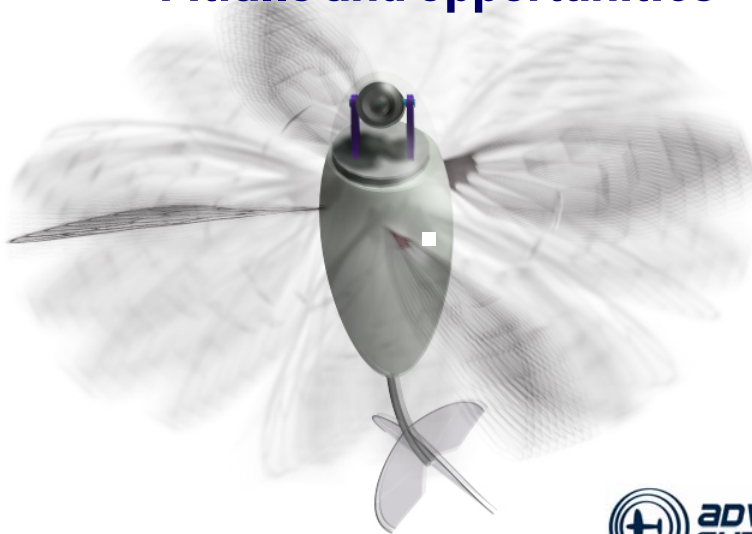
16. Weis Fogh, T., "Quick Estimates of Flight Fitness in Hovering Animals, Including Novel Mechanisms for Lift Production", J. Exp. Biol., 1973
17. Lehmann, F.-O. et al., "The aerodynamic effects of wing–wing interaction in flapping insect wings", The Journal of Experimental Biology 208, 3075-3092, 2005
18. Bilyk, D., "The Development of Flapping Wings for a Hovering Micro Air Vehicle", UTIAS M.A.Sc. Thesis, 2000
19. Frampton et al., "Passive Aeroelastic Tailoring for Optimal Flapping-Wings", Progress in Astronautics and Aeronautics Series, V-195, pp. 26, 2001
20. MacMaster, M., "Stability of a Flapping Wing Micro Air Vehicle", UTIAS M.A.Sc. Thesis, 2001
21. Huang, X., Brown, T., "Preliminary Experiment of Flapping Wing in Three-Degrees-of-Freedom Motion" paper presented at the 25th International Congress of the Aeronautical Sciences, Hamburg, Germany, September 2006
22. Hanff, E.S., "A Novel Facility for Testing at Low Reynolds Number", 24th International Congress of the Aeronautical Sciences, ICAS 2004
23. Jones et al., "Experimental and Computational Investigation of Flapping-Wing Propulsion for Micro-Air Vehicles", Progress in Astronautics and Aeronautics Series, V-195, pp. 421-445, 2001
24. Khalid, M. and Yuan, W., "Use of CFD methods on unsteady aerodynamics at low Reynolds numbers", VKI lecture series RTO/AVT-104, 2003
25. Larijani, R.F., DeLaurier, J.D., "A Nonlinear Aeroelastic Model for the Study of Flapping Wing Flight", Progress in Astronautics and Aeronautics Series, V-195, pp. 399-428, 2001
26. Zdunich, P., "System Considerations for directions to flapping wing aerodynamic studies – AERO-NAV Final Report", DRDC Valcartier Contract Report CR 2007-087, Advanced Subsonics Inc, March 2007
27. Freymuth, P., "An Unsteady Model of Animal Hovering", Lecture notes in Engineering – Low Reynolds Number Aerodynamics, June 5-7, 1989.
28. Gessow, A. and Myers, G. Jr., Aerodynamics of the Helicopter, 8th edition, College Park Press, 1985.
29. DeLaurier, J.D. An aerodynamic model for flapping-wing flight, Aeronautical Journal, April 1993, 97, (964), pp 125-130
30. DeLaurier, J.D. The development of an efficient ornithopter wing, Aeronautical Journal, May 1993, pp 153-162

31. Hamel, N., Lesage, F., "Model Comparison of Viscous Flow over a Pitching and Plunging Wing for Nano-Air Vehicles", paper presented at the 15th Annual Conference of the CFD Society of Canada, Toronto, June 2007
32. Yuan, W., Khalid, M., "Computation of Unsteady Flows past Aircraft Wings at Low Reynolds Numbers", Canadian Aeronautics and Space Journal, 50(4): 261-271, 2004.
33. Patankar, S. V., Numerical Heat Transfer and Fluid Flow, Hemisphere Publishing Corporation, Washington New York London, 1980.
34. Ferziger, J. H., Perić, M., Computational Methods for Fluid Dynamics, Springer-Verlag, Berlin & Heidelberg, 1996.
35. Smagorinsky, J., "General Circulation Experiments with Primitive Equations", Monthly Weather Review, 93:99-164, 1963.
36. Yuan, W., Schilling, R., "Numerical Simulation of the Draft Tube and Tailwater Flow Interaction", Journal of Hydraulic Research, 40(1):73-81, 2002.
37. Demirdžić, I., Perić, M., "Finite Volume Method for Prediction of Fluid Flow in Arbitrarily Shaped Domains with Moving Boundaries", International Journal for Numerical Methods in Fluids, 10:771-790, 1990.
38. Yuan, W., Khalid, M., "Preliminary CFD Simulations of Flapping-Wing Aerodynamics", paper presented at the 12th CASI Annual Aerodynamics Symposium, Toronto, Canada, April 2007

Annex 1 – Small scale flapping flight: pitfalls and opportunities – July 2006

This page intentionally left blank.

Small Scale Flapping Flight: Pitfalls and Opportunities



Introduction: Bio



Patrick Zdunich

- Involved in micro and mini UAV projects since 1999
- Incorporated Advanced Subsonics 2002
 - Developed intelligent Grasshopper UAV system
 - DARPA contract to develop morphing aircraft technology
- Analytical and experimental flapping-wing experience:
 - Developed a separated unsteady flow 2D panel method for thin airfoils undergoing arbitrary motion
 - Mechanical design of flapping-wing UAV



This presentation is property of Advanced Subsonics Inc. Duplication is permitted with written permission. Copyright © 2006 Advanced Subsonics Inc.

Introduction to MAV Program



DARPA Program Overview: 1998-2002

Prime Contractor: SRI International (EPAM Actuator Development, Simulation)

Subcontractor: UTIAS (Flight Vehicle Development and Control System Integration)

Significant Achievements:

- World's first hovering flapping-wing aircraft
- Took from concept to controllable vehicle in 10 months
- Pilot in the loop flight sim accurately modeled prototype's dynamic behavior



This presentation is property of Advanced Subsonics Inc. Duplication is permitted with written permission. Copyright © 2006 Advanced Subsonics Inc.

Introduction to MAV Program



1998-2001: DARPA MAV Program at UTIAS

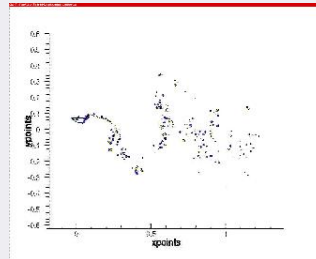
- Research program to develop "rules and tools" for low-Re flapping-wing flight
- Developed specialized wing and wing actuation methods for small, hovering MAV (< 6 inch max dimension, 150g maximum)
 - Designed and tested aeroelastically tailored wings suited to single degree of freedom actuation
 - Conducted wind tunnel tests to acquire flapping-wing forces and moments
 - Time-marching model of 2-D unsteady aerodynamic flow about thin wing



Experimental Wing Testing



Wind Tunnel Stability Testing



Unsteady Aerodynamic Model

This presentation is property of Advanced Subsonics Inc. Duplication is permitted with written permission. Copyright © 2006 Advanced Subsonics Inc.

Introduction to MAFC Program



2002: DARPA MAFC Program at UTIAS

- Take rules and tools from previous years and develop a stable, unthethered, flying vehicle in <1 yr
- Develop wings suitable for increased disk loading to account for entire system mass
- Refined aerodynamic analyses
- Created simulation for control system development and vehicle layout
- Develop light weight on-board PID controller
- Developed and flew two different vehicles – IC and battery powered



New Wings



IC motor power



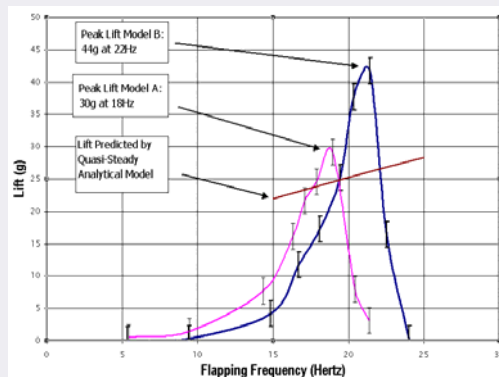
Electric Power

This presentation is property of Advanced Subsonics Inc. Duplication is permitted with written permission. Copyright © 2006 Advanced Subsonics Inc.

Quasi-Steady Model



- The goal of the quasi-steady method was not detailed prediction, but to guide experimental method and wing development
- Uses chordwise strip model
- Local flow velocity a superposition of velocity due to kinematics and through flow (from momentum theory)
- Local lift curve slope is 2π - adjusted using conventional aspect ratio corrections
- Results:
 - Predicted to within about 20-30% the necessary flapping frequency for a given amount of thrust
 - This model predicts significantly lower lift at a given flapping frequency than experimental results
 - Reason: Quasi-steady assumption is invalid in this Reynolds number regime. Does not account for clapping effect

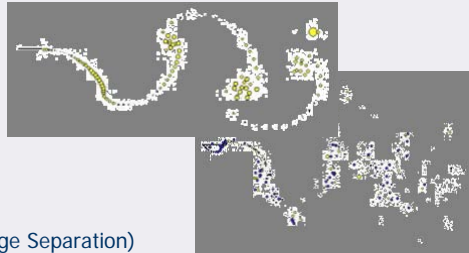


This presentation is property of Advanced Subsonics Inc. Duplication is permitted with written permission. Copyright © 2006 Advanced Subsonics Inc.

Unsteady Aerodynamic Model



- An unsteady engineering model was developed:
 - Discrete vortex thin airfoil
 - Time marching
 - Arbitrary unsteady motion
 - Models separated flow
 - Low advance ratio to hover
- Model was linear and fast
 - Modeled the necessary and dominant flow characteristics
 - Allowed variables of interest to be modified rapidly
- Simple Case:
 - Low maximum angle of attack
 - No flow separation
- Complex Case:
 - High maximum angle of attack
 - Models dynamic stall (Leading Edge Separation)



This presentation is property of Advanced Subsonics Inc. Duplication is permitted with written permission. Copyright © 2006 Advanced Subsonics Inc.

Unsteady Aerodynamic Model



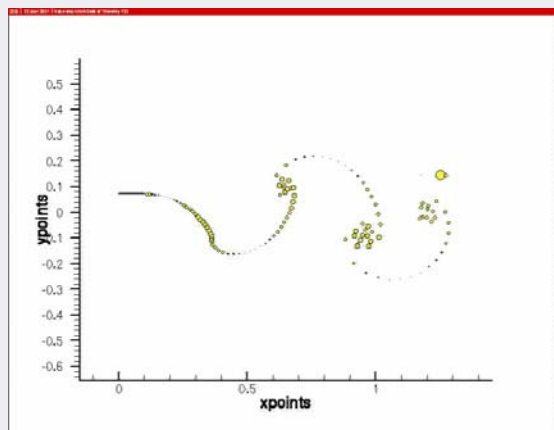
Simple Case: Unsteady, Discrete Vortex Trailing Edge (TE) Wake

Utilizes:

- Discrete wake elements to model continuous sheet of TE wake vorticity
- Fully interactive wake

Boundary Conditions:

- Flow tangency at airfoil (Kutta condition at TE)
- Conservation of vorticity (Change in bound vorticity between time steps is shed into wake)



This presentation is property of Advanced Subsonics Inc. Duplication is permitted with written permission. Copyright © 2006 Advanced Subsonics Inc.

Unsteady Aerodynamic Model



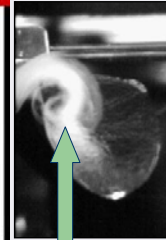
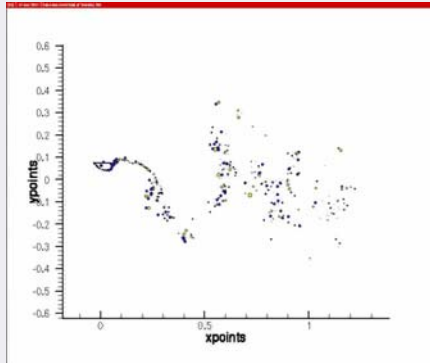
Separated, Unsteady, High AOA Flows (Low advance ratios)
Discrete Vortex Leading Edge (LE) and Trailing Edge (TE) Wake

Utilizes:

- Discrete vortex elements and control points to model bound circulation
- Discrete wake elements to model continuous sheet of LE and TE wake vorticity
- Fully flexible wake
- Linear approximation of Kutta condition yields a linear system of equations at each time step (Solves easily and quickly)

Boundary Conditions:

- Flow tangency (Kutta condition at LE and TE)
- Conservation of vorticity



Smoke in flow shows LEV

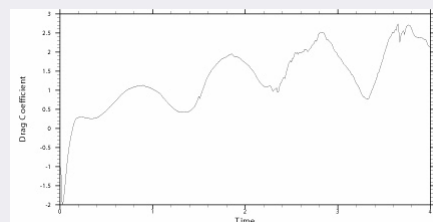
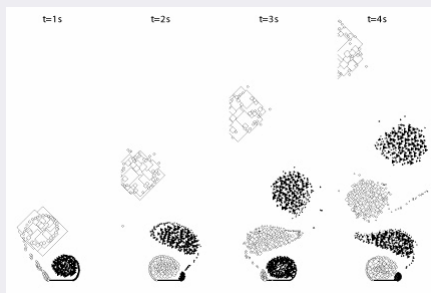
This presentation is property of Advanced Subsonics Inc. Duplication is permitted with written permission. Copyright © 2006 Advanced Subsonics Inc.

Unsteady Aerodynamic Model



● Applicability and Test Cases

- Flat plate in normal flow
- Flow features representative of flow about flapping wings (large scale, unsteady separation)
- Here drag is analogous to thrust
- Under predicts drag by 8%



This presentation is property of Advanced Subsonics Inc. Duplication is permitted with written permission. Copyright © 2006 Advanced Subsonics Inc.

Model Output and Results

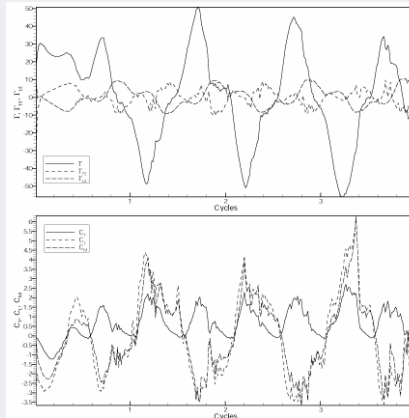
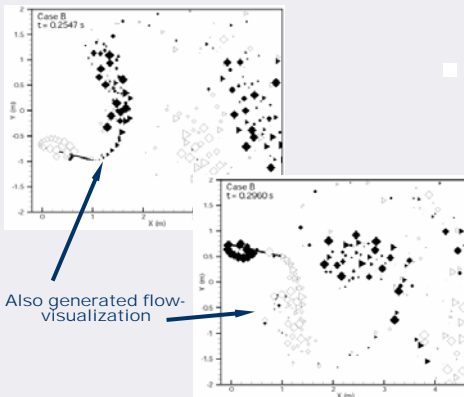


Model Capabilities:

- Models both forward flight and the more difficult hover case
- Generates a through flow with time in calm air
- Used to find operating points of maximum efficiency

Results:

- Generates instantaneous force and moment coefficients as seen at the right



Separated Flow
Test Case B

Test Parameters

$C = 1 \text{ m}$
 $H = 0.75 \text{ m}$
 $\delta = 90^\circ$
 $V_\infty = 15 \text{ m/s}$
 $f = 10 \text{ Hz}$
 $Re = 67300$

Calculated Values

$H/c = 0.75$
 $St = 1$
 $\Delta W/c = 0.02$
 $\Delta W_{\text{strip}}/c = 0.044$

Average Force and Moment Coefficients
(Using average speed due to pitch and plunge)

$C_L = 0.552$
 $C_D = 0.06$
 $C_m = 0.04$
 $\eta = 0.268$

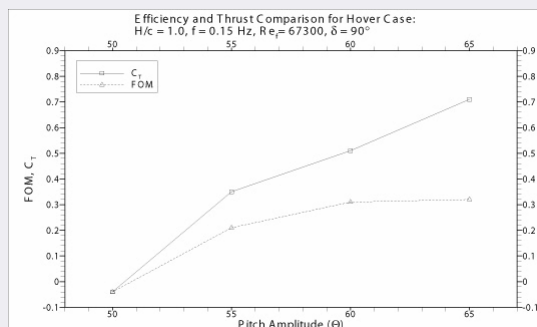
This presentation is property of Advanced Subsonics Inc. Duplication is permitted with written permission. Copyright © 2006 Advanced Subsonics Inc.

Model Output and Results



Best performance for 2D flat plate wing given by:

- Plunge amplitude to chord ratio ~ 1
- Pitch amplitude = 65 degrees (each side of vertical)
- Pitching lags plunging by 90 degrees

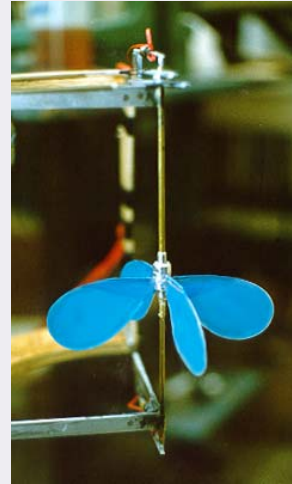


This presentation is property of Advanced Subsonics Inc. Duplication is permitted with written permission. Copyright © 2006 Advanced Subsonics Inc.

Thrust/Lift Measurement



- First test-rig developed to experimentally measure thrust production and power consumption
 - Could measure lift from isolated or interacting wing
 - Measured *average* lift
 - Measured *average* power consumption
 - Allowed superposition of free stream velocity from any angle



This presentation is property of Advanced Subsonics Inc. Duplication is permitted with written permission. Copyright © 2006 Advanced Subsonics Inc.

Wing Development



- Early Experimental Wing Designs



Fabric Covered Ellipsoid Wings:

- first wings to show promising lift values
- difficult to construct, materials fatigue rapidly



Steel Frame Mylar Wings:

- first wing type to exceed lift target of 50 g
- easier to construct, lighter weight
- high power consumption



Carbon-Fiber Frame Mylar Wings:

- exceeds thrust target of 50 g with reasonable power consumption
- very light weight (0.25 g ea..) reduces inertial energy requirements
- simple construction means wings could be mass produced in a cost-effective manner

This presentation is property of Advanced Subsonics Inc. Duplication is permitted with written permission. Copyright © 2006 Advanced Subsonics Inc.

Wing Development

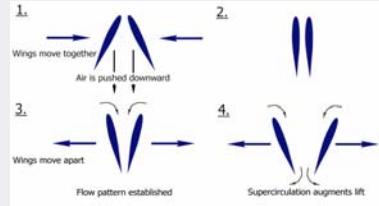


- What is "Clap-Fling"?
 - First described by Weis-Fogh
 - Wings operate in close proximity to one another at extremes of stroke
 - Trailing edges often touch
 - Generates "super-circulation"
 - Nature's afterburner

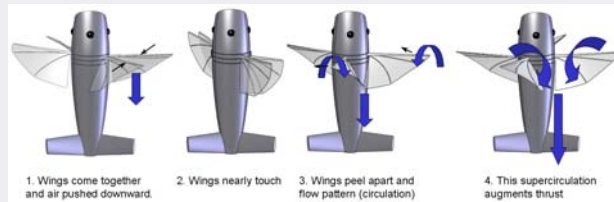
Stroboscope used to capture high-speed motion



BIRIB-06 Wing "Stiff" Mass = 0.69 g
Net Thrust = 68 g
FOM = .13



Explanation of Clap-Fling

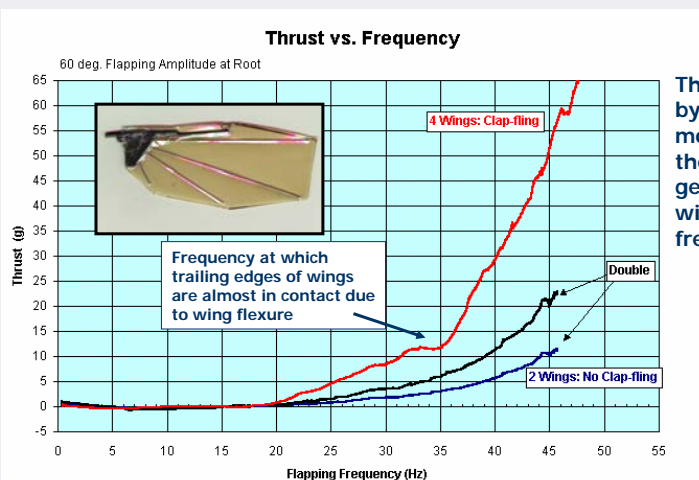


This presentation is property of Advanced Subsonics Inc. Duplication is permitted with written permission. Copyright © 2006 Advanced Subsonics Inc.

Wing Development



- Evidence of Clap-Fling Thrust Augmentation



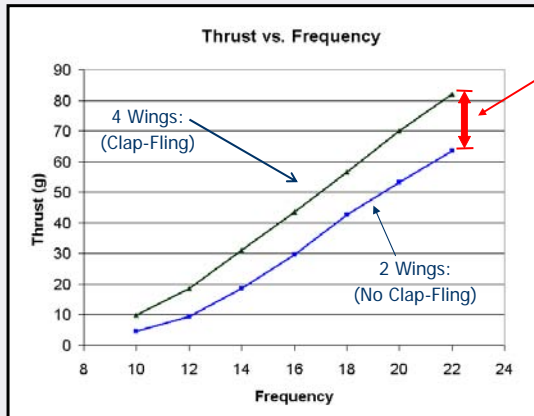
Thrust generated by four wings is more than double the thrust generated by two wings at same frequency

This presentation is property of Advanced Subsonics Inc. Duplication is permitted with written permission. Copyright © 2006 Advanced Subsonics Inc.

Clap-Fling Evaluated: Thrust



- Clap-Fling increases thrust



- Percentage increase in thrust due to Clap-Fling at 22Hz = 31%
- Lower curve represents TWICE the thrust from 2 wings that flap opposite one another on the test rig - No Clap-Fling

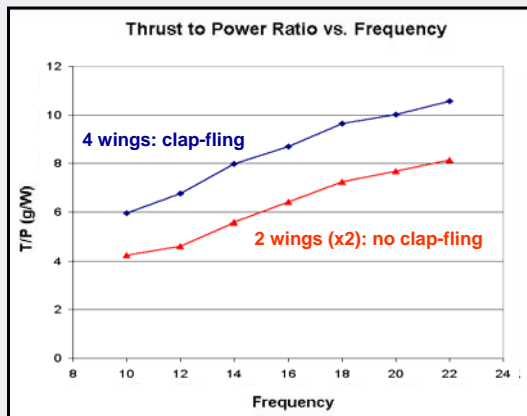
BIRIB-04: 76 deg. Flapping Amplitude

This presentation is property of Advanced Subsonics Inc. Duplication is permitted with written permission. Copyright © 2006 Advanced Subsonics Inc.

Clap Fling Evaluated: Efficiency



- More importantly, clap-fling increases thrust to power ratio



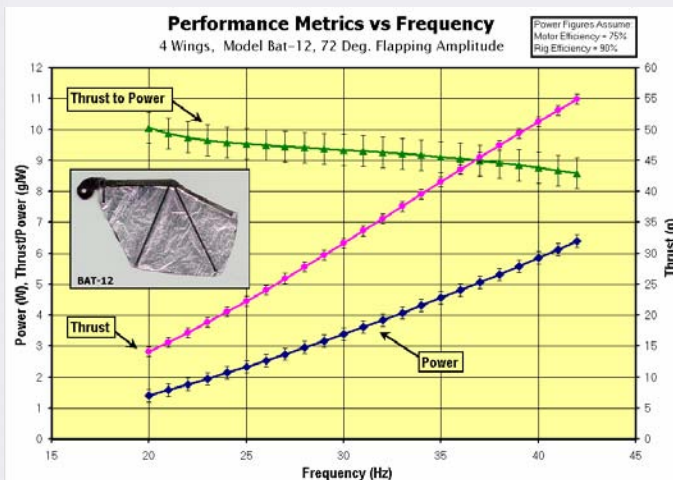
- Average percentage increase in Thrust- to- Power Ratio = 36%
- Similar test on 6 in dia. wing set showed a 40% increase in thrust to power ratio due to Clap-Fling

This presentation is property of Advanced Subsonics Inc. Duplication is permitted with written permission. Copyright © 2006 Advanced Subsonics Inc.

Wings: Early Results



BAT-12 Performance Metrics



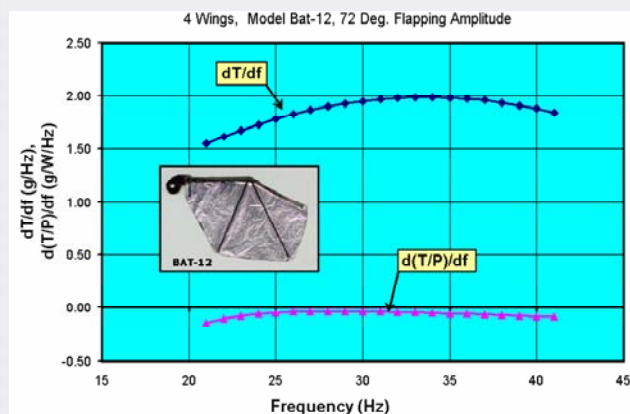
The BAT-12 wing design met the preliminary performance goal of 50g of thrust at a thrust-to-power ratio of 8g/W

This presentation is property of Advanced Subsonics Inc. Duplication is permitted with written permission. Copyright © 2006 Advanced Subsonics Inc.

Wings: Early Results



Frequency Derivatives of Performance Metrics for BAT-12 Wing



These curves illustrate the sensitivity of the performance metrics to changes in flapping frequency

Note that the thrust to power ratio of this flapping wing set is not very frequency dependent

This presentation is property of Advanced Subsonics Inc. Duplication is permitted with written permission. Copyright © 2006 Advanced Subsonics Inc.

Instantaneous Measurement



- A second test-rig was designed and built to capture instantaneous data
- Strain gauges at wing root gave wing-specific torque
- Allowed for derivation of instantaneous power consumption
- Allowed wings to be tested in an arbitrary freestream velocity

Measurable Quantities:

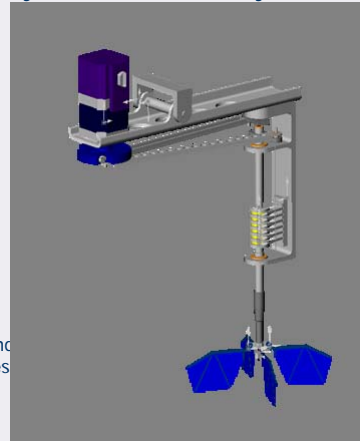
- Net thrust produced and power required by wing set
- Instantaneous root bending torque for single wing

Actuation Capability:

- Single D.O.F. wing root flapping: 4 wings
- 0-60 Hz wing beat frequency
- 60-80 deg. root flapping amplitude (4 wings)

Control and Stability Experiments:

This device was used in conjunction with an open throat wind tunnel to derive experimental control and stability derivatives



This presentation is property of Advanced Subsonics Inc. Duplication is permitted with written permission. Copyright © 2006 Advanced Subsonics Inc.

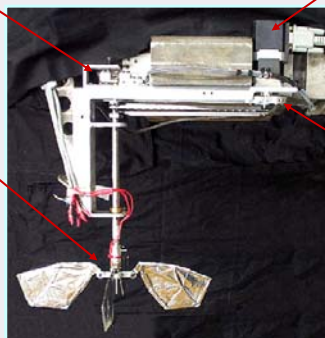
Instantaneous Measurement



- Individual test-rig components are described below:

Parallel-beam strain gauge balance measures net thrust from all four wings

Miniature cantilevered strain gage balance measures instantaneous root bending moment



Computer controlled, 'Quick Silver' servo motor

Phase-adjustable hub varies flapping amplitude

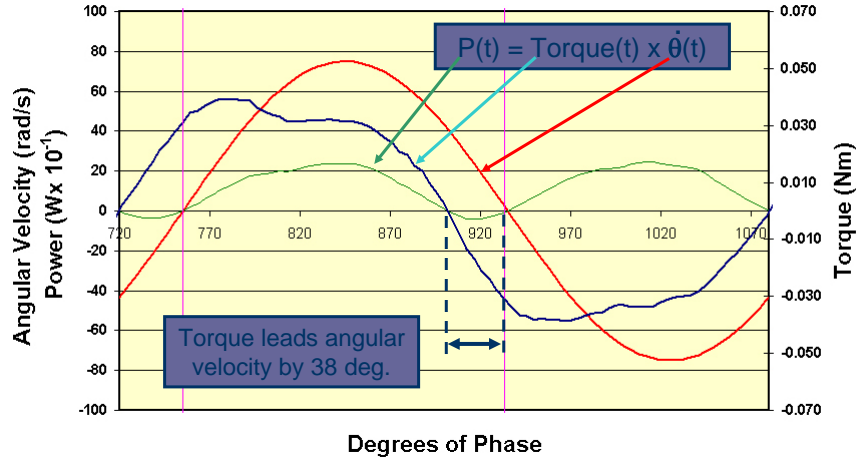
Magnets and hall-effect sensor provide sync cue for phase measurements

This presentation is property of Advanced Subsonics Inc. Duplication is permitted with written permission. Copyright © 2006 Advanced Subsonics Inc.

Instantaneous Results



Measuring Power Absorbed by Wings



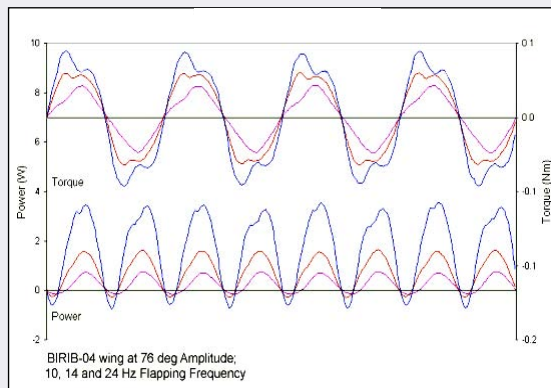
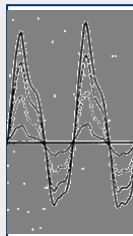
This presentation is property of Advanced Subsonics Inc. Duplication is permitted with written permission. Copyright © 2006 Advanced Subsonics Inc.

Instantaneous Results



Changes in Root Torque and Power Waveforms with Increasing Frequency

- Note broadening of torque waveform and development of a "double peak" as frequency increases
- This "double peak" is characteristic of unsteady phenomena such as dynamic stall delay
- Waveforms to the right represent the bending moment in the leading edge of a full-size ornithopter



This presentation is property of Advanced Subsonics Inc. Duplication is permitted with written permission. Copyright © 2006 Advanced Subsonics Inc.

Aside: Large Flapping Wings



First successful flight of C-GPTR on July 8, 2006

This presentation is property of Advanced Subsonics Inc. Duplication is permitted with written permission. Copyright © 2006 Advanced Subsonics Inc.

Flow Visualization: Wake



Computer controlled traverse



Hot-wire probe below wing set

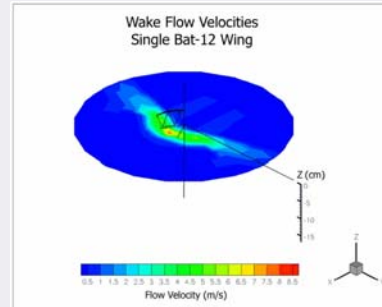
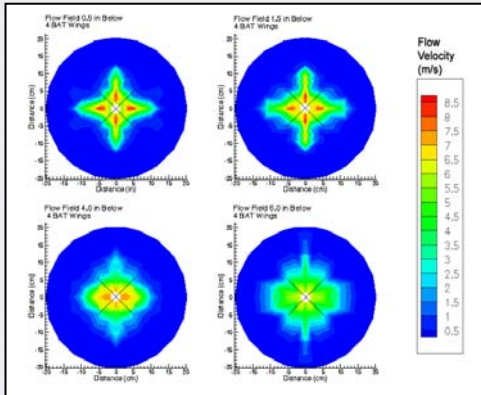
- Averaged velocity data was collected for a set of four BAT-12 wings at a wing beat frequency of 40 Hz
- The peak to peak flapping amplitude for each wing is 72 degrees
- The wing set produces approximately 50g of thrust under these conditions
- Each data point collected represents an average of 10,000 data samples at specific location
- Data was collected for a ninety degree quadrant at distances from 0 to 18 inches below the trailing edges of the wings

This presentation is property of Advanced Subsonics Inc. Duplication is permitted with written permission. Copyright © 2006 Advanced Subsonics Inc.

Flow Visualization: Wake



- Wake velocity measurements
 - Used hot wire anemometer
 - Examined single and four wing scenarios
 - Showed the high speed flow areas where symmetry negates momentum in non-useful direction

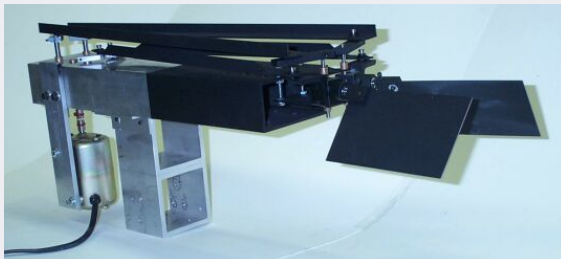


This presentation is property of Advanced Subsonics Inc. Duplication is permitted with written permission. Copyright © 2006 Advanced Subsonics Inc.

Flow Visualization: Smoke



- Flow Visualization Rig
 - Allows for flow quantification with all parameters precisely known (position, velocity, angle of attack)
 - Flapping and twisting driven actively
 - Aeroelastic deformation is eliminated in this test rig to facilitate more accurate measurements of relevant parameters
 - Fully adjustable flapping and twisting amplitude
 - Adjustable flapping/twisting phase relationship
 - With a force measurement capability, could be used to experimentally test wing with position and velocity known precisely

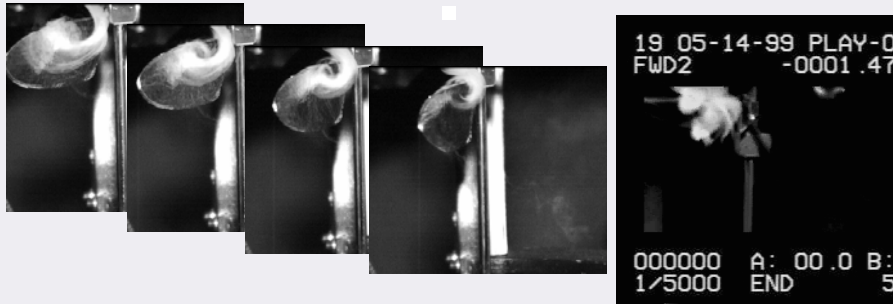


This presentation is property of Advanced Subsonics Inc. Duplication is permitted with written permission. Copyright © 2006 Advanced Subsonics Inc.

Flow Visualization: Smoke



- Flow-vis also done with smoke and actual wings
- We got a bit caught up in "vortex chasing"
 - Similar to those formed on delta-wings at high AOA, these are simply a feature of this thin wing lift mechanism
 - A robust phenomenon that affects the flow over the entire wing



This presentation is property of Advanced Subsonics Inc. Duplication is permitted with written permission. Copyright © 2006 Advanced Subsonics Inc.

Systems Considerations



- Road Map of System Considerations
 - efficiency
 - power supply
 - actuation methods
 - simulation
 - control system
 - wing design/manufacture
 - vehicle missions
 - control
 - performance metrics

This presentation is property of Advanced Subsonics Inc. Duplication is permitted with written permission. Copyright © 2006 Advanced Subsonics Inc.

Efficiency



• Comparing Aerodynamic Efficiency

Propeller efficiency equation is not valid in hovering since free stream velocity is zero

$$\eta_{\text{prop}} = \frac{TV}{P} \quad (1)$$

Helicopter hovering figure of merit uses induced velocity instead

$$M = \frac{TV}{P} \quad (2)$$

Equation (2) disguises the fact that induced velocity depends on thrust and disc area

$$V = \sqrt{\frac{T}{2A\rho}} \quad (3)$$

Because of this, vehicles with higher disk loadings have artificially higher figures of merit than vehicles with lower disk loadings.

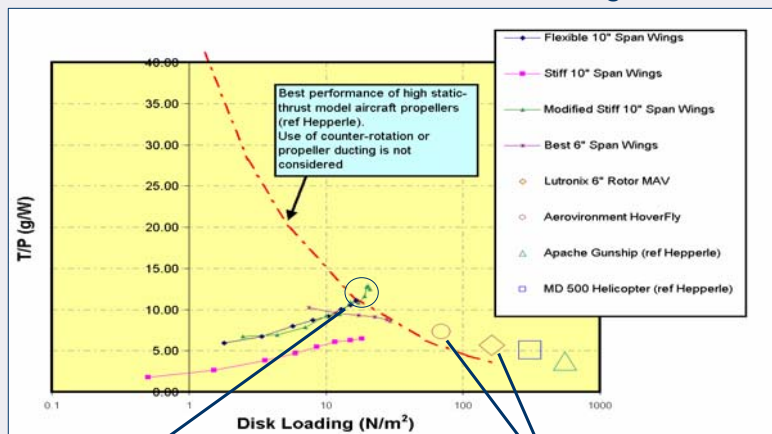
As a result, a better way to compare wing performance is to specify the thrust to power ratio for a given disc loading.

This presentation is property of Advanced Subsonics Inc. Duplication is permitted with written permission. Copyright © 2006 Advanced Subsonics Inc.

Efficiency



• The Bottom Line: T/P vs. Disk Loading



At their design point, our wings match the efficiency of propellers

Must consider disk loading when comparing efficiency to other hovering MAVs

This presentation is property of Advanced Subsonics Inc. Duplication is permitted with written permission. Copyright © 2006 Advanced Subsonics Inc.

Energy Sources



- Critical considerations:
 - Energy density (total energy per unit mass)
 - Power density (NiMH vs. NiCd)
 - Conversion efficiency (fuel to rotary motion or fuel to electricity)
 - Total system efficiency (rotary motion to oscillatory motion)
- Holistic approach needed
 - Wing and wing actuation designs must consider, from the outset, system efficiency

This presentation is property of Advanced Subsonics Inc. Duplication is permitted with written permission. Copyright © 2006 Advanced Subsonics Inc.

Energy Sources

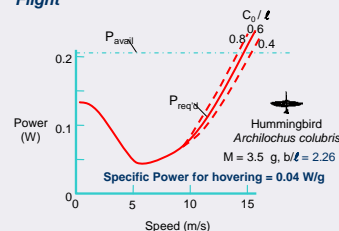


Energy Storage and Supply Limitations

- Biological creatures have good duration
 - Ruby-throated hummingbird crosses the Gulf of Mexico (30 hr flight)
- Fuel-burners are still the best but batteries are narrowing the gap
- Battery performance can be similar to biological energy storage
- Power density may also be an issue with many batteries

Primary Source	Specific Energy (MJ/kg)	Conversion Efficiency	System Specific Energy (MJ/kg)
Protein (e.g. meat)	4	10% (muscle)	0.4
Carbohydrates (e.g. honey)	15	10% (muscle)	1.5
Fat (e.g. vegetable oil)	36	10% (muscle)	3.6
Hydrocarbon Fuel (e.g. diesel, gasoline)	42	5 - 20% (engine, turbine or fuel cell/motor)	2.1 to 8.4
Rechargeable Battery (e.g. lithium metal)	0.5	20 to 80% (motor, piezo or electrostrictor)	0.1 to 0.4
Non-rechargeable Battery (e.g. lithium vinyl chloride)	2.4	20 to 80% (motor, piezo or EAP)	0.48 to 1.9

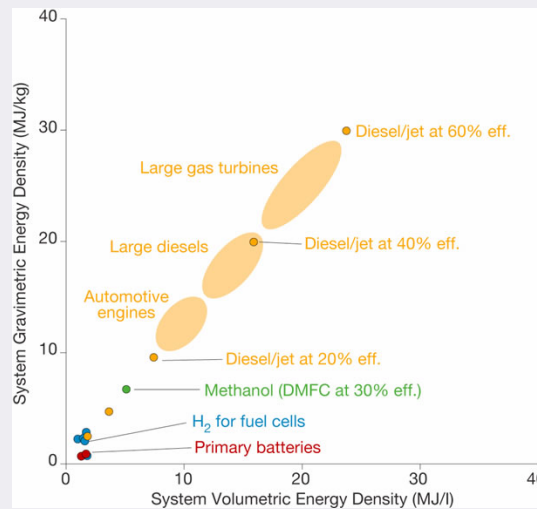
Source: H. Tennekes, *The Simple Science of Flight*



Source: R.J. Templin, "The Spectrum of Animal Flight", 1998

This presentation is property of Advanced Subsonics Inc. Duplication is permitted with written permission. Copyright © 2006 Advanced Subsonics Inc.

Energy Sources



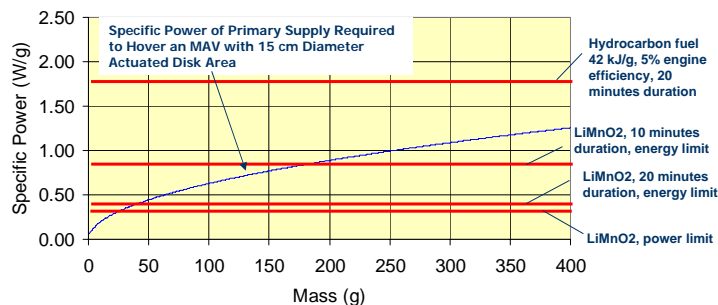
Source: Epstein, A.H., MIT

This presentation is property of Advanced Subsonics Inc. Duplication is permitted with written permission. Copyright © 2006 Advanced Subsonics Inc.

Energy Sources: Batteries



- Reasonable assumptions of FOM for wings show that MAV-sized vehicles can fly for useful durations on battery power
- 50 g represents a compromise where we can still fly a useful payload and have sufficient duration with quiet battery powered flight



Notes:

- 50% of electrical power is converted to mechanical work of wings
- 30% of mechanical work of wings goes into moving the air downward (Figure of Merit = 0.3)
- 50% of the total vehicle mass is the primary power supply (batteries or fuel)
- representative best off-the-shelf battery:
 - Tadrian
 - LiMnO₂, 17g, 800 mAh, 3V, 2A, 508 J/g, 0.35 W/g

This presentation is property of Advanced Subsonics Inc. Duplication is permitted with written permission. Copyright © 2006 Advanced Subsonics Inc.

Energy Sources: Batteries



- Battery development occurs in step-wise manner (difficult to predict too far into the future)
- One must be careful when extrapolating the performance of very small batteries
 - packaging concerns
 - electrode geometry and size
- Definition: Primary chemistries cannot be recharged; secondary can
- Common primary cells (not necessarily small sized):
 - $\text{LiSO}_2 = 170 \text{ Wh/kg}$
 - $\text{LiMnO}_2 = 290 \text{ Wh/kg}$
 - $\text{LiSOCl}_2 = 760 \text{ Wh/kg}$
 - Zn-air = 460 Wh/kg
 - Li-air (= 1000 Wh/kg in theory)
- Common secondary cells:
 - NiCd, NiMH, Li-ion,
 - Li-polymer = 150 Wh/kg

In all cases one must consider the drain rate. High drain rates substantially diminish capacity! Some batteries simply not capable of delivering required power.

This presentation is property of Advanced Subsonics Inc. Duplication is permitted with written permission. Copyright © 2006 Advanced Subsonics Inc.

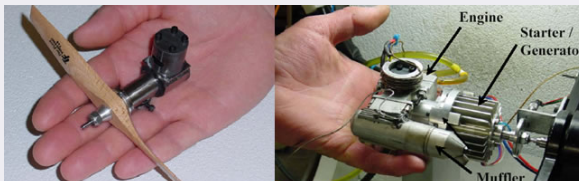
Energy Sources: Hydrocarbons



- The energy density of hydrocarbon fuel is exceptionally high
- Most common fuel at small size is methanol (glow fuel) though diesel has higher energy density and better availability to military user
- Even with low efficiency, IC engines at this size, overall energy density exceeds that of batteries
- Piston, rotary and turbine engines are in development



Source: M-Dot Aerospace (left), MIT (right)



Source: D-Star engineering



Source: UC Berkeley

This presentation is property of Advanced Subsonics Inc. Duplication is permitted with written permission. Copyright © 2006 Advanced Subsonics Inc.

Energy Sources: Fuel Cells



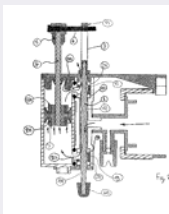
- Fuel cells convert fuel directly to electricity
- Commonly use hydrogen as the fuel (or hydrogen derived from hydrocarbons)
- As with batteries, as the size diminishes, proportionally more mass goes to packaging
- Currently, power density is the limiting factor

This presentation is property of Advanced Subsonics Inc. Duplication is permitted with written permission. Copyright © 2006 Advanced Subsonics Inc.

Energy Sources: Chemical



- Direct linear oscillatory motion from chemical energy is possible
 - Possible to construct a very simple actuation scheme that automatically produces linear oscillatory motion
- Could possibly exploit fuels with very high energy density
- External combustion
 - Solid fuels burning slowly to produce a supply of high pressure gas
- 'Chemical Muscles'
 - The CIA's dragonfly of the 1970s used nitric acid and lithium hydride as fuel. Vehicle was free flying



Source: Dr. Robert Michelson, Georgia Tech

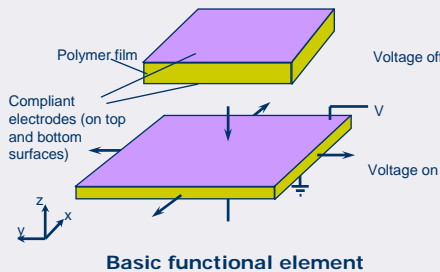
This presentation is property of Advanced Subsonics Inc. Duplication is permitted with written permission. Copyright © 2006 Advanced Subsonics Inc.

Actuation Methods: EPAMS



Principle of Operation of Dielectric Elastomer Actuators

- Focused on soft elastomeric polymers
- Polymer film is sandwiched between compliant electrodes and acts as a dielectric (insulator)
- The polymer shrinks in thickness and expands in area when a voltage is applied
- Response is dominated by electrostatic effects



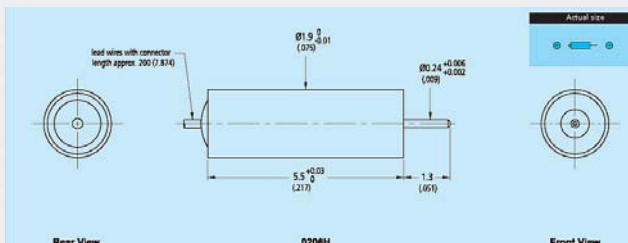
Video shows how a circular electroded area expands when the voltage is applied

This presentation is property of Advanced Subsonics Inc. Duplication is permitted with written permission. Copyright © 2006 Advanced Subsonics Inc.

Actuation Methods: Elec Motors



- Electric motors
 - brushed and brushless
 - brushed commercially available in diameters down to 1.9 mm
 - high performance brushless motors and controllers not yet available in sizes applicable to NAV
 - efficiencies of 5 – 20%
 - Often need additional gear heads to operate at peak efficiency and output at appropriate RPM



This presentation is property of Advanced Subsonics Inc. Duplication is permitted with written permission. Copyright © 2006 Advanced Subsonics Inc.

Actuation Methods: Elec Motors

- Ultrasonic motors
 - are piezoelectric rotary actuators
 - piezoceramic stator in sections that establish a standing wave causing a rotor to orbit due to friction
 - often no gearhead needed as torques higher and speeds lower
 - not easily commercially available in necessary sizes



Seiko's co-axial helicopter uses two proprietary ultrasonic motors



This presentation is property of Advanced Subsonics Inc. Duplication is permitted with written permission. Copyright © 2006 Advanced Subsonics Inc.

Resonance

- Resonance in the wings can **NOT** be exploited for efficiency
- Effective flapping-wing systems are highly damped
 - That is they put all available energy into the flow (damping is the useful work)
- Resonant aero-mechanical systems such as bridges, power-lines, and stop signs extract energy from the flow.
- Flapping wings impart energy to the flow. Any energy that is stored as 'resonance' is not going into the flow and therefore not helping you fly.

This presentation is property of Advanced Subsonics Inc. Duplication is permitted with written permission. Copyright © 2006 Advanced Subsonics Inc.

Free-Flight Vehicle



Free Flight Demonstrator



Free Flight Demonstrator

The first successful free flight of a mentor prototype was achieved with the model shown on the left.

Model Specifications:

Wing Model: BAT-13

Disk Area (Wing span): 6.75 in

Gross Vehicle mass: 40 g

Power Source: Four 3.3F 2.5 V capacitors in series charged to 14 V

Actuation: WesTechnik DC 5-2.4 coreless DC motor with modified Micro-Mo planetary gear head. (16:1) drive reduction.



This presentation is property of Advanced Subsonics Inc. Duplication is permitted with written permission. Copyright © 2006 Advanced Subsonics Inc.

Stability Derivatives



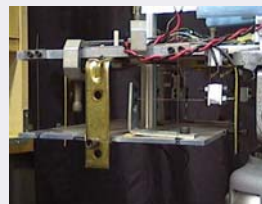
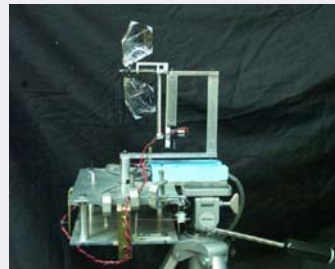
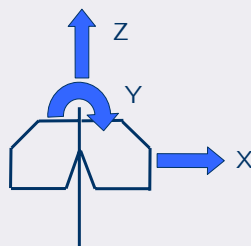
Experimental Evaluation of Vehicle Stability Characteristics

Purpose:

- supplement dynamic simulation with experimental data

Force Balance Design:

- 3 degree-of-freedom
 - X, Z forces
 - Y Moment

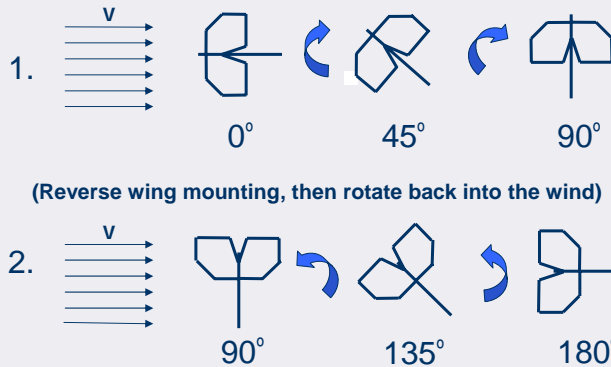


This presentation is property of Advanced Subsonics Inc. Duplication is permitted with written permission. Copyright © 2006 Advanced Subsonics Inc.

Stability Deriv: Test Procedure



- Variable advance ratios, J (ratio of free stream velocity to wing flapping speed)
- Attitudes from 0° - 180°
- Static forces and moments only



This presentation is property of Advanced Subsonics Inc. Duplication is permitted with written permission. Copyright © 2006 Advanced Subsonics Inc.

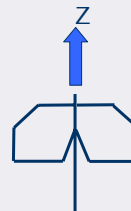
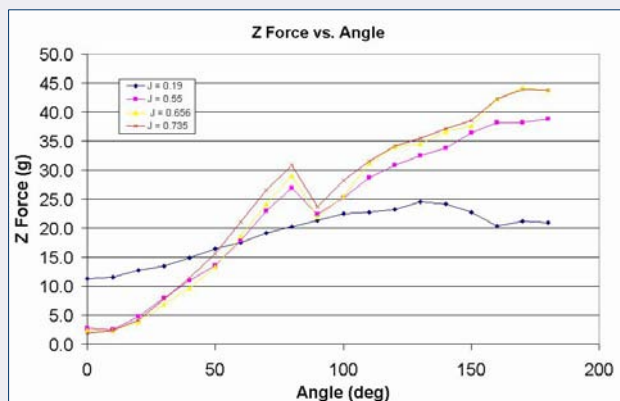
Stability Derivatives



Thrust vs. Alpha

(for various advance ratios)

- Jump in Z -force at 90° due to wing inversion and force balance interference effects
- Repeatability maintained

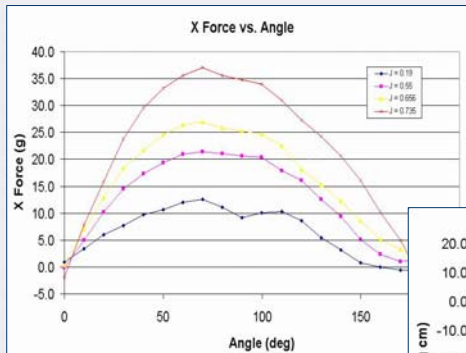


This presentation is property of Advanced Subsonics Inc. Duplication is permitted with written permission. Copyright © 2006 Advanced Subsonics Inc.

Stability Derivatives

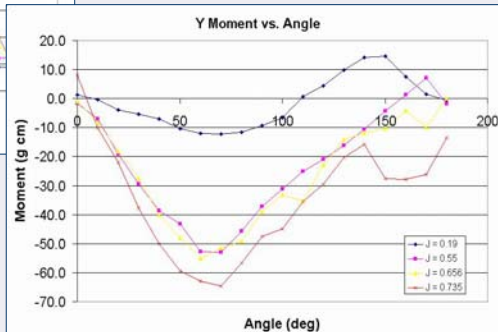


Lateral Force and Pitching Moment vs. Alpha (for various advance ratios)



Lateral force measurements
reveal anticipated trends

Pitching moment trends
vary with advance ratio



This presentation is property of Advanced Subsonics Inc. Duplication is permitted with written permission. Copyright © 2006 Advanced Subsonics Inc.

Flight Dynamic Simulation



Control and Stability Analysis/Simulation

• Approach

- Experimentally or analytically derived wing force and moment data
- Experimentally or analytically derived wing slipstream data
- Strip-theory for wing and tail damping and control moments
- Time marching algorithm
- Open-closed Tustin integrators for high real-time performance, high numerical stability, and acceptable accuracy
- User defined geometry and mass properties

This presentation is property of Advanced Subsonics Inc. Duplication is permitted with written permission. Copyright © 2006 Advanced Subsonics Inc.

Flight Dynamic Simulation



Simulation



Actual Flight



- SRI developed simulation
- Vehicle control system modeled at UTIAS (and added to Simulation)
- Accurately predicts vehicle behavior and allows proper selection of control coefficients and C.G. Location
- Allows for pilot practice
- Suggests routine for transition from hover to translational flight



This presentation is property of Advanced Subsonics Inc. Duplication is permitted with written permission. Copyright © 2006 Advanced Subsonics Inc.

Flight Dynamic Simulation



Simulation Predictions

Because of simulation's ability to accurately predict reasonable PID controller coefficients for all three axes, as well as an appropriate C.G. location, we have faith in its other predictions:

- 1) Predicts that our current vehicle can translate at up to 35 mph.
With current fuel tank, over 4 miles could be covered.
- 2) Predicts that rapid/violent maneuvers can be performed and vehicle will remain controllable.
- 3) Predicts that in translation, power could be reduced to approximately 80% percent of hover power, increasing endurance.

This presentation is property of Advanced Subsonics Inc. Duplication is permitted with written permission. Copyright © 2006 Advanced Subsonics Inc.

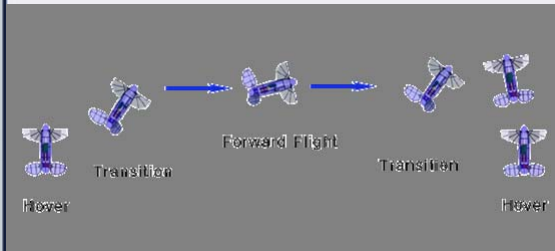
Simulation Application



Translation and Transition

Stability and Control in Forward Flight

- Flapping wings provide thrust and lift
- All moving fins automatically provide longitudinal dihedral for stability
- PID controller can easily compensate for lack of roll stability



Transitioning Between Flight Modes

- Flapping wings allow smooth transition from hover to forward flight
- Flight sim indicates that current vehicle configuration able to transition to/from hover

This presentation is property of Advanced Subsonics Inc. Duplication is permitted with written permission. Copyright © 2006 Advanced Subsonics Inc.

Simulation Application



- Simulation allowed the newer electric MENTOR to “fly right off the drawing board”



This presentation is property of Advanced Subsonics Inc. Duplication is permitted with written permission. Copyright © 2006 Advanced Subsonics Inc.

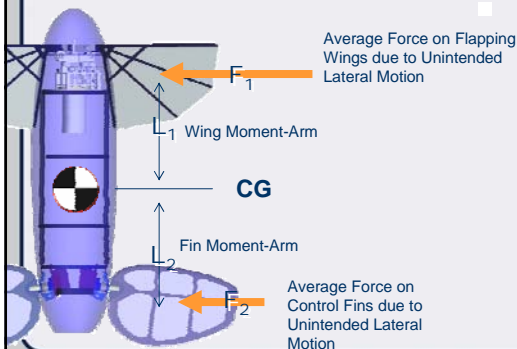
Simulation Application



Centre of Gravity Location

Vehicle controllability in hover highly sensitive to location of CG relative to thrust line.

Best longitudinal C.G location is one that decouples unintended lateral motions in hover from attitude changes.



- We choose a CG location so that:

$$F_1 \times L_1 = F_2 \times L_2$$

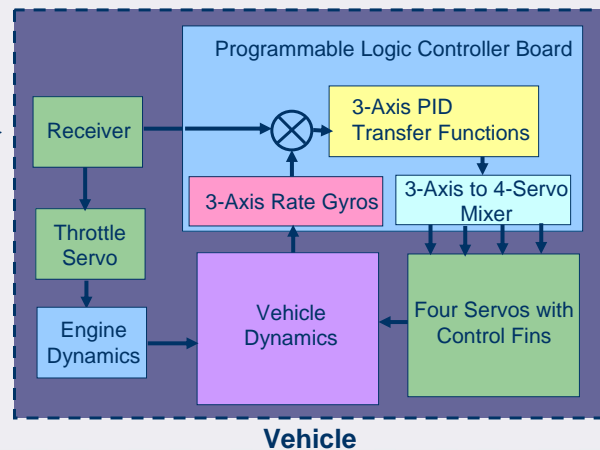
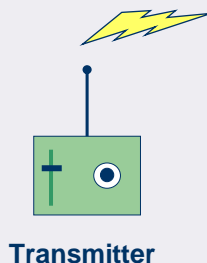
- Because of the dynamic behaviour of the flapping wings, the vehicle simulation was necessary for this task

This presentation is property of Advanced Subsonics Inc. Duplication is permitted with written permission. Copyright © 2006 Advanced Subsonics Inc.

Control System



- Sensor suite: 3-axis rate gyros, expandable to include 3-axis accelerometers and 3-axis magnetometers
- Provides greater flexibility in control algorithm than COTS systems
- SRI Simulation used extensively to guide control algorithm selection and PID coefficients



This presentation is property of Advanced Subsonics Inc. Duplication is permitted with written permission. Copyright © 2006 Advanced Subsonics Inc.

Vehicle: Wings



Design Features :

Aero-Elastically Tailored:

- Stiffness of spar elements custom tailored
- Wing deforms in response to aerodynamic loads
- Allows simple, 1 DOF kinematics



Rapid Manufacturing and Refinement:

- Wings can be batch processed for time effective manufacturing and consistency
- Constructed from multiple strips of carbon pre-preg
- Wing stiffness can be modified without re-tooling
- "Flat" wing is symmetric about vehicle centerline - no right or left-handed wings



Performance:

- Re Regime ~ 200,000
- Peak Thrust: 590 g @ 28 Hz
- Disk Loading (Hover): 54 N/m²
- Wing Loading (Translation): 92 N/m²
- T/P Ratio ~5.6 g/W

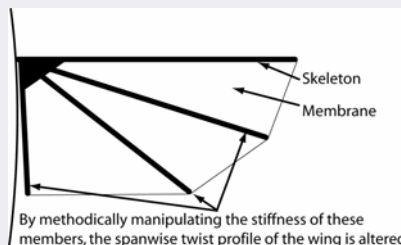
This presentation is property of Advanced Subsonics Inc. Duplication is permitted with written permission. Copyright © 2006 Advanced Subsonics Inc.

Vehicle: Wings



Summary and Lessons Learned

- Flexible, thin airfoil wings, with single DOF actuation can function efficiently and produce requisite thrust
- Clap-fling a useful thrust augmentation device
- Thin 'single surface' wings well suited to automated batch production
- Skeleton and membrane construction allows for straightforward spanwise tailoring of bending and torsional stiffness
- Skeleton and membrane construction allows for (necessary) highly non-linear torsional stiffness



This presentation is property of Advanced Subsonics Inc. Duplication is permitted with written permission. Copyright © 2006 Advanced Subsonics Inc.

Vehicle: Wings



- Summary and Lessons Learned (Continued)
- What are the dominant variables?
 - Pitch angle (as a function of span)
 - Flap amplitude with respect to chord length (especially when in proximity to other wings)
 - Phase relationship between pitch and plunge
 - Flapping frequency
- No large planform advantage
- Airfoil thickness profile not critical (very thin airfoil used)

This presentation is property of Advanced Subsonics Inc. Duplication is permitted with written permission. Copyright © 2006 Advanced Subsonics Inc.

Nano Air Vehicles: Utility



Current UAVs are too large to penetrate buildings to provide situational awareness



**Reconnaissance inside buildings
Ability to breach interiors
Emplace important sensors
Transmitt data without being detected**

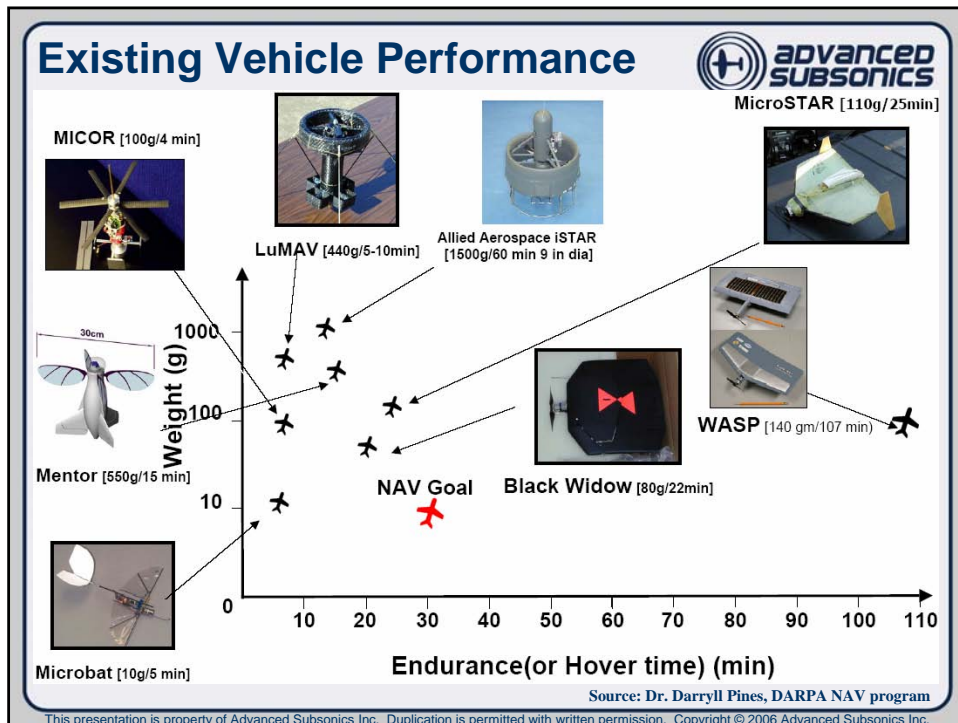
Nano Air Vehicle Definition:
Mass < 10 grams
Wingspan < 7.5 cm
Forward Speed = 3 to 7 m/sec




Need a nano scale vehicle to quietly penetrate and navigate inside buildings to obtain timely and important reconnaissance information

Source: Dr. Darryll Pines, DARPA NAV program

This presentation is property of Advanced Subsonics Inc. Duplication is permitted with written permission. Copyright © 2006 Advanced Subsonics Inc.



NAV: Candidate Missions



Mission 1: DARPA NAV Program mission requirements

- 10g max GTOW with 2g payload (inclusive)
- <7.5 cm maximum dimension
- 1000m range at 7-10 m/s
- 60 sec of flight at low speed (~0.5m/s)
- 60 sec of hovering flight
- Controlled placement at landing from hover
- Communications, navigation and sensors must function indoors
- Return capable
- Mission duration: 20 –30 minutes

This presentation is property of Advanced Subsonics Inc. Duplication is permitted with written permission. Copyright © 2006 Advanced Subsonics Inc.

NAV: Candidate Missions



Mission 2: Outdoor urban perch and stare

- 10g max GTOW with 2g payload (inclusive)
- <7.5 cm maximum dimension
- 5 minutes of hovering flight outdoors
- Outdoor perch and release capability
- Mission duration (sensor function): 1-2 hours

This presentation is property of Advanced Subsonics Inc. Duplication is permitted with written permission. Copyright © 2006 Advanced Subsonics Inc.

NAV: Vehicle considerations



- The following mass breakdown was used recently in the DARPA NAV program:
 - Energy supply (batteries) 4.9 g = 49%
 - Avionics 2.0 g = 20%
 - Structure 1.1 g = 11%
 - Payload 2.0 g = 20%
- Note that the structural weight is small component of overall weight. (Favours simple actuation schemes)
- For comparison, consider the hummingbird:
 - wingspan = 9.5 cm (25% more wingspan)
 - mass = 3.5 to 4.0 g (60% less mass)

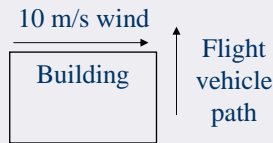
This presentation is property of Advanced Subsonics Inc. Duplication is permitted with written permission. Copyright © 2006 Advanced Subsonics Inc.

NAV: Control Schemes



Wind Considerations and Reaction Time

Example: Moving around a building on windy day



Case 1: Full-Size Helicopter with 10m rotor, 3000 kg mass (that is, almost 30,000 N force in hover)

downwash speed from rotors = 12.5 m/s

drag force in 10 m/s wind (estimated) = 300 N

Therefore, to maintain slow hovering flight path, force vector must change by approximately $\arctan(300/30,000) = 0.6$ degrees

Reaction time to limit downwind drift to: 0.5 m = 3.2 seconds
1 rotor diameter = 14 seconds

Case 2: Piccolo helicopter with 0.5 m rotor, 300 grams mass (almost 3 N force in hover)

downwash speed from rotors = 2.5 m/s

drag force in 10 m/s wind (estimated) = 0.6 N

Therefore, to maintain slow hovering flight path, force vector must change by approximately $\arctan(0.6/3) = 11.3$ degrees

Reaction time to limit downwind drift to: 0.5 m = 0.7 seconds
1 rotor diameter = 0.7 seconds



Seiko Epson MFR
10g, < 6in.

Case 3: Dragonfly-size vehicle with 0.1 m rotor, 5 grams mass (almost 0.05 N force in hover)

downwash speed from rotors = 1.6 m/s

drag force in 10 m/s wind (estimated) = 0.18 N

Therefore, to maintain slow hovering flight path, force vector must change by approximately $\arctan(0.18/0.05) = 74.5$ degrees

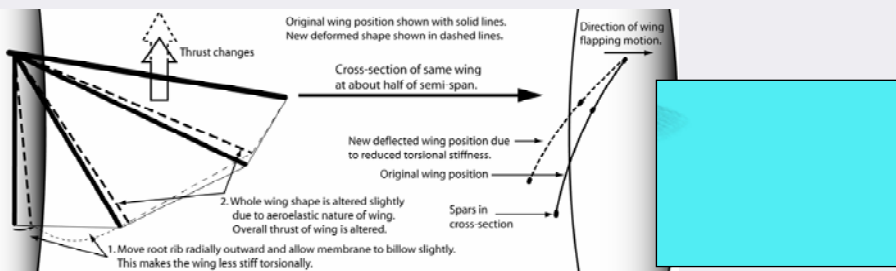
Reaction time to limit downwind drift to: 0.5 m = 0.17 seconds
1 rotor diameter = 0.075 seconds

This presentation is property of Advanced Subsonics Inc. Duplication is permitted with written permission. Copyright © 2006 Advanced Subsonics Inc.

NAV: Control Schemes



- The previous slide shows that at small sizes, the time constant becomes small
 - Reaction times must be fast (affects control system and sensors)
 - Application of control forces must be fast and effective
 - Mass budget also means that control actuators must be very light
- These constraints favour the generation of control forces using the wings with simple and light-weight actuators
 - Actuators need not respond at the rate of wing frequency
- Candidate actuators include:
 - shape memory alloys
 - pressure (byproduct of some candidate energy sources)



This presentation is property of Advanced Subsonics Inc. Duplication is permitted with written permission. Copyright © 2006 Advanced Subsonics Inc.

NAV: On-board Electronics



- Moore's Law has consistently predicted advances in semiconductor performance
 - These advances suggest that avionics electronics not likely to be the bottleneck in NAV development
 - Even sensors (accelerometers and gyros) are at useful sizes already
- Challenges likely to be:
 - Communications (power and line-of-sight requirements)
 - Navigation (GPS denied indoors)
 - Electronics integration

This presentation is property of Advanced Subsonics Inc. Duplication is permitted with written permission. Copyright © 2006 Advanced Subsonics Inc.

NAV: On-board Electronics



- Mass ~ 2 g
- Navigation/Control Solution could employ (at minimum):
 - 80x60 monochrome imager with 10 frames/sec rate
 - self stabilized using MEMS accelerometers and gyros with approx 5 kHz control loop (MENTOR used 1 kHz)
 - directed to objective by operator using visual feedback
 - collision avoidance assisted by optical flow



This presentation is property of Advanced Subsonics Inc. Duplication is permitted with written permission. Copyright © 2006 Advanced Subsonics Inc.

Definition of Metrics



- For reasons given previously, the Thrust to Power Ratio is proposed as the appropriate measure of hover efficiency.
 - T/P is a 'real world' number that relates directly to vehicle development
- It is suggested that a T/P=10 g/W (measured at the wings) be used as a starting target for wing development.
 - Note that Froude actuator disk theory gives $P_{req\ min} = 0.3\ W$.
 - The goal thrust to power ratio is about three times larger than the theoretical ideal.

$$P = \sqrt{\frac{T^3}{2\rho A}} = \sqrt{\frac{(0.1N)^3}{2(1.225kg/m^3)(0.0044m^3)}} = 0.3W$$

- For comparison, consider these vehicles:
 - MENTOR disk loading = 49 N/m²; T/P ~ 8 - 10 g/W
 - MICOR disk loading = 55 N/m²; T/P ~ 12 g/W
 - NAV disk loading = 22 N/m²; T/P ~ 10 g/W



This presentation is property of Advanced Subsonics Inc. Duplication is permitted with written permission. Copyright © 2006 Advanced Subsonics Inc.

Definition of Metrics



- Consider what this means for a representative vehicle and Sample Mission 2

- Power required at battery: $P_{battery} = \frac{m_{vehicle}}{\left(\frac{m}{P}\right)_{wings} * \eta_{mechanical} * \eta_{motor}} = \frac{10g}{(10g/W) * 0.7 * 0.2} = 7.14W$
- Capacity of a Li-ion battery: $C_{battery} = 170Wh/kg$
- Duration in a hover (assumes additional other power requirements such as communications, avionics, payload add 30%):

$$t = \frac{C_{battery} * m_{battery}}{P_{req,battery}} = \frac{170Wh/kg * .0049kg}{7.14\ W * 1.3} = 5.4\ minutes$$

This presentation is property of Advanced Subsonics Inc. Duplication is permitted with written permission. Copyright © 2006 Advanced Subsonics Inc.

Possible Pitfalls



- Shotgun approach
 - A very large test matrix with many variable parameters is inefficient and historically an ineffective way to develop wings
 - CFD and Experiment must run identical cases and the earlier the better
- Inconsistent metrics
- Resonance
 - Resonance in the wings can **NOT** be exploited for efficiency
 - Effective flapping-wing systems are highly damped
 - That is they put all available energy into the flow (damping is the useful work)
 - Resonant aero-mechanical systems such as bridges, power-lines, and stop signs extract energy from the flow.
 - Flapping wings impart energy to the flow. Any energy that is stored as 'resonance' is not going into the flow and therefore not helping you fly.

This presentation is property of Advanced Subsonics Inc. Duplication is permitted with written permission. Copyright © 2006 Advanced Subsonics Inc.

Program Opportunities



1. Develop an accurate 3D CFD model of low Re wings operating in proximity
2. Verify CFD with experimental results
 - CFD and experiments must test the exact same case and the earlier the better
 - Focus on critical variables ■
 - Test case should reflect realistic wing loading and flapping frequency
3. Eventually integrate an aeroelastic model with aerodynamic model for a comprehensive design tool

This presentation is property of Advanced Subsonics Inc. Duplication is permitted with written permission. Copyright © 2006 Advanced Subsonics Inc.

Conclusion



Thank you

Discussion/Questions?



Patrick Zdunich
patrick@advancedsubsonics.com
905.760.5556

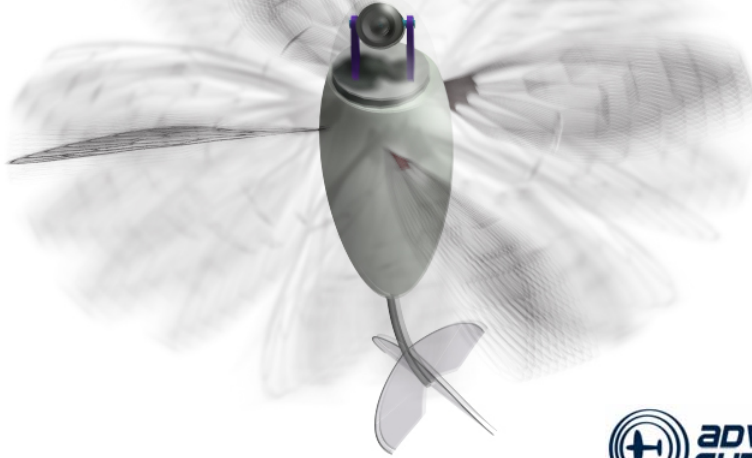
This presentation is property of Advanced Subsonics Inc. Duplication is permitted with written permission. Copyright © 2006 Advanced Subsonics Inc.

This page intentionally left blank.

Annex 2 - Highlights of systems considerations for flapping-wing NAV – April 2007

This page intentionally left blank.

Highlights of Systems Considerations for Flapping-Wing NAV



Aero-NAV Program Review



Advanced Subsonics' Tasks:

- To provide guidance based on past work, and systems level considerations
- Work was front loaded to best benefit the team
 - Kick-off presentation presented comprehensive summary of the successful Mentor hovering flapping-wing vehicle and 4 year research program
 - Standard test case described for CFD and experimental work
 - Presented a starting point for consistent definitions and terminology
 - Representative NAV geometry and performance extrapolated
 - Test case geometry and kinematics developed to model said NAV
 - Suitable test case constructed for NRC experimental facility

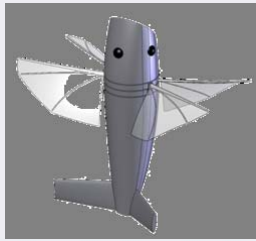


This presentation is property of Advanced Subsonics Inc. Duplication is permitted with written permission. Copyright © 2006 Advanced Subsonics Inc.

Aero-NAV Program Review



- Report describing systems-level considerations that drive aerodynamic research prepared
 - Presented at mid-project meeting
 - Described sample military missions for NAV and resulting broad performance requirements
 - Described current state of necessary complementary technologies such as energy storage, energy conversion, micro-electronics, control actuators, etc.
 - Extrapolated NAV performance goals for aerodynamic research
 - Estimated control force requirements and effect of aerodynamic design
 - Described a notional representative system concept



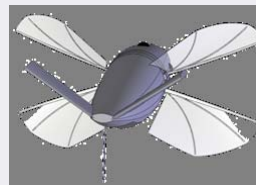
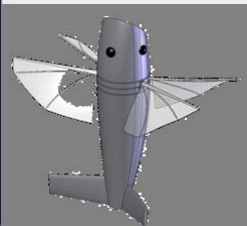
This presentation is property of Advanced Subsonics Inc. Duplication is permitted with written permission. Copyright © 2006 Advanced Subsonics Inc.

NAV Target System: Geometry



Geometry:

- 4 wing "Double-Hummingbird" X-wing configuration
- Capable of hover and fast translational flight
- Single DOF root-flapping actuation
- Very thin flat wings
- Aeroelastic tailoring gives camber and span dependent twist
- Span: 7.5 cm
- Chord: ~2 cm
- Root flapping angle nominally 75 degrees



This presentation is property of Advanced Subsonics Inc. Duplication is permitted with written permission. Copyright © 2006 Advanced Subsonics Inc.

NAV Target System: Clap-Fling



Advantages to configuration:

- Exploits the clap-fling phenomenon
 - Improved thrust to power ratio (already verified up to 40%)
 - Offers very high thrust in limited disk area (high disk loading)



- Single DOF actuation
 - Flapping mechanism need not be overly complicated = heavy and fragile
 - Wings aeroelastically tailored: have appropriate camber and twist in both directions
- Wings easy to manufacture



This presentation is property of Advanced Subsonics Inc. Duplication is permitted with written permission. Copyright © 2006 Advanced Subsonics Inc.

NAV Target System: Performance



Vehicle Parameters:

mass (m)	10 g = 0.01 kg
weight (W) = thrust (T)	~0.1 N
span (b)	7.5 cm = 0.075 m
semi-span (b/2)	3.75 cm = 0.0375 m
chord (c)	0.019 m
frequency (f)	80 Hz (best estimate of req'd freq)
peak plunge amplitude angle (γ)	75 deg (= 1.31 rad)
disk area (A)	$= \pi^2 = \pi(0.0375\text{m})^2 = 0.00418\text{m}^2$
disk loading (T/A)	23.9 N/m ²

Performance Targets

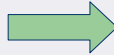
- Systems considerations dictate the following targets:
 - Thrust = 0.1 N total (0.1N/4 per wing)
 - Thrust to Power = 16 g/W (wings only)
 - Figure of Merit = 0.5 (50% Conversion efficiency to thrust power)
 - At this efficiency, expect an average of 0.6 W (input at wings) to drive wings

This presentation is property of Advanced Subsonics Inc. Duplication is permitted with written permission. Copyright © 2006 Advanced Subsonics Inc.

NAV Target System: Control



- Goal: generate all control forces using wings alone
 - more maneuverable
 - less susceptible to changes in induced velocity (descent and gusts)



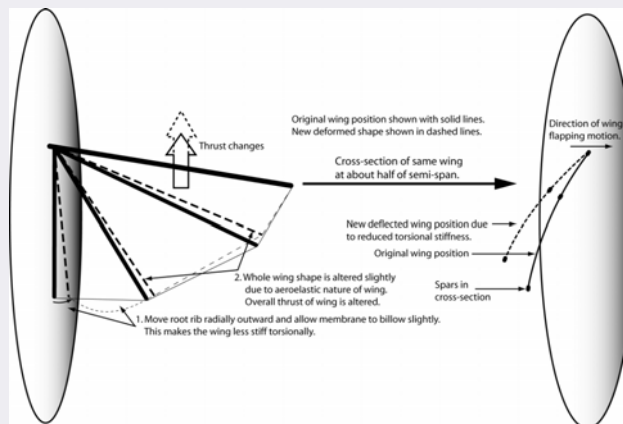
- Keep representative NAV within 20 cm of prescribed path
 - Need to alter thrust by only 5% per wing
 - Must achieve control force within about 0.1 to 0.2 seconds (8 to 16 flaps)
 - Based on gusts of nearly double the induced velocity

This presentation is property of Advanced Subsonics Inc. Duplication is permitted with written permission. Copyright © 2006 Advanced Subsonics Inc.

NAV Target System: Control



- Difficult to manipulate the large scale wing flapping motion on a per-wing basis
- Instead, make small changes to wing to affect thrust production
 - Sweep
 - Root twist angle
 - Stiffness change
 - Skeleton
 - Membrane



This presentation is property of Advanced Subsonics Inc. Duplication is permitted with written permission. Copyright © 2006 Advanced Subsonics Inc.

Non-dimensionalization



- Traditional method of non-dimensionalization not suited to flapping-wing vehicles (Especially in a hover)

$$L = \frac{1}{2} \rho V^2 C_L S \quad T = \frac{1}{2} \rho V^2 C_T S$$

- Force (and moment) not just functions of freestream velocity
- At low advance ratios (low reduced frequencies) force production dependent mainly, or only, on flapping frequency and therefore wing speed:

	Θ	H/c	St	f	V_∞	$(\bar{C}_T)_{V_\infty}$	$(\bar{C}_T)_{V_{plunge}}$	$(\bar{C}_T)_{V_{fp}}$
Case 1	50 deg	0.75	1	7 Hz	10.5 m/s	4.2	0.85	0.57
Case 2	50 deg	0.75	1	7 Hz	15 m/s	1.9	0.79	0.53
Case 3	50 deg	0.75	1	10 Hz	15 m/s	3.9	0.79	0.53

- Instead use the mean square plunge speed:

$$(\bar{V}_{plunge})^2 = \frac{(V_{plunge})_{min}^2 + (V_{plunge})_{max}^2}{2} = \frac{0^2 + (2\pi fH)^2}{2} = 2(\pi fH)^2$$

This presentation is property of Advanced Subsonics Inc. Duplication is permitted with written permission. Copyright © 2006 Advanced Subsonics Inc.

Non-dimensionalization



- This is similar to how Reynolds number was defined as a function of flapping frequency rather than freestream velocity:

$$Re_f = \frac{2\pi H f c}{\nu}$$

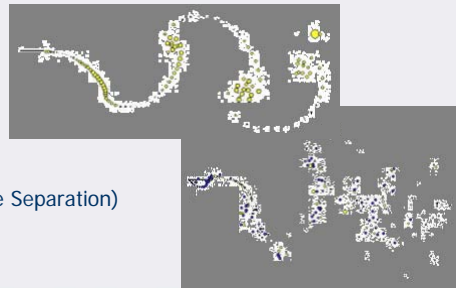
- If freestream velocity is on the order of wing flapping speed, some combination of the two velocities is appropriate.
- Can alternately present dimensional results
 - Gives immediate intuitive understanding of results
 - Easy to compare to identical experimental results
 - Not suitable to compare performance between cases

This presentation is property of Advanced Subsonics Inc. Duplication is permitted with written permission. Copyright © 2006 Advanced Subsonics Inc.

TIF - Engineering Model



- 3D Engineering model to be based on an existing 2D model:
 - Discrete vortex thin airfoil
 - Time marching
 - Arbitrary unsteady motion
 - Models separated flow by imposing Kutta condition(s)
 - Low advance ratio to hover
- Model is linear and fast
 - Models the necessary and dominant flow characteristics
 - Allows variables of interest to be modified rapidly
- Simple Case:
 - Low maximum angle of attack
 - No flow separation
- Complex Case:
 - High maximum angle of attack
 - Models dynamic stall (Leading Edge Separation)



This presentation is property of Advanced Subsonics Inc. Duplication is permitted with written permission. Copyright © 2006 Advanced Subsonics Inc.

Unsteady Aerodynamic Model



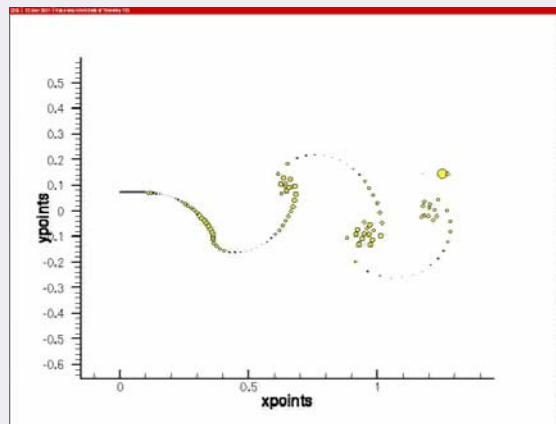
Simple Case: Unsteady, Discrete Vortex Trailing Edge (TE) Wake

Utilizes:

- Discrete wake elements to model continuous sheet of TE wake vorticity
- Fully interactive wake

Boundary Conditions:

- Flow tangency at airfoil (Kutta condition at TE)
- Conservation of vorticity (Change in bound vorticity between time steps is shed into wake)



This presentation is property of Advanced Subsonics Inc. Duplication is permitted with written permission. Copyright © 2006 Advanced Subsonics Inc.

Unsteady Aerodynamic Model



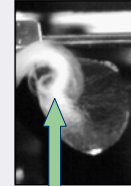
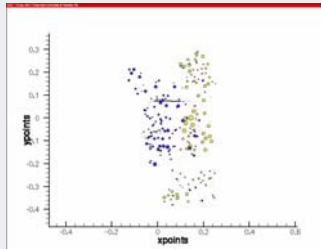
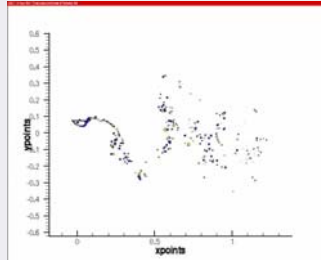
Separated, Unsteady, High AOA Flows (Low advance ratios)
Discrete Vortex Leading Edge (LE) and Trailing Edge (TE) Wake

Utilizes:

- Discrete vortex elements and control points to model bound circulation
- Discrete wake elements to model continuous sheet of LE and TE wake vorticity
- Fully flexible wake
- Linear approximation of Kutta condition yields a linear system of equations at each time step (Solves easily and quickly)

Boundary Conditions:

- Flow tangency (Kutta condition at LE and TE)
- Conservation of vorticity



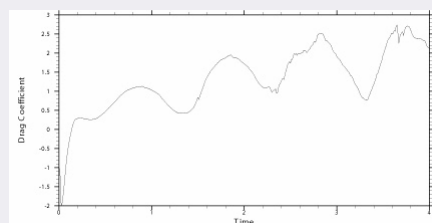
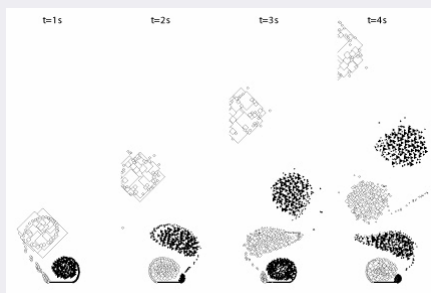
Smoke in flow shows LEV

This presentation is property of Advanced Subsonics Inc. Duplication is permitted with written permission. Copyright © 2006 Advanced Subsonics Inc.

Unsteady Aerodynamic Model



- Applicability and Test Cases
 - Flat plate in normal flow
 - Flow features representative of flow about flapping wings (large scale, unsteady separation)
 - Here drag is analogous to thrust
 - Under predicts drag by 8%

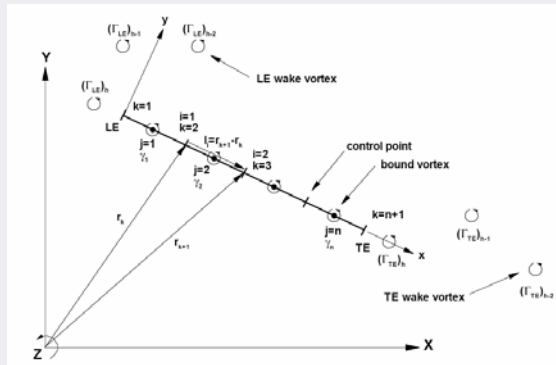


This presentation is property of Advanced Subsonics Inc. Duplication is permitted with written permission. Copyright © 2006 Advanced Subsonics Inc.

TIF - Engineering Model



- Step 1:
 - Original 2D model
 - Vortices modeled as infinite vortex strands (into page)
 - Compare to 2D experimental results

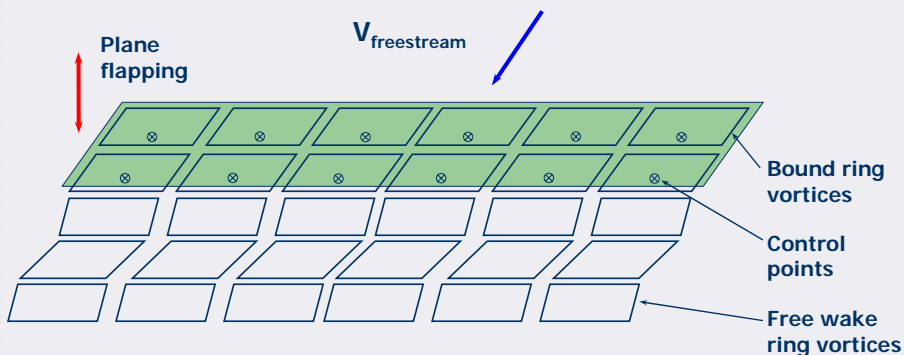


This presentation is property of Advanced Subsonics Inc. Duplication is permitted with written permission. Copyright © 2006 Advanced Subsonics Inc.

TIF - Engineering Model



- Step 2:
 - Adapt 2D infinite vortices to 2D ring vortices
 - High AR wing to mimic 2D flow
 - Compare against previous model and experimental results

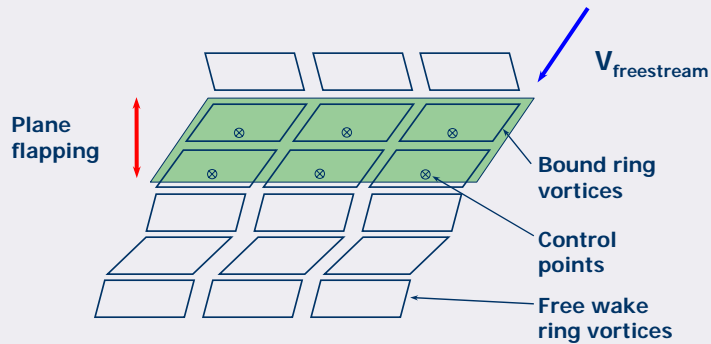


This presentation is property of Advanced Subsonics Inc. Duplication is permitted with written permission. Copyright © 2006 Advanced Subsonics Inc.

TIF - Engineering Model



- Step 3:
 - Migrate 2D ring vortex model to 3D
 - Plane flapping first (as in 2D case)
 - Low AR wing
 - Compare to experimental results

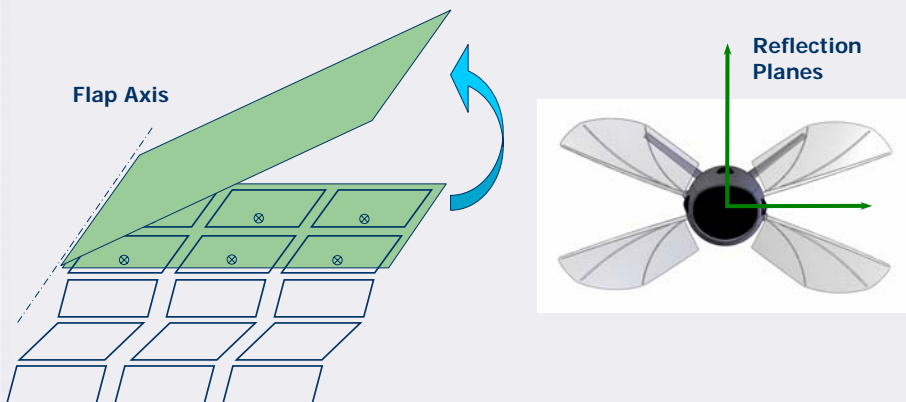


This presentation is property of Advanced Subsonics Inc. Duplication is permitted with written permission. Copyright © 2006 Advanced Subsonics Inc.

TIF - Engineering Model



- Step 4:
 - Add root flapping (as in NAV concept)
 - Add two reflection planes to model 4 wing clap-fling design



This presentation is property of Advanced Subsonics Inc. Duplication is permitted with written permission. Copyright © 2006 Advanced Subsonics Inc.

This page intentionally left blank.

Annex 3 – CFD 2007 Conference paper; June 2007

This page intentionally left blank.

Model Comparison of Viscous Flow over a Pitching and Plunging Wing for Nano-Air Vehicles

Nicolas Hamel ¹ and François Lesage ¹

¹*Precision Weapons Section, Defence Research & Development Canada – Valcartier
Quebec City, QC, G3J 1X5, Canada*

Email: *nicolas.hamel@drdc-rddc.gc.ca*

ABSTRACT

This study of the aerodynamics of flapping airfoil compares different viscous models available in Fluent. Two different nano-air vehicle (NAV) flapping-wing shapes were studied in 2-D, a flat plate and a NACA 0005. The same motion was applied both. To simulate the airfoil motion, a completely structured grid was generated. The laminar, k- ω SST, DES with Spalart-Almaras and LES viscous models were compared quantitatively in terms of convergence speed and drag/propulsion force coefficient, and qualitatively, by comparing contour plots of vorticity magnitude. To estimate the forces generated by a plunging and pitching flat plate airfoil, the laminar viscous model seems to be sufficient. On the other hand, to consider the vortices shed by the airfoil and interacting with the NAV airframe, the LES viscous model should be used.

1. INTRODUCTION

The development and acquisition of a new class of military system known as a Nano Air Vehicle (NAV) is possible in a not so distant future as a result of technological progress in a number of areas such as aerodynamics, micro-electronics, sensors, micro-electromechanical systems (MEMS) and micro-manufacturing. A NAV, according to DARPA's definition, will be smaller than 7.5 cm and will weigh less than 10 grams. The potential of NAVs opens up new possibilities in the formulation of military strategies with respect to information superiority in urban operations. It is expected that their main attributes will be low cost, low weight, little to no

logistical footprint, mission versatility, low visibility, covertness and precision.

Their distinct flight envelope will include hover, perching, and other high agility manoeuvres in order to perform their missions. The real mission niche for these insect-size aircraft may well be in the indoor setting where there is currently no reconnaissance asset available for military use. Fixed wing solutions are immediately discounted because they require either high forward speed or large wings. The alternative is a method of creating circulation over the wings in the absence of fuselage translation. This movement can be a circular motion as in a rotorcraft or it can be a reciprocating motion as in a flapping wing. There is strong evidence that for very small crafts (less than 5 cm), flapping-wing performance is superior to rotors due to dynamic effects that create much higher average lift coefficients at low Reynolds numbers.

The flapping wing aerodynamics, such as leading-edge vortex, dynamic stall and wake capture, are very complex and not yet fully understood. The technical difficulties relate to the complex unsteady motion required to produce high lift and the low Reynolds number of flow. DRDC has initiated an effort seeking to develop the aerodynamic tools for understanding the issues for the motion representative of insect wing beat kinematics.

2. THE AIRFOIL'S SHAPES AND MOTION

The airfoil studied should be as thin as possible to approximate an insect wing. Two different airfoil shapes were chosen. The first one is a flat plate with

a thickness of 5% of the cord. It has equilateral triangle shaped leading and trailing edges (Figure 1-a). The second airfoil is a NACA 0005 (Figure 1-b).

The same motion was studied for both airfoils. The wings were considered to have an infinite span and to be undergoing only pitching and plunging motion. The point about which the airfoils pitch is the leading edge. The plunging (V_{plunge}) and pitching (ω) velocities of the airfoils are given by equations 1 and 2.

The airfoil is also facing a constant uniform free-stream velocity in the direction perpendicular to the plunging velocity.

$$V_{\text{plunge}} = 2\pi f H \cos(2\pi f t + \delta) \quad (\text{eq. 1})$$

$$\omega = 2\pi f \Theta \cos(2\pi f t) \quad (\text{eq. 2})$$

Where: t is the time in second

f is the flapping frequency in Hz

Θ is the pitching amplitude in radian

H is the plunge amplitude in meter.

δ is the phase angle shift between the pitching and plunging phase in radian.

The target NAV for the project has a span of 7.5 cm, a chord of 1.9 cm and weighs 10 gram. It has four wings. For the NAV to hover the wings must generate 0.1 N of thrust. Based on preliminary estimates, a two-dimensional wing motion (frequency and amplitude) was defined (Table 1).

The Reynolds number based on the freestream velocity and airfoil chord is given by the equation 3.

$$\text{Re} = \frac{V_{\infty} c}{\nu} \quad (\text{eq. 3})$$

Since the speed of the airfoil is not negligible compared to the freestream velocity, the Reynolds number should be based on the maximum airfoil speed (eq. 4).

$$\text{Re}_f = \frac{2\pi H f c}{\nu} \quad (\text{eq. 4})$$

Based on eq. 4, the Reynolds number is 12 000 compared to 3 800 using eq. 3.

The reduced frequency (k) is commonly used to describe the wing motion and is defined as follows:

$$k = \frac{\pi f c}{V_{\infty}} \quad (\text{eq. 5})$$

The reduce frequency for the motion described is $k=1.6$.

Since the project involves experiments in a water tunnel, a motion representative of the NAV flight in the water tunnel was also defined. Using eqs. 4 and 5 with $\text{Re}_f=12\ 000$, $k=1.6$ and $H=c$, the motion of a wing in the water tunnel (Table 1) was defined. It is this motion that was studied using CFD.

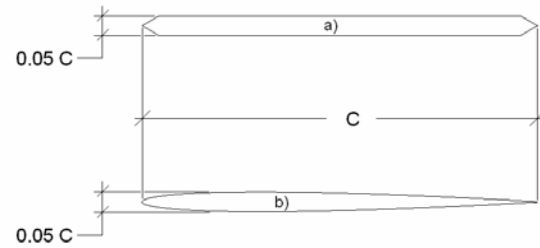


Figure 1: Shapes of the airfoils

Variable	Symbol	Value (air)	Value (water)
Frequency	f	80 Hz	1.3 Hz
Plunge amplitude	H	0.0184 m	0.0375 m
Pitch amplitude	Θ	50 deg = 0.87 rad	50 deg = 0.87 rad
Phase angle shift	δ	90 deg = 1.57 rad	90 deg = 1.57 rad
Airfoil chord	c	0.019 m	0.0375 m
Airfoil max thickness	d	0.95 mm	1.87 mm
Freestream velocity	V_{∞}	3.0 m/s	0.1 m/s
Kinematic viscosity	ν	1.51 e-5 m ² /s	1.004 e-6 m ² /s
Density	ρ	1.225 kg/m ³	998.2 kg/m ³

Table 1: airfoil motion and freestream conditions

3. CFD CODE DESCRIPTION

Unsteady simulations of the flow field were made using the commercial CFD code Fluent (version 6.3) [1]. The implicit, incompressible, structured mesh solver was used in 2-D. In Fluent, the user is able to

deform the grid by the use of user defined functions (UDF).

Fluent includes many viscous models, from the simplest laminar model to LES passing by many two-equation models. This study of the aerodynamics of flapping airfoils compares the results obtained with the laminar, k- ω SST, DES with Spalart-Allmaras and LES viscous models. The quantitative comparison is in terms of convergence speed and drag/propulsion force coefficient, and the qualitative comparison is using contour plots of vorticity magnitude.

3.1 Mesh motion technique

To simulate the airfoils' motion, a completely structured grid was generated. The emphasis was put on the region around the airfoil studied. The grid was organized in the way that the airfoil motion does not deform the grid in the surrounding area of the airfoil. To do so, a non-deforming area was shaped around the airfoil. This area had a diameter of 10 airfoil chords. The region surrounding the airfoil is showed in red in Figure 2. All the nodes in this area have the same motion, pitching and heaving as the airfoil. The grid stays the same for all time steps. To generate the motion, grid options "rigid body motion" and "non-conformal interface" were used in Fluent. To complete the airfoil motion, two other grid components were used. Figure 3 shows all mesh components. The green part is the heaving-only section, and the mesh motion is described only by an up and down motion of the grid with no pitching. Consequently, the "layering" grid motion type with a split and collapse factor of 0.2 and 0.4 respectively was used. Layering is for applications involving linear motions. Layers of mesh are added or deleted at the boundary of the grid to satisfy the split and collapse conditions. The purple region is the non-moving part of the mesh.

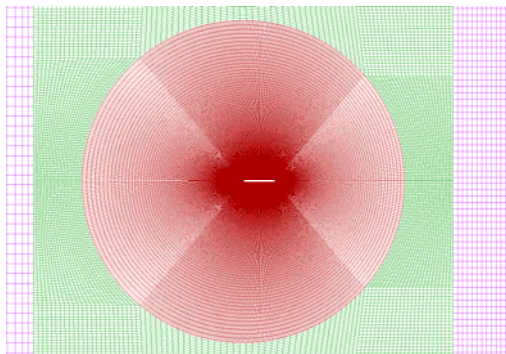


Figure 2: Airfoil surrounding area

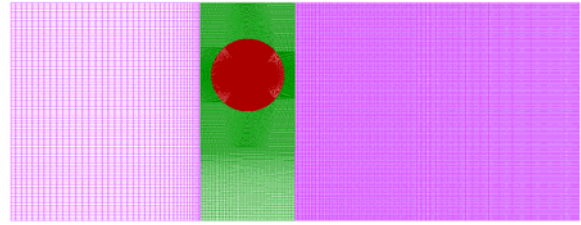


Figure 3: Complete grid

4. VERIFICATION OF TECHNIQUE

The application of Fluent for this kind of motion and this low Re was verified with three test cases found in the open literature [2, 3, 4] using the laminar model. Table 2 gives all the test conditions. The same NACA 0012 airfoil profile was used in all the test cases.

The first validation was a motionless NACA 0012 at $Re=20\,000$. The qualitative aspect of the Von Karman street was well predicted by Fluent. There was good agreement of the position and frequency of the vortices with the experimental [2] and simulation [4] results.

Variable	Case 1 refs. 2 & 4	Case 2 refs. 3 & 4	Case 3 refs. 3 & 4
Frequency [Hz]	—	2.5	0.27
Plunge amplitude [m]	—	0.0075	0.075
Twist amplitude [deg]	—	—	2.44
Phase angle shift [deg]	—	—	75
Airfoil chord [m]	0.1		
Freestream velocity [m/s]	0.2	0.2	0.4
Kinematic viscosity [m ² /s]	1.004×10^{-6} (water)		
Density [kg/m ³]	998.2 (water)		

Table 2: Validation test cases conditions [2, 3, 4]

The second test case was a pure plunge for the same Re and airfoil. Again, Fluent predicted well the position and size of the vortices shed by the airfoil (Fig. 4). The final test case included the heaving and pitching motion of the NACA 00012. For this case, the Re was 40 000. Again, the results agreed with the reference. The Fluent prediction for the drag and lift

coefficients generated by the airfoil motion are shown in the Figure 5 against those obtained by reference 4.

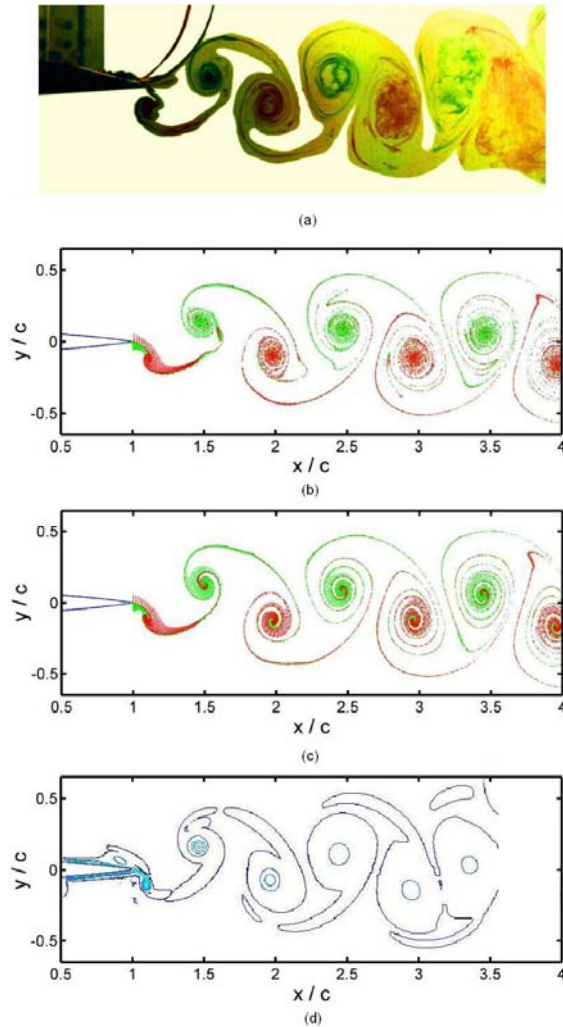


Figure 4: Vortices shed by the airfoil for case 2 conditions, (a) experimental [3], (b) numerical laminar [4], (c) numerical turbulent [4] and (d) Fluent laminar

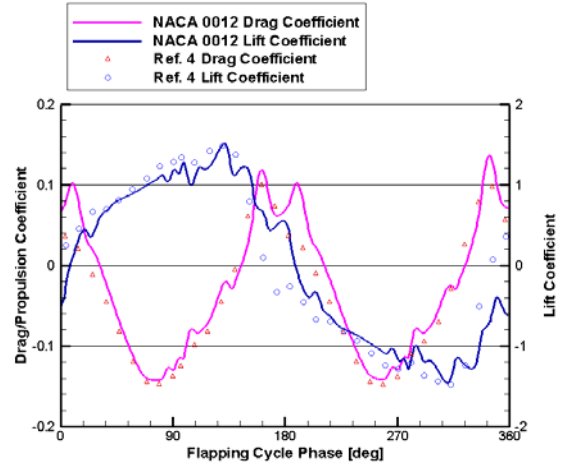


Figure 5: NACA 0012 lift and drag coefficient

5. RESULTS AND DISCUSSION

For the conditions of Table 1 in water, the drag/propulsion coefficients for the various viscous models tested are obtained as shown in Fig. 6. Drag/propulsion is the force in the x-direction (direction of the free stream velocity). There is propulsion when the coefficient is negative, and drag when it is positive. For the flat plate, the laminar model indicates less drag than the other models at the maximum plunging amplitude. This was expected since the separation point is predetermined by the geometry and a laminar boundary layer creates less viscous drag. The average propulsion forces are however of similar magnitude and the instantaneous drag/propulsion coefficient curves have the same tendency.

For the NACA 0005, the forces estimated by the LES viscous model have the same trend as the ones predicted for the flat plat but the averaged propulsion force is around 15% greater. The propulsion force enhancement is obtained by a lower drag force at the maximum plunging amplitude and higher propulsion force during the plunging motion.

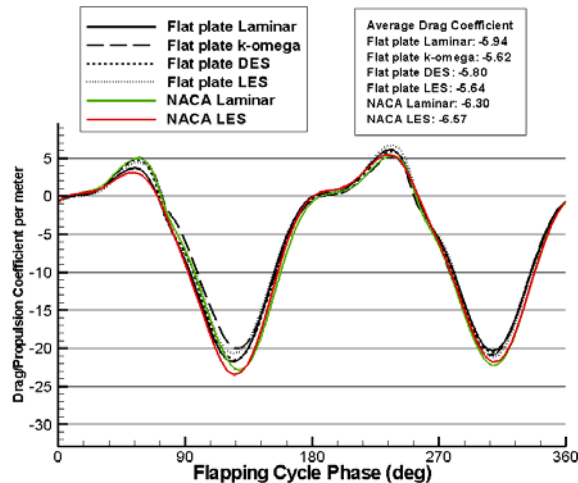


Figure 6: Drag/propulsion Coefficient for the different viscous model

Table 3 shows the computation time for one time step on 6 CPU (Pentium 4 3.2 GHz). As expected, the laminar model and K-omega have the fastest computation time. Furthermore, the LES and DES models need 3 to 4 cycles rather than one for the laminar model before having steady drag/propulsion coefficient values.

Airfoil shape	Viscous model	Time step [sec]	Convergence time per time steps [sec]
Flat plate	Laminar	0.001	28
Flat plate	k-omega	0.001	38
Flat plate	DES	0.0005	51
Flat plate	LES	0.001	45
NACA	LES	0.001	44

Table 3: Convergence time for each viscous model

Figure 7 shows the vorticity magnitude contours for the flat plate airfoil. The leading-edge vortex can be clearly seen. Figure 7 shows results at the minimum plunging location of airfoil motion. During the terminal phase of the down-stroke of the airfoil, when it is pitching up, a vortex is formed on the upper surface. During the up-stroke period, this vortex is shed. The same phenomenon occurs at the maximum plunging location of the airfoil motion but on the bottom of the airfoil.

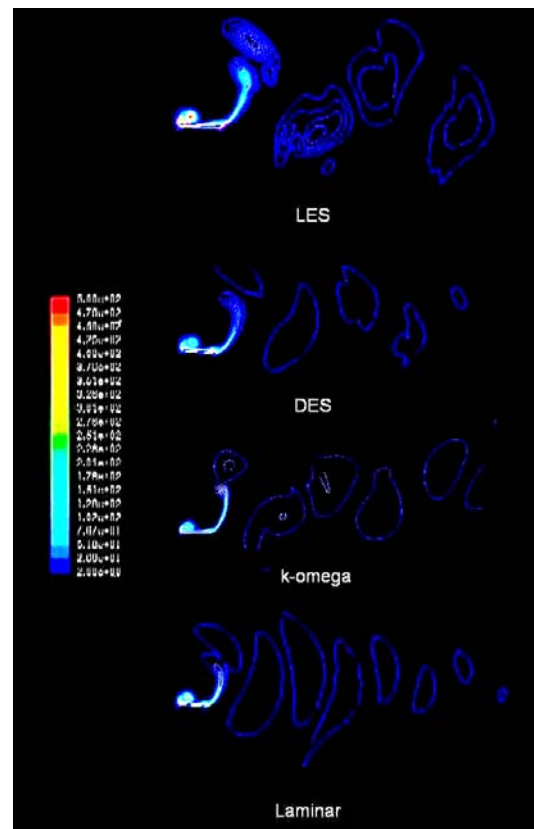


Figure 7: Vorticity magnitude contour for the flat plate airfoil

The shed vortices can be seen in the wake of the airfoil. The LES viscous model showed better vortex definition in the wake. The laminar model showed a larger and weaker vortex than LES. The leading edge vortices were however similarly predicted by all turbulence models. Same comment can be made for the NACA 0005 shown in Figure 8.

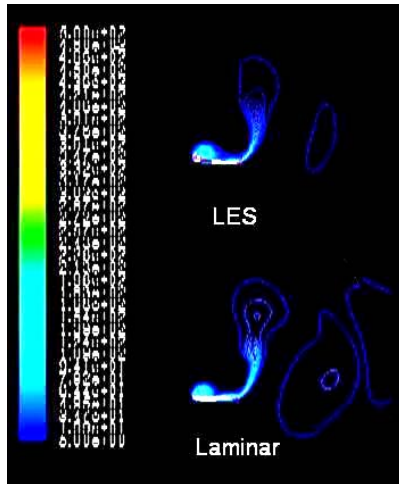


Figure 8: Vorticity magnitude contour for the NACA 0005 airfoil

The averaged propulsion force coefficient predicted by Fluent is found to be around 6 (Fig. 6). Considering that thrust is given by eq. 6 and that there are four wings, the thrust generated becomes 0.095N. This is very close to the target of 0.1N. This coarse estimation of forces based on CFD seems to indicate nearly sufficient force for the NAV to hover.

$$Thrust = Cd \cdot 1/2 V_{\infty}^2 A \rho_{air} \quad (eq.6)$$

6. CONCLUSION

The work done at DRDC Valcartier on the simulation of flapping airfoils was presented. It demonstrated that Fluent can simulate efficiently pitching and heaving airfoil. The technique was also verified against results found in the literature.

The force generated by the flapping airfoil did not vary significantly for one viscous model to the other. Also all the models predicted the same shape and strength of the leading edge vortex. This could be explained by the geometry of the thin airfoil. The flow detaches directly at the leading edge of the airfoil. Also, for all turbulence models the NACA 0005 airfoil gave superior propulsion forces than the flat plate for the same motion.

The laminar viscous model seems to be sufficient to estimate the forces generated by a plunging and pitching airfoil. On the other hand, to consider the vortices shed by the airfoil and interacting with the NAV airframe, the LES viscous model should be used.

It was also demonstrated that the propulsion obtained by CFD is sufficient to permit to 10 gram NAV to hover.

ACKNOWLEDGEMENTS

This study was made under DRDC Valcartier's project "Flapping Wing Aerodynamics for Efficient Insect-Size Craft". The authors want to express thanks to project team members Patrick Zdunich from Advanced Subsonics, Toronto, Mahmood Khalid, Weixing Yuan and XingZhong Huang from NRC-IAR for their contributions to the project.

REFERENCES

- [1] Fluent Inc. web site, Fluent 6.3 user's guide: http://www.fluentusers.com/fluent6326/doc/doc_f.htm
- [2] Anderson, J.M., Streitlien, K., Barrett, D.S. and Triantafyllou, M.S., "Oscillating Foils of High Propulsive Efficiency," Journal of Fluid Mechanics, Vol. 360, 1998, pp. 41-72.
- [3] Lai, J.C.S. and Platzer, M.F., "Jet Characteristics of a Plunging Airfoil," AIAA Journal, Vol. 37, No. 12, 1999, pp. 1529-1 537.
- [4] J. Young, "Numerical Simulation of the Unsteady Aerodynamics of Flapping Airfoils", PhD Thesis, School of Aerospace, Civil and Mechanical Engineering, University of New South Wales, Australian Defence Force Academy, Canberra, Australia, May 2005, 328pp

Annex 4 – CASI Aerodynamics Symposium 2007 conference paper; April 2007

This page intentionally left blank.

Preliminary CFD Simulations of Flapping-Wing Aerodynamics

Weixing Yuan and Mahmood Khalid
Institute for Aerospace Research (IAR)
National Research Council (NRC) Canada
Ottawa, Ontario, K1A 0R6, Canada
Email: Weixing.Yuan@nrc-cnrc.gc.ca

ABSTRACT

The Institute for Aerospace Research (IAR) of the National Research Council Canada (NRC) is carrying out research work to develop and validate efficient mathematical models and numerical algorithms for unsteady low-Reynolds-number flow solvers, as well as to investigate aeromechanical aspects of unsteady insect-like flapping wing for nano-air vehicles (NAV). The study of the insect-like flight is a discipline in itself with myriad of morphological parameters based on mass, body length, wing shape and area as well as virtual mass arising from the quantity of air shifted, all contributing towards the sophistication of flight. This paper presents some preliminary results around 2D insect-size airfoils using the in-house code INSflow developed for computing three-dimensional unsteady incompressible flows. The simulations indicate that the largest thrust occurs at the time when the leading-edge vortices form.

NOMENCLATURE

c	=	airfoil chord length
C_D	=	drag coefficient
C_L	=	lift coefficient
c_p	=	pressure coefficient
f	=	flapping frequency
F_x, F_y	=	components of integrated force acting on the airfoil
h	=	linear plunge displacement of the point about which airfoil pitches
H	=	plunging amplitude (peak value) of the point about which the airfoil pitches
k_c	=	reduced frequency
Re	=	Reynolds number
U_∞	=	freestream velocity
$V_{induced}$	=	peak velocity of the plunging motion
u', v'	=	components of velocity fluctuation
Tu	=	freestream turbulence intensity
s	=	span length
t	=	time
x, y	=	Cartesian coordinates
x_0	=	pivot location
x_{tran}	=	transition location
y^+	=	non-dimensional distance from wall
α	=	angle of attack
α_i	=	instantaneous angle of attack
μ	=	fluid dynamic viscosity
θ	=	rotational displacement (angle) of airfoil

ρ = fluid density
 ω = angular frequency
 ω_z = spanwise vorticity

1. INTRODUCTION

The evolution of a new class of military system, known as nano-air vehicles (NAV), has been made possible by reliable and fast modelling techniques in aerodynamics and other advances in such disciplines as micro-electronics, sensors, micro-electromechanical systems (MEMS) and micro-manufacturing. Nano-air vehicles are defined as insect-size aircraft on a five-centimetre scale. The research on such autonomous flying vehicles is motivated by a need for intelligent reconnaissance robots, capable of discreetly penetrating confined spaces and manoeuvring inside such spaces without direct human interaction. Agile flight inside buildings, stairwells, shafts and tunnels is of significant military and civilian value. The current surveillance assets possess little or no airborne capability for information gathering inside buildings and other confined spaces. Other applications of such miniaturized vehicles would include deployments in bomb diffusion locations or routine surveillance under anti-terrorist operations and reconnaissance to counter chemical or biological agent release. Their ready deployments in dull and dirty environments in contaminated areas surrounding nuclear reactors or in ship machine shops, where human exposure could be dangerous, make them very attractive under current security concerns. Elsewhere, human-free exploration of industrial environments will allow air quality sampling in non-attainable areas, utility inspection, and examination of confined spaces in buildings, installations and large machines.

NAVs require a distinct flight envelope including hover, perching, and highly agile manoeuvrability at low speeds, which must be achieved with high power efficiency. It does not seem likely that the fixed wing/forward thrust and rotorcraft (helicopter) designs satisfy the flight envelope specifications for NAVs. On the other hand, insect flight exhibits the required envelope and has been successful in nature for millions of years. Insects rely on unsteady aerodynamics to produce high lift coefficients and excellent manoeuvrability. The high lift is a major factor in the high efficiency of the scheme. Therefore, engineering realisation of the functionality of insect flight is attractive.

Although progress in many technology areas will be required for a practical insect-size craft, NRC-IAR and DRDC (Defence R&D Canada), amongst other disciplines, have focused on the efficient generation of propulsive forces through the flapping motion. Even though there has been considerable analysis of bird and insect flight mechanisms, no machine for example of the hummingbird size has been successfully demonstrated. The dramatic lift-boosting unsteady aerodynamic phenomena that are exploited by insect flapping wings are not yet fully understood. Insect wing kinematics involves non-trivial, instinctive, reciprocal motions. The wing flapping plane continuously adjusts with the body axis which also changes rapidly to bring about a certain type of flight. In steady forward flight the wing flaps in a well guided fashion to control the leading-edge vortex as it traverses downstream so the horizontal thrust generates the right amount of lift as well as precisely balancing the body drag. In a hovering motion the body can be aligned vertically but the wings must open and close in such a “clap and fling” [1] manoeuvre that the large vortex at the opening (fling motion during downstroke) end together with the small vortex generated at the hinge bring about such outer circulation to provide precisely the lift to balance the insect weight. At the end of upstroke, the leading edges touch and the wings clap together. The wings remain clapped for about 20% of the cycle period, which is believed to correspond to elastic storage of the high mechanical energy needed for the subsequent fling motion [2]. The velocity distribution on the wing surface resulting from flapping is non-uniform, resulting in a complex airflow. It is also unsteady, i.e. the aerodynamic force varies in amplitude and direction during each wingbeat cycle. The variability of the force is compounded by the strong influence of the viscosity of air and significant interaction of the wing with its wake, especially in hover. However, our understanding of the resulting aerodynamics is incomplete even on the phenomenological level. Not only is the qualitative picture unfinished, but also the quantitative analysis is wanting. From the perspectives of both the insect flight analysis and NAV design, there is a need for an analysis framework and numerical algorithms for aerodynamic modelling and simulation of flapping wings. In fact, the few mathematical approaches attempted thus far involve either simple algebra or advanced computational fluid dynamics (CFD). In the former case, the framework is incapable of capturing the essential unsteady characteristics of the flow. The CFD approach is challenging, owing to the complicated kinematics of wing motion and inadequacy of experimental data for full verification. Capturing the leading-edge separation is a well-known major obstacle in the CFD simulation for low-Reynolds-number airfoil flows. NRC-IAR

is conducting numerical investigations of this low-Reynolds-number flapping type aerodynamics. This paper presents the preliminary results obtained during the collaboration with DRDC Valcartier under SDA06-28.

2. DESCRIPTION OF THE CFD CODE AND THE NUMERICAL METHODS

The in-house code INSflow [3] developed for computing three-dimensional (3D) unsteady incompressible flows was applied in the study. In the code, the integral form of the conservation law for mass and momentum was used. A fully implicit second-order temporal differencing scheme was used in the discretisation, which made the algorithm stable for large timesteps. The discretisation of the convective and diffusive fluxes was carried out in a co-located variable arrangement using the finite-volume approach which was second-order accurate in space. The coupling of the pressure and the velocity was handled using the SIMPLE algorithm [4]. The continuity equation was transformed into a pressure-correction equation, which had the same general form as the discretized momentum equations. The use of the co-located variable arrangement on non-orthogonal grids required that the SIMPLE algorithm be modified slightly to dampen numerical oscillations. A pressure-velocity coupling method for complex geometries used by Ferziger and Perić [5] was implemented, where an additional pressure gradient term was subtracted from the velocity value at the surface of the control volume to prevent non-physical oscillations. To enable large-eddy simulation (LES) practices for complex geometry flows, the Smagorinsky [6] SGS model was implemented as a standard SGS model in the code.

The calculations were performed on moving grid configurations. The velocity of the grid movement was included in the governing equations [3], [7] in an inertial frame of reference. In order to avoid artificial mass sources generated by the grid velocity, as applied by Demirdžić and Perić [8], a space conservation law was introduced to ensure a fully conservative property in the computations.

3. CODE VALIDATION AT LOW REYNOLDS NUMBERS

The in-house code INSFlow has been used for a number of LES and URANS (unsteady Reynolds-averaged Navier-Stokes) calculations for various flows in incompressible regimes, see [3], [9]-[11]. To demonstrate the effectiveness of the CFD code, two test cases in low-Reynolds-number regimes were chosen from earlier investigations.

Large-eddy simulations have been performed for flows past an SD7003 airfoil at $Re = 6 \times 10^4$. The resulting Reynolds shear stress distribution accumulated from 15000-timestep LES without SGS model on a $737 \times 65 \times 17$ grid is illustrated on Figure 1. The 3D LES predictions of the laminar separation bubble (LSB) and the transition process across the LSB compared reasonably to the experiments from the LNB wind tunnel of the Technical University Braunschweig (TUBS) and the water tunnel at the Air Force Research Laboratory (AFRL). Details can be found in [11].

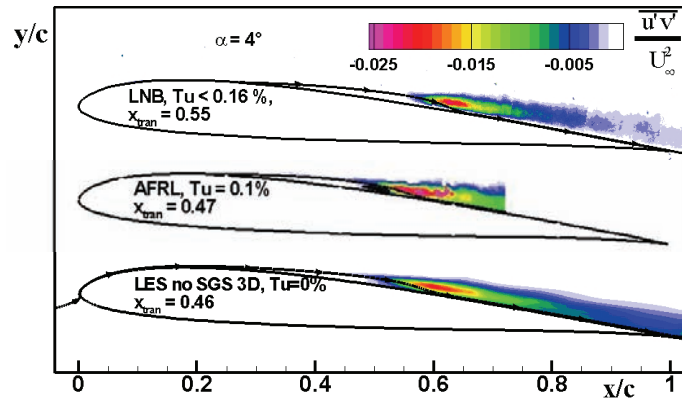


Figure 1. Comparisons of LES (without SGS model) results with experimental observations. Non-dimensional Reynolds shear stress $\overline{u'v'}$ contours over the SD7003 airfoil at $Re = \rho c U_\infty / \mu = 6 \times 10^4$ and $\alpha = 4^\circ$.

As recommended by the NATO AVT low-Re task group, a plunging case of the SD7003 airfoil was also considered [12]. For the numerical simulations, the chord length of the airfoil was set to 202.6 mm. Other parameters were as

follows: $U_\infty = 0.3$ m/s, $\alpha_i = 5.5^\circ + 3^\circ \sin(2\pi ft)$, $f = 0.25$ Hz. The Reynolds number was 6×10^4 . Computations were performed for different setups: $\Delta t = T/384$ and $T/3840$ on the $737 \times 65 \times 4$ mesh (quasi 3D) and $\Delta t = T/384$ on the $737 \times 65 \times 17$ mesh (3D). Figure 2 shows the non-dimensionalized Reynolds shear stress of the 3D calculations for the mid-upstroke location at $t = T + 3T/4$ and $\alpha_i = 2.5^\circ$. For a more detailed comparison, magnified views of the appropriate regimes of the experimental and computational flowfields are shown in Figure 2a and Figure 2c. Regimes of increasing turbulent flow are clearly identified past the axial location $x/c = 0.4$. The turbulence statistics analysis was carried out based on the calculations of 20 plunging cycles using the Smagorinsky SGS model. Although the contour is not smooth owing to the limited calculation periods, the Reynolds shear stress is qualitatively comparable to the experimental data. As the freestream turbulence ($Tu = 1\%$) observed in the experiments at the TUBS was not considered in the calculations, the calculations reasonably predicted larger laminar separation bubble. Further quantitative comparisons would be performed as soon as suitable experimental data become available.

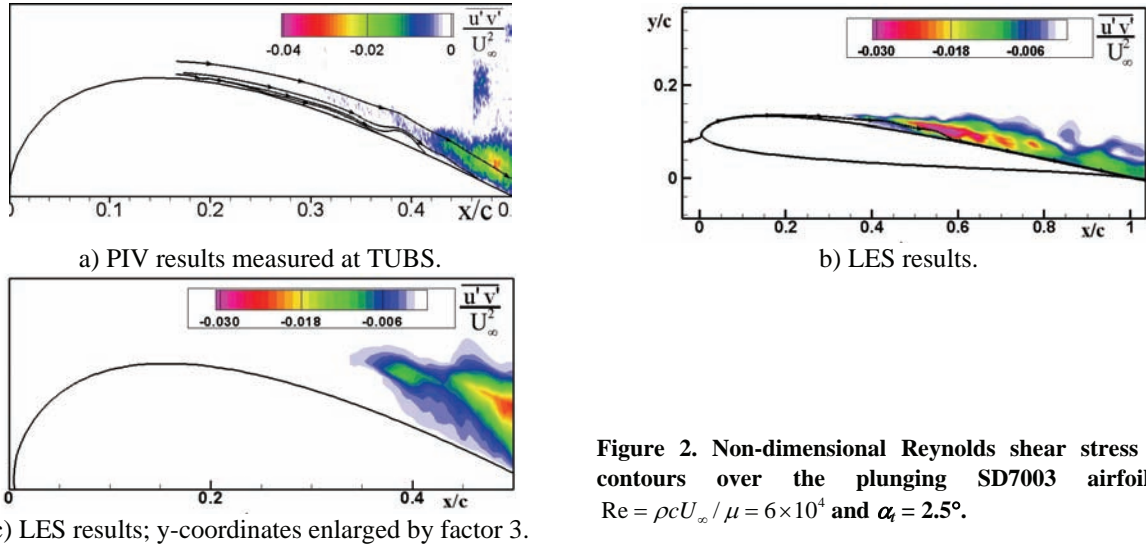


Figure 2. Non-dimensional Reynolds shear stress $\overline{u'v'}$ contours over the plunging SD7003 airfoil at $Re = \rho c U_\infty / \mu = 6 \times 10^4$ and $\alpha_i = 2.5^\circ$.

4. PRELIMINARY RESULTS OF FLAPPING-WING AERODYNAMICS

4.1 Description of Problem and Test Conditions

As mentioned earlier, the objective of the present study is to understand better the flapping-wing aerodynamics of nano-air vehicles. During the collaborative project with DRDC, a symmetrical NACA 0005 and a flat-plate airfoil were recommended. The relative thickness of the flat-plate airfoil is approximately equivalent to that of the NACA 0005 airfoil. The leading and trailing edges of the flat plate are equilateral triangles. The airfoils oscillate with combined plunging and pitching motions under a very low-speed (U_∞) freestream flow condition. The plunging motion of the airfoil is defined as follows:

$$h(t) = H \sin(\omega t + 90^\circ), \quad (1)$$

where H is the plunging amplitude and the circular frequency is $\omega = 2\pi f$. The pitching motion of the airfoil about the leading edge is described as:

$$\theta(t) = 50^\circ \sin(\omega t), \quad (2)$$

with positive angle when pitching in the counter-clockwise direction as illustrated in Figure 3.

In this study, the total airfoil length was set to $c = 3.75$ cm and the freestream velocity was specified as $U_\infty = 0.1$ m/s, which resulted in a Reynolds number $Re_\infty = \rho U_\infty c / \mu = 3,750$. The motion was such scheduled that the plunging amplitude was equal to the airfoil chord length ($H = c$) with a frequency of $f = 1.3$ Hz. The reduced frequency was

$k_c = \omega c / 2U_\infty = 1.53$. Taking into account the peak velocity of the plunging motion $V_{induced} = H\omega$, the induced Reynolds number and the reduced frequency can be obtained: $Re_{induced} = \rho V_{induced} c / \mu = 11,486$ and $k_{induced} = \omega c / 2V_{induced} = 0.5$, respectively. In this study, a generalized Reynolds number based on the combination of these two is introduced:

$$Re = \frac{\rho \|U_\infty + V_{induced}\| c}{\mu}, \quad (3)$$

which works for hover conditions too. At the flow conditions mentioned above, the Reynolds number is $Re = 12,083$.

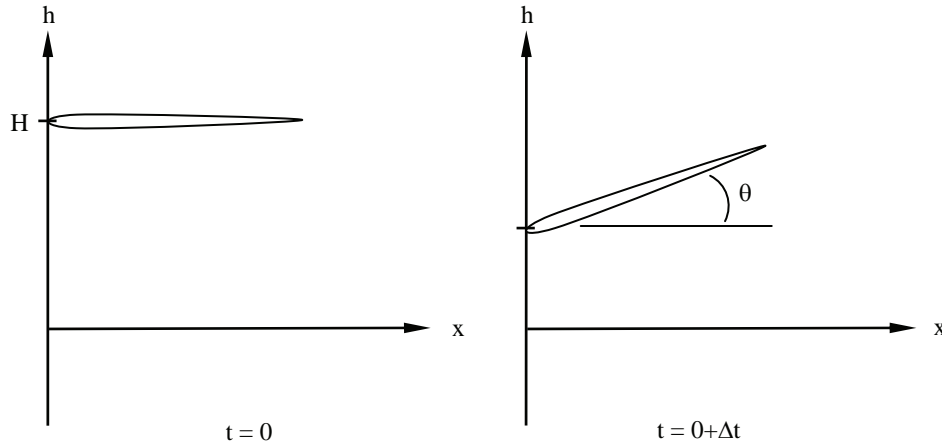


Figure 3. Schematic of the airfoil plunging and pitching motion.

The complex flapping motion will cause deviation of the local angle of attack from the steady case. For a flapping airfoil in a plunging motion combined with a pitching oscillation about x_0 , at any chordwise location x , the local angle of attack can be expressed as

$$\alpha(x, t) = -\theta(t) - \tan^{-1} \left[\frac{h'(t) + \dot{\theta}(t)(x - x_0) \cos(\theta)}{U_\infty + \dot{\theta}(t)(x - x_0) \sin(\theta)} \right], \quad (4)$$

where x_0 indicates pivot centre and $x_0 = 0$ when it is located at the leading edge. In the equation, the first term in the brackets stands for the part of the instantaneous angle of attack at the pivot centre induced by the plunging motion while the second term is additional change in the local angle of attack induced by the pitching oscillation causing an equivalent cambered wing effect. The derivatives of the motion displacements are

$$h'(t) = H\omega \sin(\omega t), \quad (5)$$

$$\dot{\theta}(t) = \frac{50\pi\omega}{180} \cos(\omega t). \quad (6)$$

For H , ω and U_∞ chosen in this paper, the combined motion induced a complex variation of the instantaneous angle of attack at the airfoil leading edge as shown in red in Figure 4. It can be easily verified that the instantaneous flow incidence induced by the plunging motion is much stronger than that from the pitching motion at this selected condition.

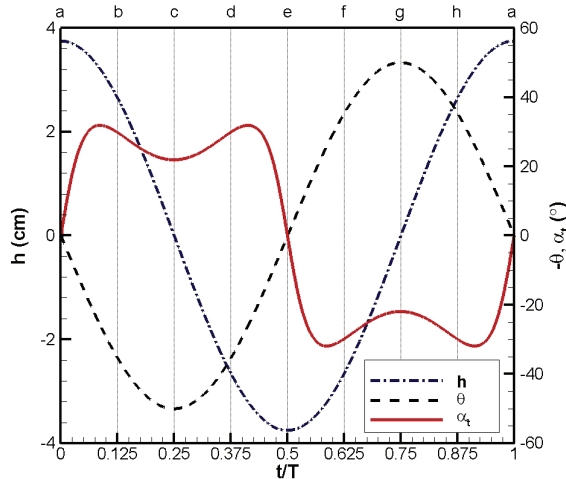


Figure 4. Time history of effective airfoil incidence in accordance with the airfoil plunging and pitching motion.

4.2 Flow Field over NACA 0005

Preliminary investigations were carried out for the NACA 0005 and the flat-plate airfoils mentioned above. Laminar solutions were obtained on 2D 481×129 O-type meshes. Figure 4 shows the compound instantaneous angle of attack at the airfoil leading edge produced from the combined pitching and plunging motion schedules. The flowfield resulting from such complex motions would be difficult to interpret in terms of the actual instantaneous displacement owing to the presence of the phase lag between the flowfield and the model. Since the flowfield was dominated by the presence of the leading-edge vortex which pervaded across the entire flowfield as the airfoil motion progressed, the flowfield shown in Figure 5 must be interpreted alongside with the vorticity development traced out in Figure 6 during both upstroke and downstroke portions of the entire flight regime.

The top left picture in Figure 5a is the start of the downstroke movement at the end of the upstroke after the bottom right snapshot of Figure 5h. It is clear that a leading-edge vortex had already started to take shape at the bottom surface of the airfoil at the ending phase of the upstroke (Figure 5h) which was further strengthened at the onset of the down beat in Figure 5a. This leading-edge vortex continued to grow with a baby vortex (Figure 5b) that seems to have taken birth at the end of the upstroke (Figure 5a). Eventually, the vortex is shed into the wake where it continued to travel downstream (Figure 5c) and disappeared. It should be noted that even though the moment corresponding to Figure 5b has passed the first peak instantaneous angle of attack, no vortex formed on the upper surface owing to the phase delay. By the time that the instantaneous angle of attack was approaching the second maximum peak in Figure 5d, a new system of leading-edge vortex now on the upper surface has started to take form. Similar to the vortex that grew on the lower surface, the vortex on the upper surface, too, gave rise to a baby vortex as it traveled downstream before it shed into the wake in Figure 5g.

Figure 6 shows the spanwise vorticity over the NACA 0005 airfoil. Although the preliminary results are somewhat noisy, the vortex rolling up can be clearly seen. During the downstroke period, the primary vortex rolled counter-clockwise (red) on the lower surface while the vortex rolled clockwise (blue) on the upper surface during the upstroke period. As mentioned earlier, a small secondary vortex was generated while the primary vortex was shedding. As shown in Figure 6b and f as well as in Figure 5b and f, the secondary leading-edge vortices shed for a while and then disappeared. A similar phenomenon was also observed over the flat plate discussed later. This complex phenomenon needs to be confirmed by experimental observations and further investigation by more comprehensive 3D simulations. The vorticity history corresponding to the evolution of the leading-edge vortex during both up and downstroke motions was well captured in Figure 6. Perhaps, a more intriguing phenomenon is the “fingering” distribution of the vorticity noted when the vortices were shed passed the trailing edge at the conclusion of the up and downstroke motions.

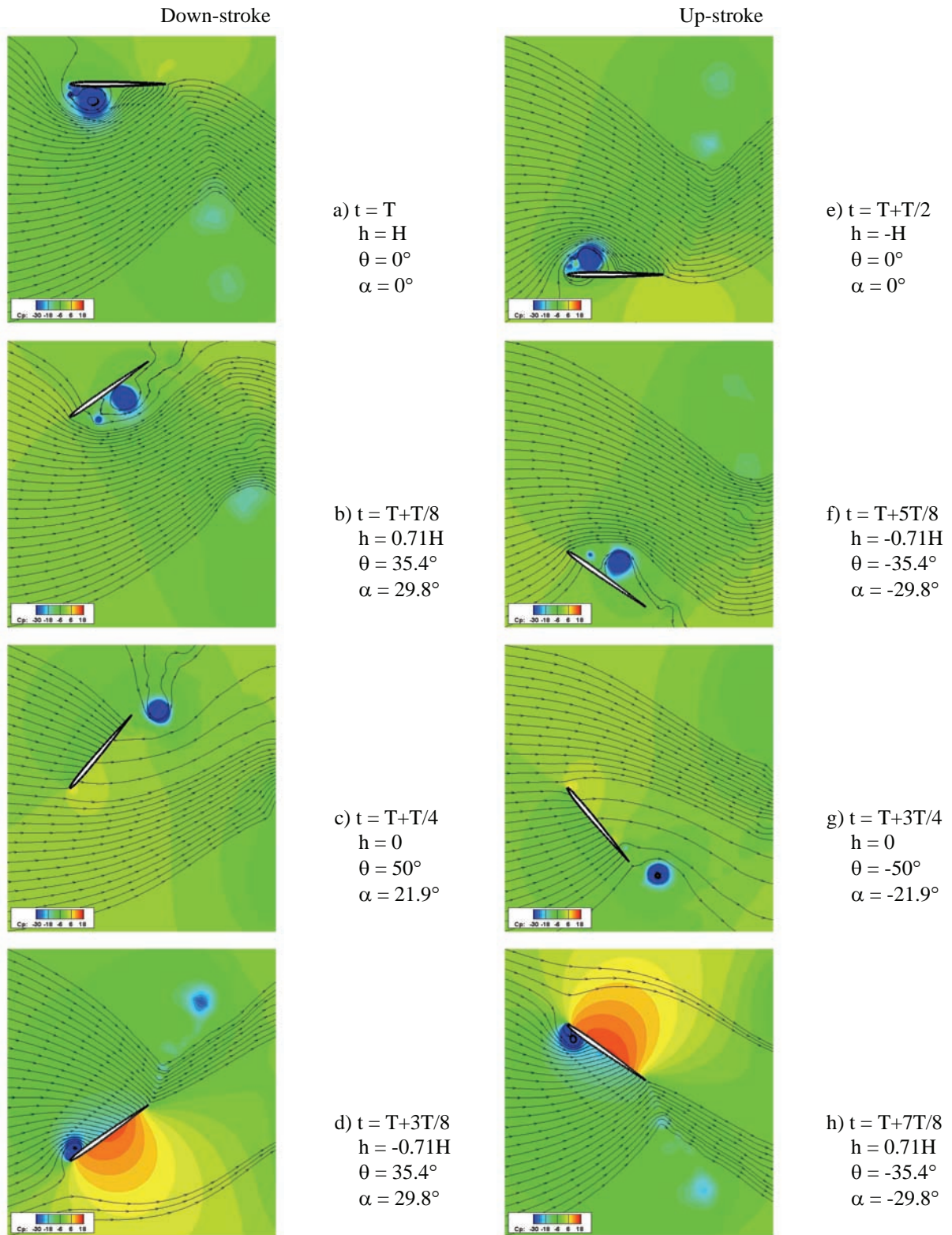


Figure 5. Laminar solution of the flowfield over the flapping NACA 0005 airfoil at $Re = 1.2 \times 10^4$.

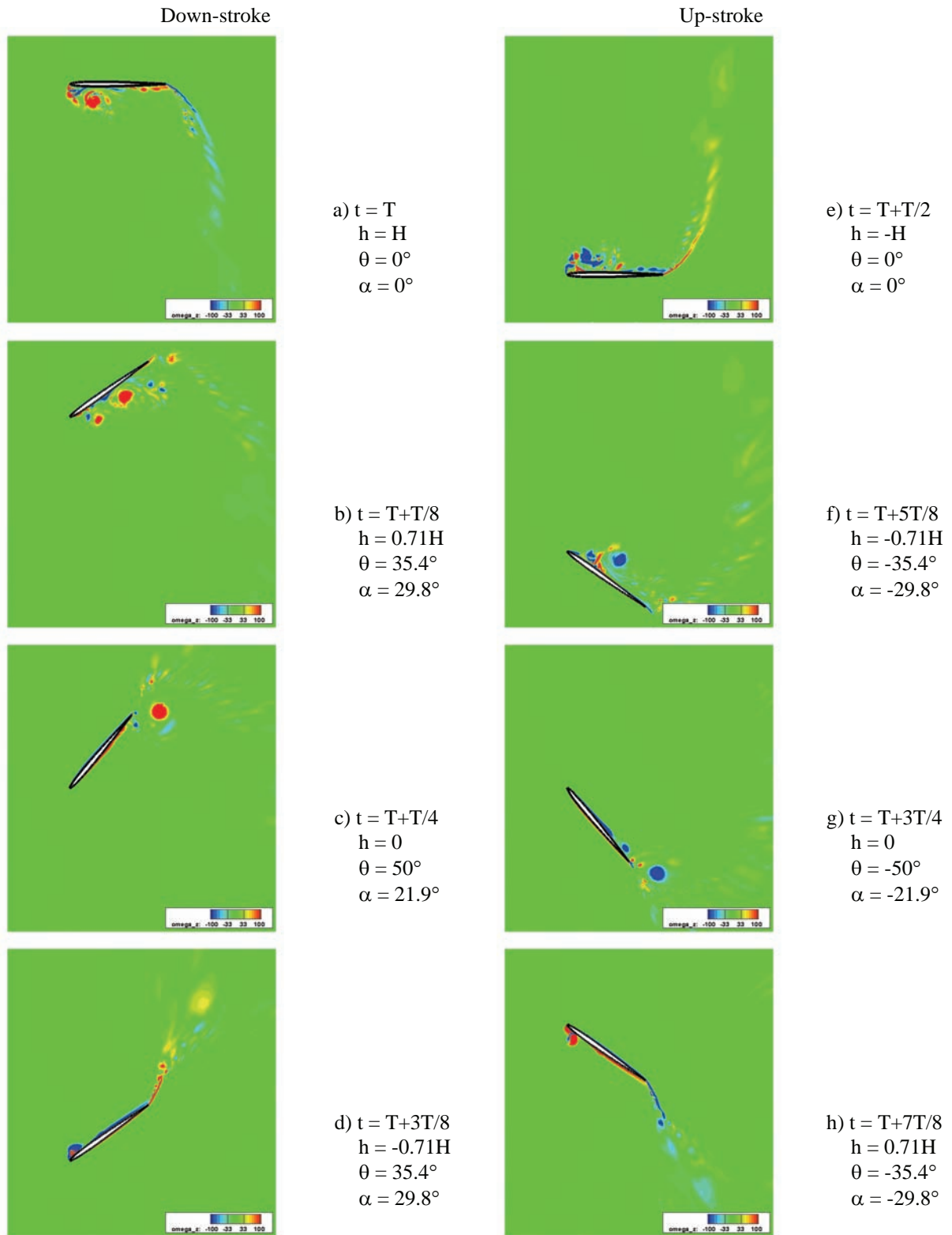


Figure 6. Non-dimensional spanwise vorticity over the flapping NACA 0005 airfoil at $Re = 1.2 \times 10^4$.

4.3 Preliminary Parametric Studies

4.3.1 Grid Resolution Effect

To assess the grid convergence effects, calculations on a different mesh were performed. The grid density in the normal-to-the-wall direction of the aforementioned grid was reduced resulting in a coarse mesh with 481×65 grid points. Figure 7 shows the integrated lift and drag coefficients on two meshes. The negative value of the drag indicates the thrust. As the integrated coefficients did not show chaotic variations, it is believed that the flow was in the laminar regime. The lift and drag coefficients did not show big difference between the two meshes indicating that the prediction of integrated results on the coarse mesh is acceptable for engineering purposes at pre-design stage. The simulations exhibited that the largest lift occurred when the instantaneous angle of attack reached the second peak, with slightly lagging the maximum thrust. The maximum thrust coefficients occurred at the time that the leading-edge vortex formed (Figure 5d, h). The lift coefficient on the fine grid showed sudden drop during the down stroke and rise during the up stroke period, which is believed to be related to the flow hysteresis and needs to be confirmed. However, this phenomenon was not so clear on the coarse grid. This was attributed to the difference of vortex shedding processes as shown in Figure 8. The shedding vortices disappeared much faster on the coarse grid. In addition, the rolling of shedding vortices on the coarse grid was not clear either, see Figure 9. Therefore, to get deep insight of the flow physics, the grid resolution must satisfy the physical requirements even for laminar flow simulations.

It should be noted that consistent with the definition of the generalized Reynolds number, the induced velocity by the plunging motion was considered for calculating the lift and drag coefficients:

$$C_L = \frac{F_y}{\frac{1}{2} \rho \|U_\infty + V_{induced}\|^2 cs}, \quad (7)$$

$$C_D = \frac{F_x}{\frac{1}{2} \rho \|U_\infty + V_{induced}\|^2 cs}. \quad (8)$$

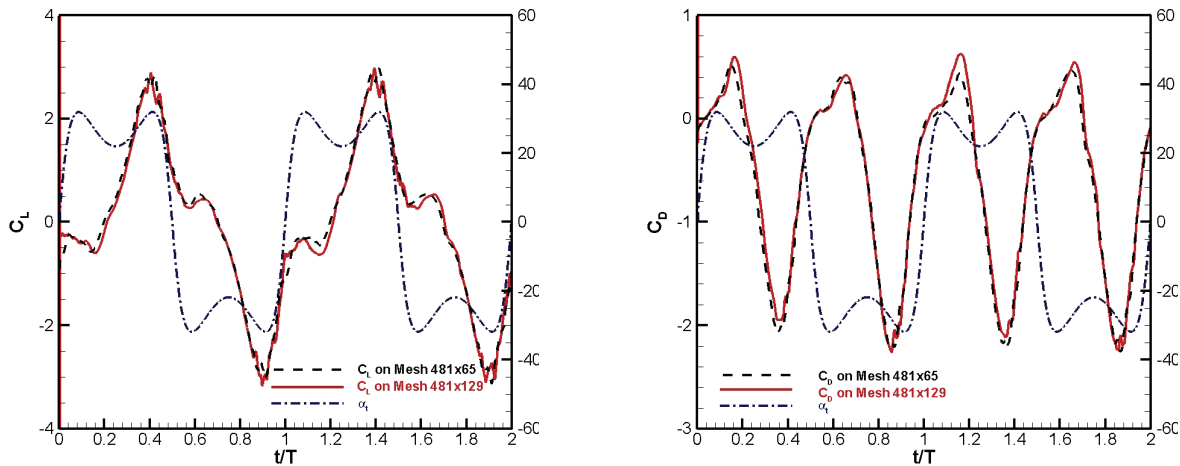


Figure 7. Grid resolution effect: Time history of lift and drag coefficients.

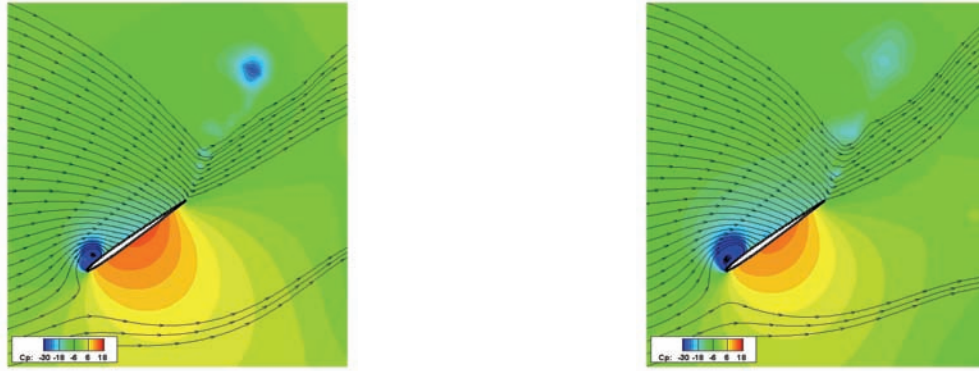


Figure 8. Grid resolution effect: Flow fields on fine (left) and coarse (right) grids at $t=T+3T/8$.

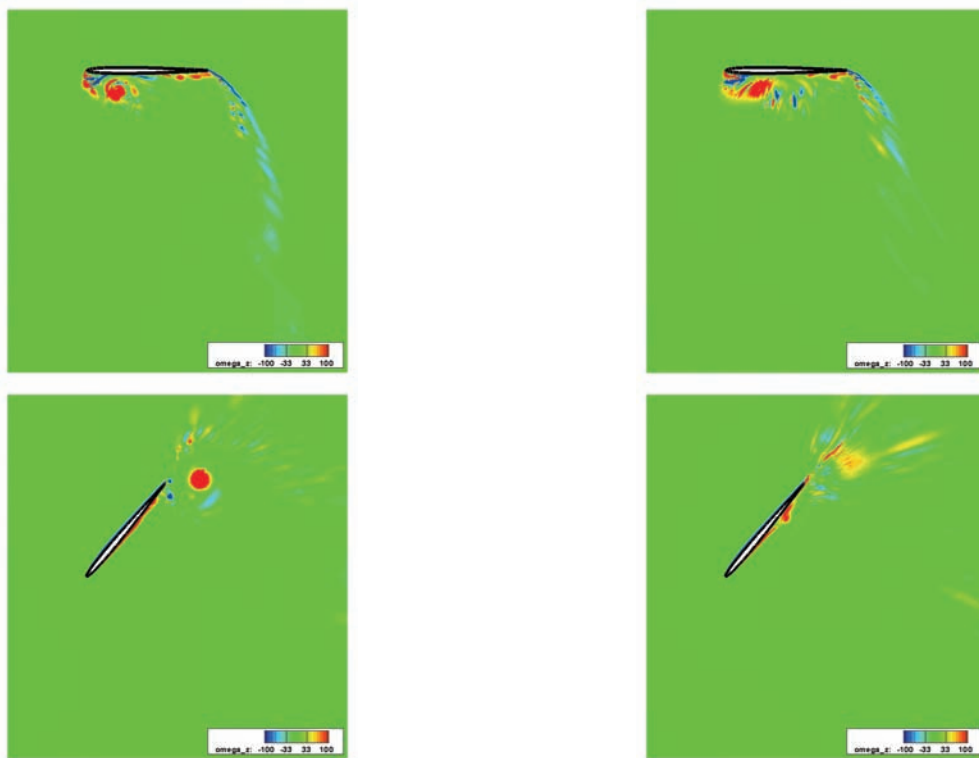


Figure 9. Grid resolution effect: Spanwise vorticity over NACA 0005 on fine (left) and coarse (right) grids at $t=T$ (top) and $t=T+T/4$ (bottom).

4.3.2 Airfoil Effect

A second test case was a flow past a flat-plate airfoil with equilateral triangles at the leading and trailing edges as shown in Figure 10. The thickness of the flat plate was 5% chord, which is comparable to the NACA 0005 airfoil. The flat-plate airfoil showed a similar vortex formation and shedding process as the NACA 0005 airfoil. The flowfields around the NACA 0005 and the flat-plate airfoils were similar, which resulted in the comparable integrated lift and drag coefficients, see Figure 11. Small humps were observed for the flat-plate airfoil. They may contribute to the flight stability. A closer look at the flow field over the flat plate (Figure 12) showed that the vortex rolling over the flat-plate airfoil was not as cylindrical as over the NACA 0005 airfoil.

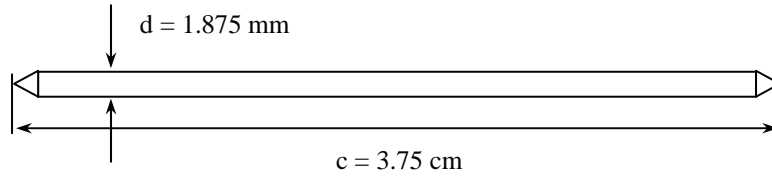


Figure 10. Schematic of the flat-plate airfoil.

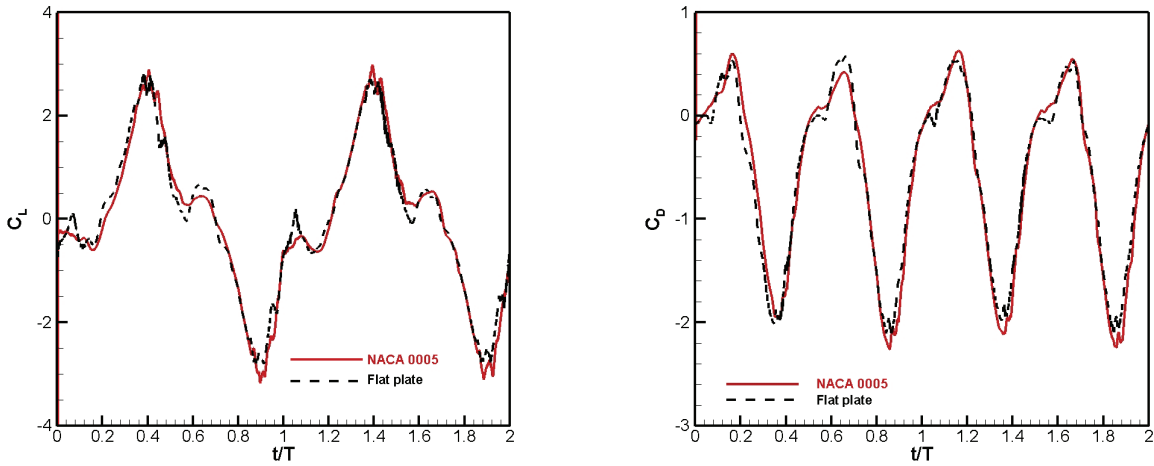


Figure 11. Airfoil effect: Time history of lift and drag coefficients.

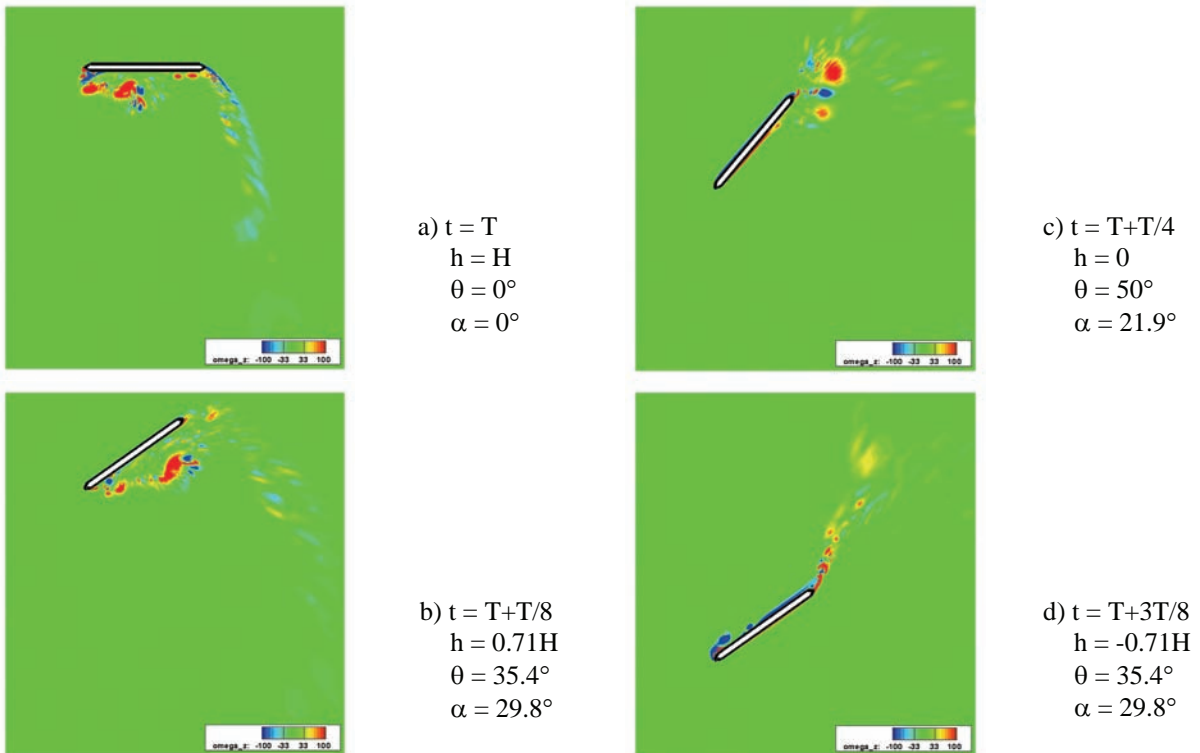


Figure 12. Spanwise vorticity over the flapping flat-plate airfoil during the downstroke period at $Re = 1.2 \times 10^4$.

4.3.3 Airfoil Thickness Effect

To check the airfoil thickness effect, a test case with NACA 0012 airfoil was chosen. As expected, the drag coefficient of the NACA 0012 was a little higher than that of the NACA 0005, see Figure 13. However, the thrust was nearly the same, as the kinematic motion generated the thrust.

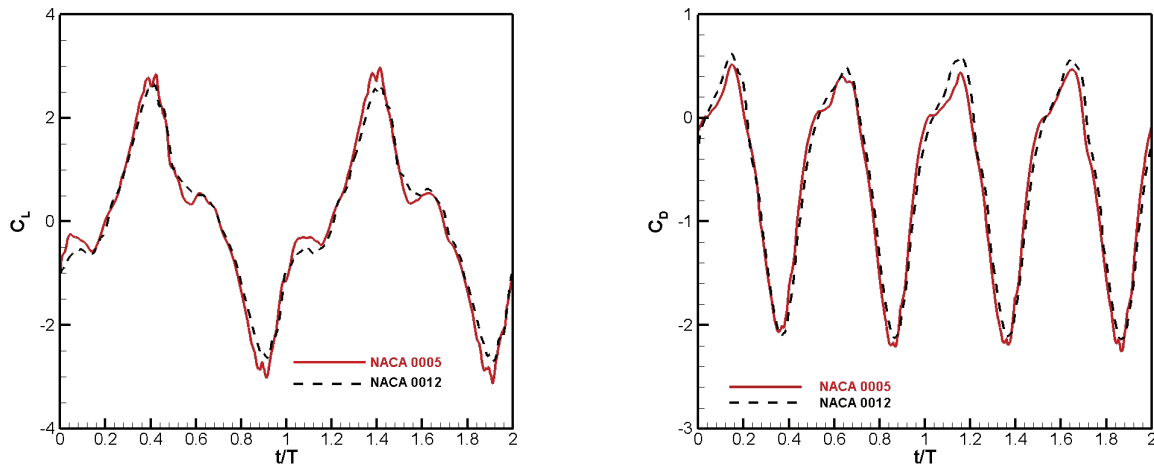


Figure 13. Airfoil thickness effect: Time history of lift and drag coefficients of NACA 0005 and NACA 0012 airfoils.

4.3.4 Pitching Axis Effect

In addition, another test case with the pitching axis located at the centre of the chord was calculated. As seen in Figure 14, the integrated lift and drag coefficients were completely different from the previous case with the pitching axis located at the leading edge. This is because that the rotation around the mid chord caused different local angles of attack as indicated in Eq. 4. The pitching motion induced an effect equivalent to a cambered airfoil. Figure 15 illustrates the equivalent cambered wing effect induced by the pitching motion at zero pitching angle for the pitching axes located at $x_0/c = 0.5$ and $x_0/c = 0$. As the flow was unsteady, the immediate local angle of attack changed instantly depending on the axial location, pitching angle and the freestream angle of attack. The resulting instantaneous effective angle of attack at the airfoil leading edge with $x_0/c = 0.5$ is shown in Figure 16 against the case with $x_0/c = 0$. The largest difference reached was about 53° . Therefore, it is not surprising that the results from these two cases differ from each other. Figure 17 shows snapshots of the spanwise vorticity distributions around the airfoil when pitching around $x_0/c=0.5$. As the down stroke started at the maximum instantaneous angle of attack in this case, flow separated on the upper surface at the leading edge noticeably earlier than that at the nominal case with $x_0/c=0$. When the vortex started taking shape on the upper surface at the leading edge, the lower surface vortices formed during the up stroke period were still shedding downstream.

5. CONCLUSIONS

The preliminary simulations of plunging airfoils combined with a pitching motion about the airfoil leading edge showed the leading-edge vortex formation and shedding process. When the effective angle of attack approached the second of the two maximum peaks, the leading-edge vortex formed and started shedding through the other half motion cycle. The largest thrust occurred when the leading-edge vortex was forming. However, the largest lift appeared when the effective angle of attack reached the second maximum followed by a flow hysteresis. It seems that the effect of the airfoil on the averaged lift/drag coefficients is limited. However, thin airfoil seems to be superior to thicker ones causing less drag and larger thrust coefficients. In addition, grid resolution affected the vortex shedding prediction and the pitching axis had clear influence on the integrated lift and thrust coefficients.

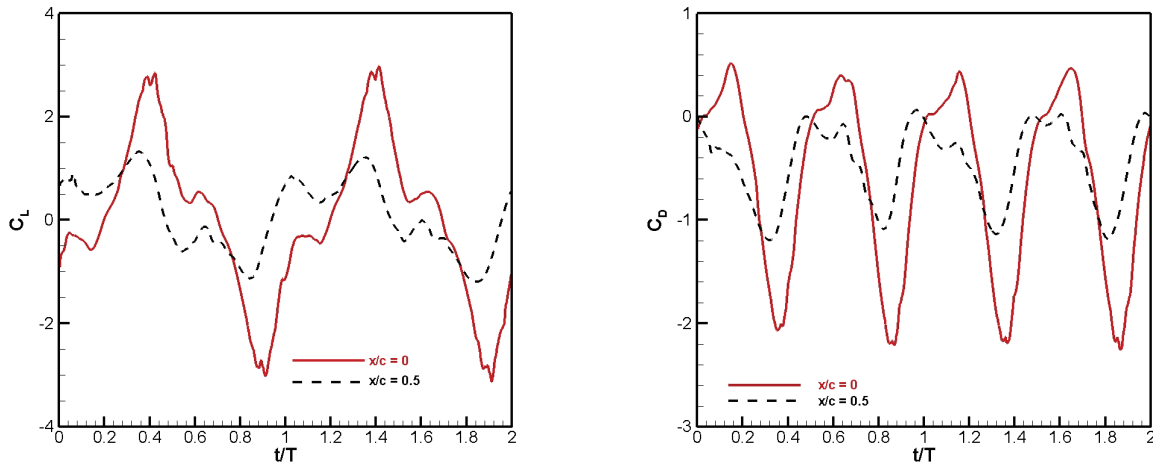


Figure 14. Pitching axis effect: Time history of lift and drag coefficients.

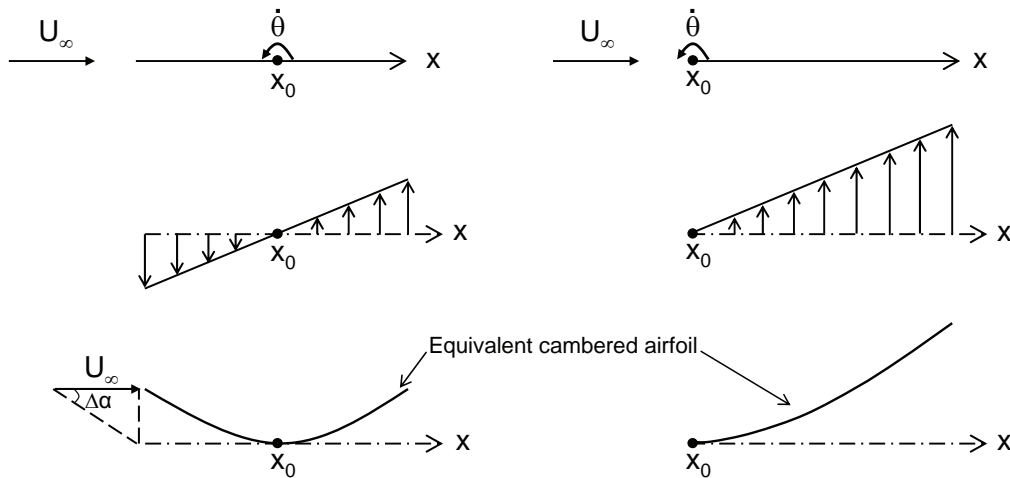


Figure 15. Illustration of pitching induced cambered-wing effect. Left: $x_0/c = 0.5$; right: $x_0/c = 0$.

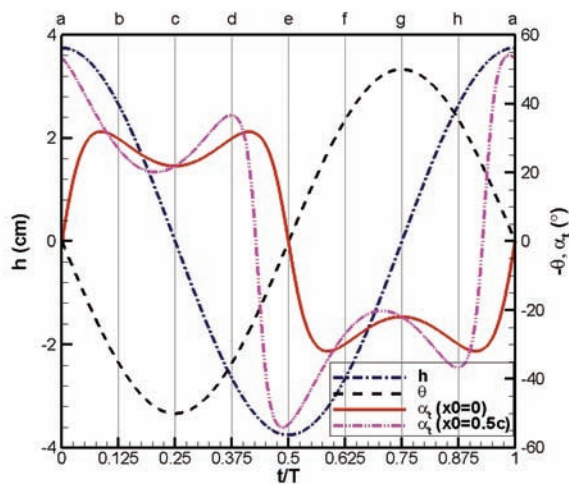


Figure 16. Influences of pitching axis locations ($x_0/c = 0$ vs. $x_0/c = 0.5$) on instantaneous angle of attack at leading edge of the flapping airfoil.

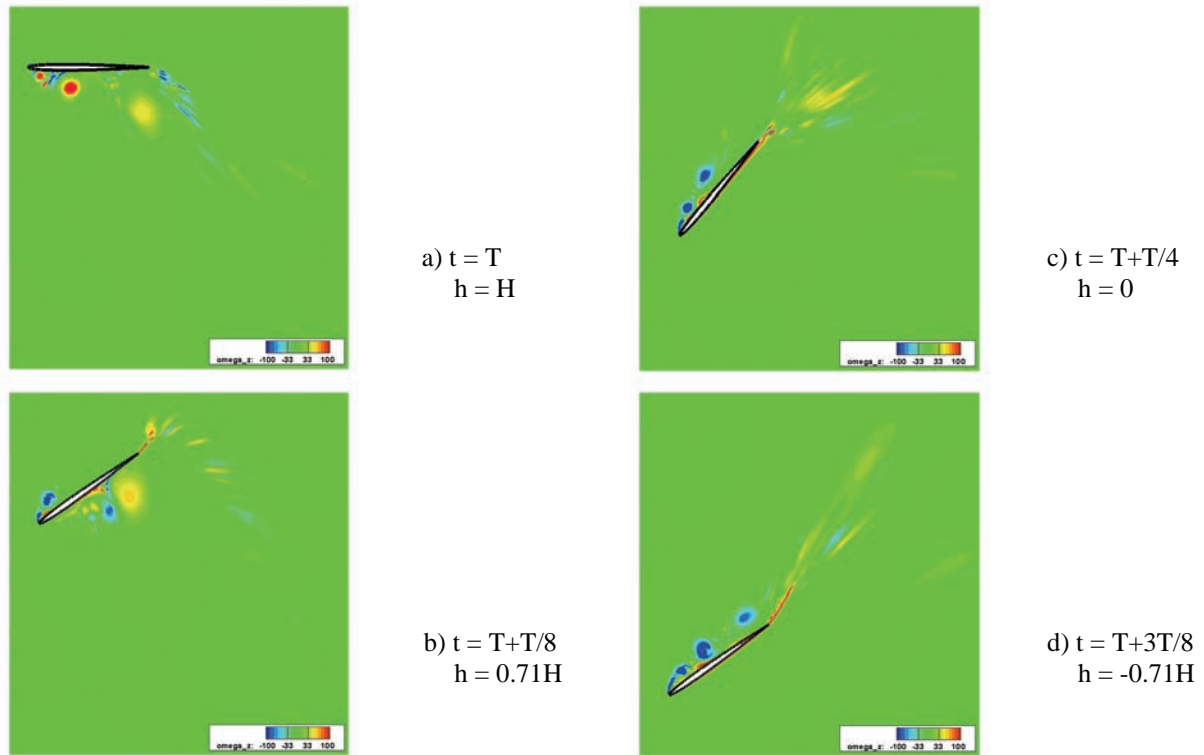


Figure 17. Spanwise vorticity over the flapping NACA 0005 airfoil during the downstroke period with pitching axis $x_0/c=0.5$ at $Re = 1.2 \times 10^4$.

ACKNOWLEDGMENTS

The authors gratefully acknowledge the support of DRDC Valcartier under grant SDA06-28 that partially funded this research during the project “Flapping wings at low Reynolds numbers”. Sincere thanks are given to the project team members F. Lesage and N. Hamel from DRDC Valcartier, P. Zdunich from Advanced Subsonics in Toronto for meaningful discussions. X. Huang from NRC-IAR made some valuable suggestions towards cambered-wing effects in the analysis portion of the paper.

REFERENCES

- [1] Weis-Fogh, T., “Quick Estimates of Flight Fitness in Hovering Animals, including Novel Mechanisms for Lift Production”, *Journal of Experimental Biology*, 59:169-230, 1973.
- [2] Ellington, C. P., “The Aerodynamics of Hovering Insect Flight”, *Philosophical Transactions of the Royal Society of London, Ser. B Biological Sciences*, 305, 1984.
- [3] Yuan, W., Khalid, M., “Computation of Unsteady Flows past Aircraft Wings at Low Reynolds Numbers”, *Canadian Aeronautics and Space Journal*, 50(4):261-271, 2004.
- [4] Patankar, S. V., *Numerical Heat Transfer and Fluid Flow*, Hemisphere Publishing Corporation, Washington New York London, 1980.
- [5] Ferziger, J. H., Perić, M., *Computational Methods for Fluid Dynamics*, Springer-Verlag, Berlin & Heidelberg, 1996.
- [6] Smagorinsky, J., “General Circulation Experiments with Primitive Equations”, *Monthly Weather Review*, 93:99-164, 1963.
- [7] Yuan, W., Schilling, R., “Numerical Simulation of the Draft Tube and Tailwater Flow Interaction”, *Journal of Hydraulic Research*, 40(1):73-81, 2002.
- [8] Demirdžić, I., Perić, M., “Finite Volume Method for Prediction of Fluid Flow in Arbitrarily Shaped Domains with Moving Boundaries”, *International Journal for Numerical Methods in Fluids*, 10:771-790, 1990.

- [9] Yuan, W., Mamou, M., Khalid, M., Wokoeck, R., Radespiel, R., "LES/RANS Simulations of Airfoil Flows near Combined Leading-Edge Trailing-Edge Stall", *24th AIAA Applied Aerodynamics Conference*, San Francisco, AIAA 2006-3177, June 5-8, 2006.
- [10] Yuan, W., Xu, H., Khalid, M., Radespiel, R., "A Parametric Study of LES on Laminar-Turbulent Transitional Flows past an Airfoil", *International Journal of Fluid Dynamics*, 20(1): 45-54, 2006.
- [11] Yuan, W., Khalid, M., Windte, J., Scholz, U., and Radespiel, R., "Computational and Experimental Investigations of Low-Reynolds-Number Flows past an Airfoil", *The Aeronautical Journal*, 111(1115):17-29, 2007.
- [12] Arina, R., Atkin, C., Hanff, E., Jones, K., Lekas, T., Ol, M., Khalid, M., McAuliffe, B., Paquet, J.-B., Platzer, M., Radespie, R., Rist, U., Windte, J., Yuan, W., AVT-101 Final Report: *Experimental and Computational Investigations in Low Reynolds Number Aerodynamics, with Applications to Micro Air Vehicles*, RTO Technical Report, NATO, 2006.

This page intentionally left blank.

Annex 5 – ICAS 2006 conference paper; September 2006

This page intentionally left blank.

PRELIMINARY EXPERIMENTS OF A FLAPPING WING IN THREE-DEGREES-OF-FREEDOM MOTIONS

X. Huang and T. Brown
Aerodynamics Laboratory/IAR/NRC Canada

Keywords: *flapping wing aerodynamics, water tunnel experiment, three-degree-of-motion*

Abstract

A preliminary water tunnel experiment was conducted on an insect wing performing three-degrees-of-freedom motions. A bi-fold five-component strain-gauge balance has been developed to measure the aerodynamic behavior of insect's flapping wings.

It has been found that at low to mid- range angles of attack, the normal force and pitching moment of the wing increase as the angle of attack increases. While at high angles of attack, the phase shift between the motion and the aerodynamic loads becomes obvious. The maximum normal force appears much ahead of the maximum angle of attack and decrease dramatically thereafter as the angle increases further.

Introducing second and third degrees-of-freedom motions could further increase the maximum normal force compared with one-degree-of freedom motion, indicating possible delayed stall caused by the additional motions.

1. Introduction

There is keen interest in insects' flapping wing aerodynamics. To support the insects' body weight, their wings typically produce two to three times more lift than can be accounted for by conventional aerodynamics^[1]. Research results from biologists and zoologists show that insects with flapping wings can fly thousands miles at extremely high lift-to-drag ratios and with great stability and maneuverability which cannot be explained by conventional aerodynamic principles. It is hoped that a better understanding of aerodynamics and flight dynamics of these highly successful creatures

might provide insights for the design of realistic micro air vehicles.

Although the solution is not clear at this time, insects' flapping wings have at least three remarkable features: 1) complex three-degrees-of-freedom motions, 2) deforming wing structure during the motion history and 3) micro surface devices for active flow control (Fig. 1 and Fig. 2). With those features insects achieve their excellent aerodynamic performance by delayed stall, rotational circulation, wake capture and interaction of these distinct mechanisms. For a hovering Hawkmoth^[2], for example, the vortical unsteady and highly non-linear flow at low Re numbers, caused by rapid up/down stroke in combination with rotating about its long axis and tilting the wings to appropriate angles, must be responsible for creating sufficient lift and control power (Fig. 1). Understanding the complex aerodynamic flow around the insect as it is controlled by these remarkable features is a prerequisite to building a real robotic "insect".

In the past few years, much progress has been made in revealing the unsteady high-lift mechanisms of flapping wings^[3]. Among others, Dickinson et al. have developed instruments and procedures used in their experiments to measure the two-dimensional forces (lift and drag) in still fluid^[4,5]. However, as the high aerodynamic performance of insect's wings is achieved by three-degrees-of-freedom (3DOF) motions, it will be very important to study its aerodynamic behavior under 3DOF conditions. Thus, a 3DOF system, i.e. pitch motion (α), dihedral motion (γ) and sweep motion (Λ), has been developed and the preliminary experimental studies were conducted on a flapping wing in the IAR water

tunnel. This paper presents the development of the experimental techniques and some preliminary experimental results.

2. Experimental set-up

The experiments were conducted in the IAR water tunnel (Fig. 3). The water tunnel has an open surface test section with a vertical return circuit. The test section is 15in wide and 20in high. The free-stream turbulence level in the tunnel is rated at $u/U_\infty < 1\%$. Much care was exercised in ensuring that the turbulence screens were always free of trapped air bubbles and that a constant temperature of $22^\circ\text{C} \sim 24^\circ\text{C}$ was maintained. The uniformity of the velocity field in the empty tunnel has been validated by the PIV measurements at all Reynolds number conditions of interest.

A half model test method was used in the experiments (Fig. 4). An insect-like wing was set vertically in the water flow. Except for the wing, all of the equipment was above the water surface, including a 3DOF gearbox, a 3DOF control system and a small five-component strain gauge balance (Fig. 5 to Fig. 7).

The 3DOF system controlled three angular motions: pitch motion (α), dihedral motion (γ) and sweep motion (Λ). The standard terminologies and nomenclatures used in fixed wing aerodynamics are adopted here. The body axes system is shown in Fig. 8. Three angles are taken as the motion parameters, i.e. angle of attack (α), sweep angle (Λ) and dihedral angle (γ), corresponding to feathering motion angle, elevation angle and position angle in some bioflight literature. For example, Fig. 9a shows the three angular motion histories. The consonant wing tip motion history is shown in Fig. 9b.

Pitch angle was mechanically independent but sweep angle and dihedral angle were mechanically linked such that actuating either motor caused the other angle to move. The interaction relationship between sweep angle and dihedral angle is 1:1, degree for degree. That is, if the sweep angle is commanded to move one degree, the dihedral angle will also

move one degree and vice versa. Therefore the equations of motion for these two axes will reflect the interdependent relationship by subtracting one angle from the other.

The gear ratio between the motors and the wing angles was the same for all three axes and equalled 1245:1, 415:1 through the gearhead and 3:1 through the open gearing. One motor revolution caused 0.29° deflection in wing angle. Although the maximum no-load speed of the motors is 28,000 rpm, the maximum continuous motor speed recommended for the gearhead was 5,000 rpm, making the maximum recommended rate of change in wing angles equal to $24^\circ/\text{s}$. The stall torque for the motor was 1.6 oz-in. but the recommended continuous motor torque load for 5,000 rpm is 0.42 oz-in. However the recommended maximum continuous torque output from the gearhead is 42.5 oz-in. generated by 0.18 oz-in of motor torque, well within the motor's capability. This translates to a maximum torque available at the wing center of rotation of approximately 100 oz-in for pitching moment and yawing moment and 65 oz-in for rolling moment. Rolling moment is reduced by two additional sets of 80% efficient gears and bearings that the other axes do not have. The instantaneous torque values are permitted 150% higher than the continuous values. The system was carefully adjusted to reduce the backlash. However it has been found that there was about 1° in yawing motion which causes some inaccuracy in the measurements and has to be modified in the future.

The 3DOF system was controlled by three stepping motors. Faulhaber 1628T012BK312 brushless motors, Series 16/7 415:1 gearhead and HEM1626T16 encoder were installed and connected to the gearbox. The LabView software was used to control the motors that actuated the 3-axes-of-motion gearbox. Model motion programming also included safety limits; 1) load limits provided by the strain gauge balance output, 2) torque (current) limits on the motors, 3) a warning to the operator if limits were approached and 4) halt the motion if limits were exceeded.

A Discrete Fourier Transform (DFT) program computed on equal frequency intervals. The related motion control system was determined by Fourier series in the corresponding Fourier equations:

$$F(t) = a_0 + \sum a_n \cos(n * kt) + b_n \sin(n * kt)$$

The results composed of four parts: real part, imaginary part, correspond frequency and amplitude. The Inversed Fourier Transform (IFT) was used to transfer the output into the time domain. A trail candidate in the Fourier equations was adopted by analyzing the flapping motions of the birds with hover motion the following series. In that example the following Fourier series were taken from a photo of insect's flight.

	Pitching motion		Yawing motion		Rolling motion	
n	an	bn	an	bn	an	bn
0	-0.8615	0.0000	-0.1653	0.0000	1.9644	0.0000
1	-0.1255	1.1978	1.6732	0.2239	1.7860	0.7745
2	0.0233	0.1214	0.4018	-0.1053	0.3367	-0.0280
3	-0.1048	0.1477	0.1002	0.0154	0.1936	0.0960
4	-0.0097	0.1958	-0.0115	0.0314	0.0691	0.0408
5	0.0894	0.1017	0.0110	0.0355	0.0134	0.0004
6	0.0503	0.0403				
7	0.0399	0.0634				
8	0.0377	0.0410				
9	0.0227	0.0170				

The comparisons between calculated and raw data are shown in Fig. 10a through Fig. 10c, which give confidence to the program.

The five-component strain gauge balance supported the wing on one end and was connected to the motion system on other end (Fig. 5b). The balance consists of five elements corresponding to each aerodynamic force or moment including normal force (N), drag (X), pitching moment (m_z), yawing moment (m_y) and rolling moment (m_x). Fig. 8 shows the coordinate axes system. As seen from Fig. 3b, the rotation center of the wing was above the balance reference center. In order to mimic real insect's flight, it is important to shorten the length of the balance as much as possible. However, shortening the length of the elements in the balance reduces sensitivity. Thus a new concept of bi-fold concept was introduced as

shown in Fig. 11 which shows all parts before its assembly. Not like conventional balances where the length of the balance is the sum of each element, the new concept of the bi-fold balance makes the length of each element close to the length of the total balance. It also has the advantages of easy manufacturing, gauging and wiring. The calibration results confirm that the balance satisfies the experimental requirements.

An insect-like wing model was used in the experiments. Its section view, plan view and 3D view are shown in Fig. 12. The corresponding plan and section coordinates are listed in Table 1. The model was constructed using a rapid prototyping (RP) and Stereolithography technique at IAR. The laser beam was guided by an X-Y stage that followed the computerized coordinates of the 3D object. The surface details resolved to $3\mu\text{m}$. The resulting model is a rigid solidified photopolymer. It is a solid wing model and obviously lacks the deformability of a real, feathered wing.

3. Preliminary Experimental Results and Discussions

The aerodynamic loads and motions were recorded synchronously during the experiments with a maximum sample rate of 100/sec. Different motion profiles were tested – from 1DOF (pitching motion) to 3DOF motion. The ranges of angle of attack, sweep angle and dihedral angle were $\pm 60^\circ$, $\pm 20^\circ$ and $\pm 20^\circ$ respectively. The tested Reynolds number, based on the mean aerodynamic chord (1.5in), ranged from 5×10^3 to 10×10^3 . The reference area for coefficients is the wing plan area. The reference length for pitching moment is the mean aerodynamic chord while for yawing and rolling moment is the wing span (5in). The reference centers for the three moment coefficients are in the center of the balance, which can be found in Fig. 3d.

Samples of preliminary results are shown from Fig. 13 to Fig. 15. As more experiments will be conducted in the near future, here only

brief analysis and discussion are given for those preliminary experiments.

First of all, the measured aerodynamic loads are not very smooth, even for one degree-of-freedom motions at low angles of attack (Fig. 13b). The data reported in those figures were recorded at $\Delta t=0.03$. No smoothing techniques were used in the data reduction. Also, mechanical backlash was checked before each test. It was found that only the sweep motion had 1° of backlash. Thus it is not very clear at this time what causes the unsmooth behavior. Nevertheless, we can still, in general, draw something from these experimental results.

Fig. 13 presents the results for 1DOF (pitching motion) from $\alpha=-2^\circ$ to 20° , where Fig. 13a is the motion profile and Fig. 13b shows the measured coefficients. The coefficients of pitching moment (m_z) and normal force (C_N) increase as the angle of attack increases until the angle of attack reaches a maximum of 20° and then decreases as α decreases. The almost synchronous increase of pitching moment and normal force indicates that the location of center of pressure may not change too much as the angle changes. Fig. 14 shows results for the angle of attack in the range of $\alpha=-8^\circ$ to 60° . Compared with Fig. 13 it can be seen that the maximum normal force does not increase linearly as the angle of attack increases. Moreover, the maximum normal force appears at $\alpha\approx 40^\circ$. Further increase of angle of attack results in the dramatic decrease in normal force and pitching moment. It indicates that the stall happens when $\alpha>40^\circ$ and eventually occurs over the whole wing area. Nevertheless, the maximum normal force coefficient could reach $C_N=1.2$ at $\alpha\approx 40^\circ$. Compared with 1DOF motion, the 3DOF motion brings more interesting results as seen in Fig. 15. When the wing performs 3DOF motion as shown in Fig. 15a, the corresponding aerodynamic coefficients are shown in Fig. 15b. The pitching motion in 3DOF motions (Fig. 15a) is the same as 1DOF motion in Fig. 14a but two other motions are added: sweep motion and dihedral motion. Compared with Fig. 14b it can be observed that the maximum normal force could reach $C_N=1.4$.

It may indicate that there is some delayed stall as 3DOF motion is involved. Also the drag in Fig. 15b is higher than that in Fig. 14b. Comparing 1DOF with 3DOF motion results, one finds that the aerodynamic coefficients exhibit quite different behavior. Dihedral and sweep motion could increase the maximum normal force and expand its area. Also it will create higher negative force when the wing is in upstroke. This negative force is actually a thrust when the angle of attack is larger than 90° , as the wing uses the mechanism of wake capture.

As mentioned above, in order to further investigate the flow behavior, the uncertainty caused by backlash in the mechanism should be minimized or eliminated. Also, in order to fully understand the flow behavior, flow visualization experiments should be conducted.

4. Conclusions

- A three-degrees-of-freedom motion system including a bi-fold five-component strain-gauge balance has been developed which can be applied to study the aerodynamic behavior of insect's flapping wings.
- At low to mid-range angles of attack, the normal force and pitching moment of the tested insect-like wing increase as the angle of attack increases.
- At high angles of attack, the phase shift between the motion and the aerodynamic loads becomes obvious. The maximum normal force appears much ahead of the maximum angle of attack. After that angle, the normal force decreases dramatically as the angle increases further, indicating that stall develops over the wing.
- Three-degrees-of-freedom motion could further increase the maximum normal force compared with one-degree-of-freedom motion, indicating possible delayed stall by the 3DOF motion.

Acknowledgement

The work was partly supported by the Department of the National Defence Canada / DRDC under the Collaboration Agreement:

“Flapping Wings Aerodynamics for Efficient Insect-Size Aircrafts.”

5. References

- [1] Ellington, C.P., “The Novel Aerodynamics of Insect Flight: Application to Micro-Air Vehicles,” *The Journal of Experimental Biology* 202, 3439-3448, 1999.
- [2] Liu, H. and Kawachi, K., “Leading-Edge Vortices of Flapping and Rotary Wings at Low Reynolds Number,” Chapter 14, Vol. 195, *Progress in Astronautics and Aeronautics*, 2001.
- [3] Mueller, T.J., “Fixed and Flapping Wing Aerodynamics for Micro Air Vehicle Application,” *Progress in Astronautics and Aeronautics*, Vol. 195, 2001.
- [4] Dickinson, M.H., Lehmann, F.O. and Sane, S.P., Wing Rotation and the Aerodynamic Basis of Insect Flight. *Science* 284, 1954-1960, 1999.
- [5] Sane, S.P., and Dickinson, M.H., The Control of Flight Force by a Flapping Wing: Lift and Drag Production. *J. Exp. Biol.* 204, 2607-2626, 2001.
- [6] Huang, X.Z., Wong Frank, T. Brown and Berlivet T., “Development of Bi-Fold Water-Tunnel Half Model Balance,” IAR Rep. 2006.

Table 1 wing coordinates (plan view)

x	y (TE)	x	y (LE)	c
0.0000	0.1700	0.0000	0.4991	0.3291
0.0652	0.1680	0.0652	0.4991	0.3311
0.1369	0.1600	0.1369	0.4997	0.3397
0.2087	0.1550	0.2087	0.5003	0.3453
0.2739	0.1350	0.2739	0.5006	0.3706
0.3325	0.1100	0.3325	0.4997	0.3897
0.3977	0.0660	0.3977	0.5027	0.4427
0.4695	0.0020	0.4695	0.5091	0.5071
0.5347	-0.0650	0.5347	0.5169	0.5869
0.5999	-0.1800	0.5999	0.5287	0.7067
0.6716	-0.4400	0.6716	0.5394	0.9794
0.7303	-0.6400	0.7303	0.5507	1.1907
0.8020	-0.7700	0.8020	0.5619	1.3319
0.8672	-0.8600	0.8672	0.5714	1.4314
0.9389	-0.9500	0.9389	0.5779	1.5279
0.9976	-1.0000	0.9976	0.5827	1.5827
1.0628	-1.0500	1.0628	0.5910	1.6410
1.1476	-1.1090	1.1476	0.5993	1.6993
1.2976	-1.1900	1.2976	0.6094	1.7994
1.4606	-1.2448	1.4606	0.6165	1.8613
1.6171	-1.2804	1.6171	0.6242	1.9046
1.7866	-1.3041	1.7866	0.6325	1.9366
1.9431	-1.3219	1.9431	0.6366	1.9585
2.1191	-1.3272	2.1191	0.6402	1.9674
2.2756	-1.3278	2.2756	0.6402	1.9680
2.4321	-1.3219	2.4321	0.6461	1.9680
2.6147	-1.3041	2.6147	0.6461	1.9502
2.7777	-1.2833	2.7777	0.6461	1.9295
2.9277	-1.2626	2.9277	0.6461	1.9087
3.0907	-1.2318	3.0907	0.6437	1.8755
3.2537	-1.1962	3.2537	0.6427	1.8389
3.4167	-1.1559	3.4167	0.6414	1.7973
3.5862	-1.1097	3.5862	0.6402	1.7499
3.7558	-1.0634	3.7558	0.6372	1.7007
3.9253	-1.0077	3.9253	0.6319	1.6396
4.0883	-0.9484	4.0883	0.6283	1.5768
4.2513	-0.8951	4.2513	0.6218	1.5169
4.4209	-0.8299	4.4209	0.6106	1.4404
4.5774	-0.7676	4.5774	0.5910	1.3586
4.7534	-0.6906	4.7534	0.5661	1.2567
4.9210	-0.6150	4.9210	0.5335	1.1485
5.0788	-0.5365	5.0788	0.4713	1.0077
5.1401	-0.4967	5.1401	0.4400	0.9235
5.2111	-0.4535	5.2111	0.4050	0.8435
5.2822	-0.3983	5.2822	0.3490	0.7362
5.3533	-0.3379	5.3533	0.2900	0.6046
5.4257	-0.2650	5.4257	0.2015	0.4665
5.4772	-0.1800	5.4772	0.0966	0.2922
5.5000	0.0000	5.5000	0.0000	0.0000

wing section coordinates

x	z (upper)	x	z (lower)
0.0002	0.0000	0.0002	0.0000
0.0010	0.0310	0.0010	-0.0280
0.0030	0.0540	0.0030	-0.0530
0.0070	0.0800	0.0070	-0.0800
0.0110	0.0960	0.0110	-0.0946
0.0153	0.1049	0.0153	-0.1059
0.0446	0.1648	0.0348	-0.1304
0.1423	0.3387	0.0934	-0.1958
0.2497	0.4897	0.1911	-0.2813
0.3571	0.6068	0.2985	-0.3485
0.4450	0.6822	0.4255	-0.4010
0.5231	0.7366	0.5915	-0.4403
0.6403	0.8004	0.7380	-0.4578
0.7380	0.8405	0.9626	-0.4681
0.8258	0.8689	1.2070	-0.4692
0.9333	0.8959	1.5290	-0.4631
1.0600	0.9198	2.0470	-0.4306
1.5190	0.9706	2.5250	-0.3610
2.0370	1.0084	3.0330	-0.2423
2.5250	1.0361	3.5310	-0.0967
3.0330	1.0492	4.0390	0.0584
3.5410	1.0428	4.5370	0.1975
4.0490	1.0212	5.0540	0.3159
4.5660	0.9899	5.5430	0.3980
5.0640	0.9537	6.0410	0.4488
5.5430	0.9109	6.5390	0.4641
6.0600	0.8503	7.0370	0.4426
6.5490	0.7753	7.5350	0.3862
7.0470	0.6815	8.0520	0.2982
7.5450	0.5758	8.5600	0.1940
8.0520	0.4631	9.0580	0.0822
8.5600	0.3462	9.5470	-0.0394
9.0680	0.2147	10.0450	-0.1802
9.5470	0.0616	10.3850	-0.2693
10.0450	-0.1205		
10.3850	-0.2126		

PRELIMINARY EXPERIMENTS OF FLAPPING WING IN THREE- DEGREE-OF-FREEDOM MOTIONS

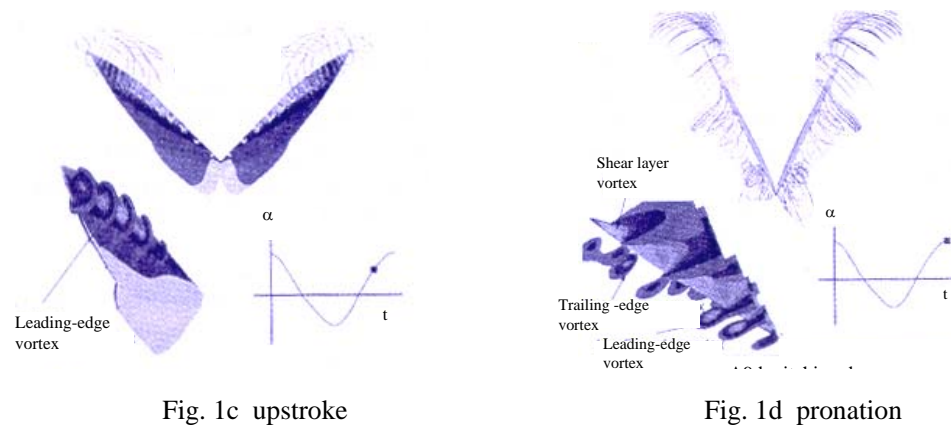
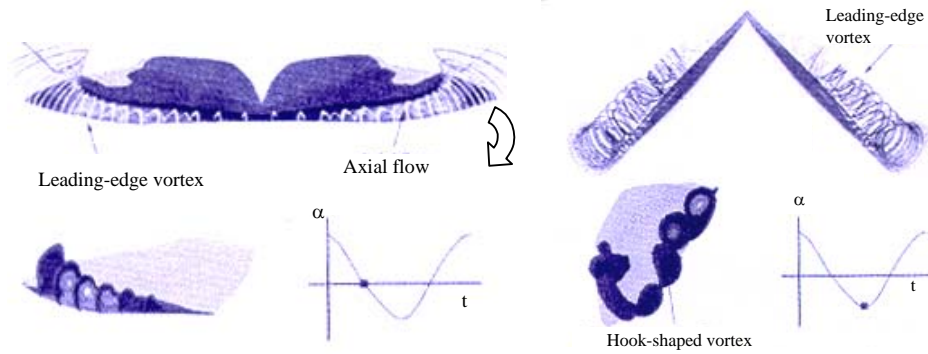


Fig. 1 Dynamic vortex structure around a flapping wing during a complete wing beat cycle^[2]

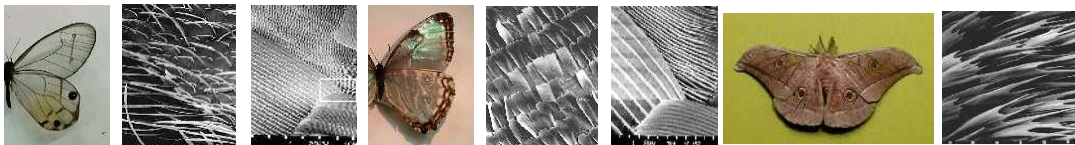


Fig. 2 Complex feather patterns on insect's wing surfaces



Fig. 3 IAR 1520 water tunnel

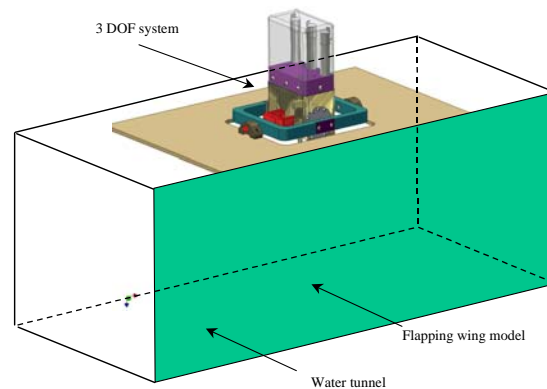
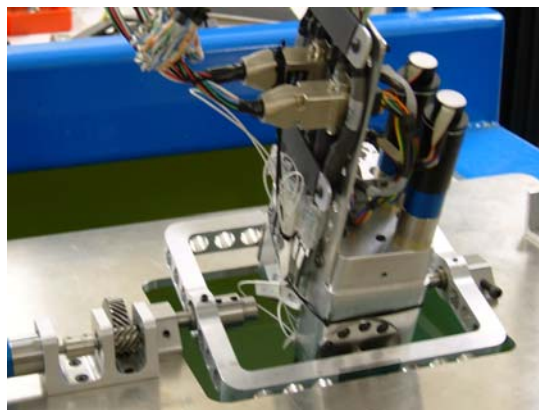
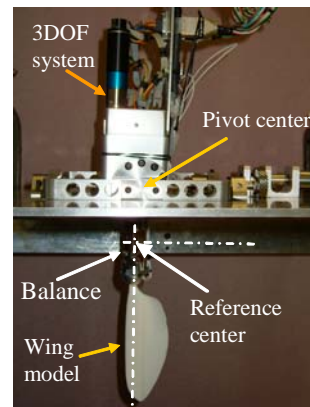


Fig. 4 Schematic 3DOF system set-up



5a top view



5b side view

Fig. 5 Three-degree-of-freedom motion system installed in the IAR water tunnel

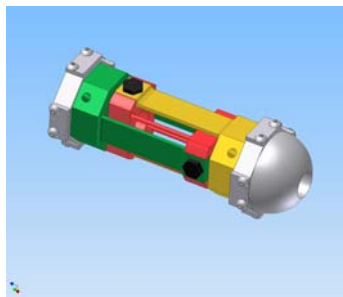


Fig. 6 Five-component strain gauge balance



Fig. 7 Insect-like wing model

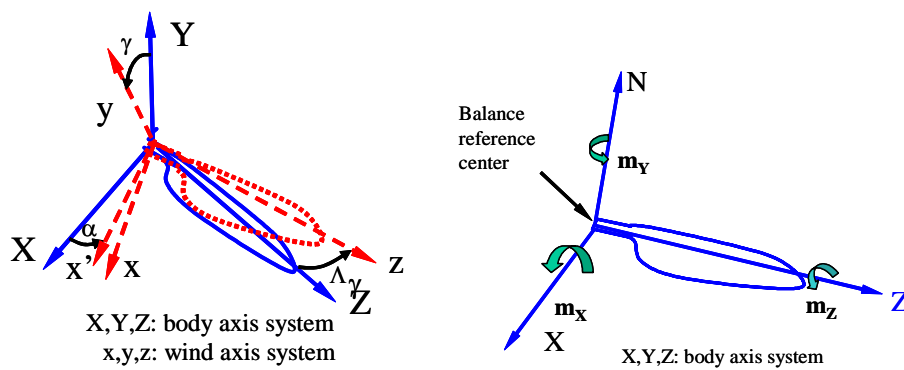


Fig. 8 Coordinate system

PRELIMINARY EXPERIMENTS OF FLAPPING WING IN THREE-DEGREE-OF-FREEDOM MOTIONS

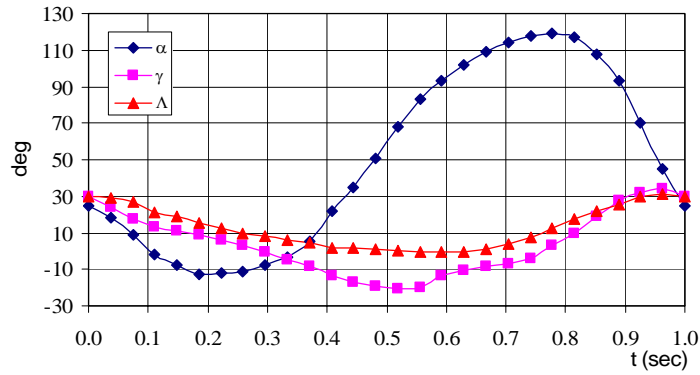


Fig. 9a Sample of three motion parameters' histories

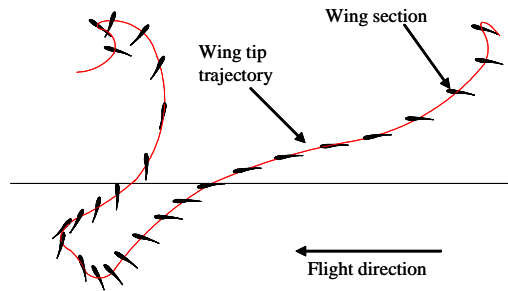


Fig. 9b consonant wing tip motion history
Fig. 9 Motion profile and corresponding parameters

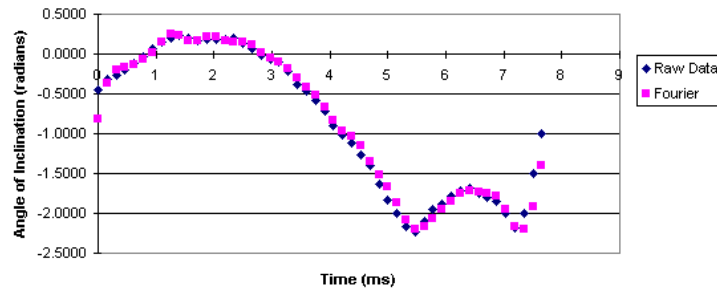


Fig. 10a Comparisons in Pitching motion

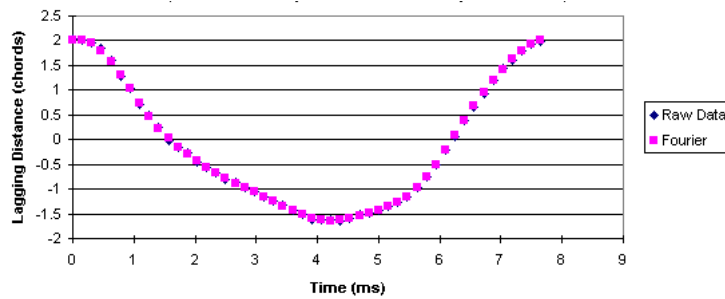


Fig. 10b Comparisons in yawing motion

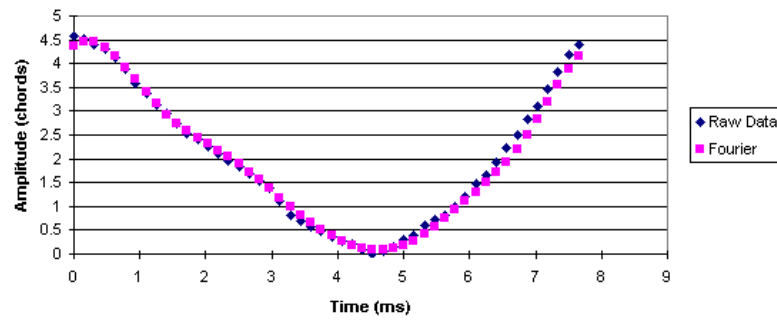


Fig. 10c Comparisons in dihedral motion
Fig. 10 Comparisons between input and output motions

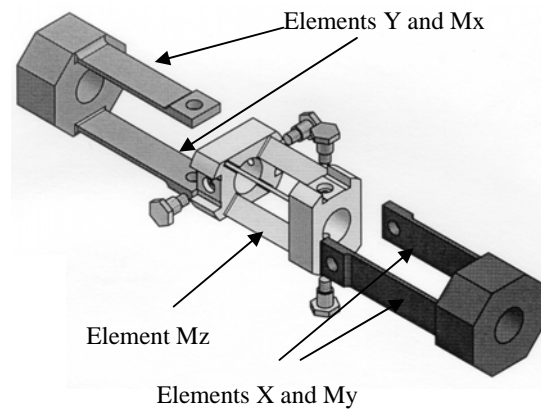


Fig. 11 Schematic of Bi-fold strain gauge balance before assembling

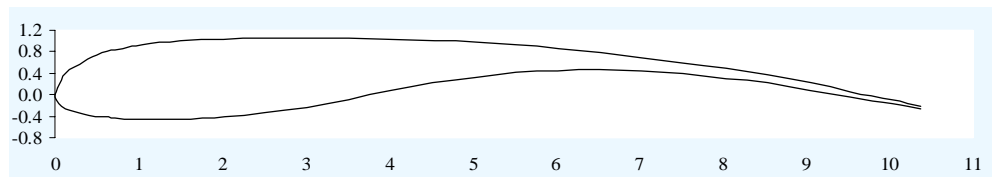


Fig. 12a Section view of the test wing

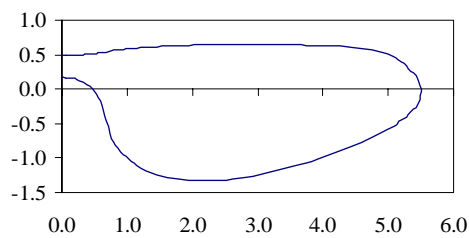


Fig. 12b Plan view of the test wing

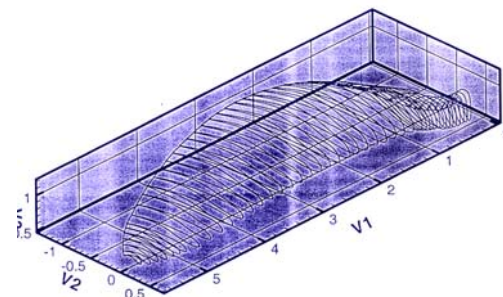


Fig. 12c 3D view of the test wing

Fig. 12 Geometry of tested insect's wing

PRELIMINARY EXPERIMENTS OF FLAPPING WING IN THREE-DEGREE-OF-FREEDOM MOTIONS

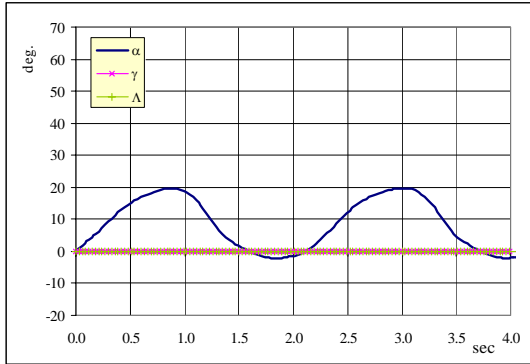


Fig. 13a Motion profile

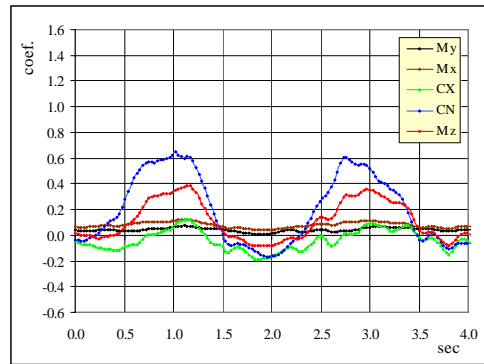


Fig. 13b Measured aerodynamic coefficients

Fig. 13 One-degree-of-freedom motion and corresponding loads

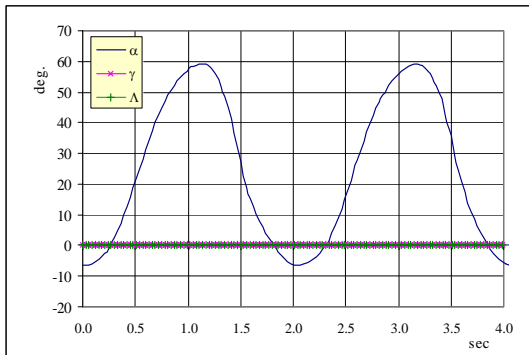


Fig. 14a Motion profile

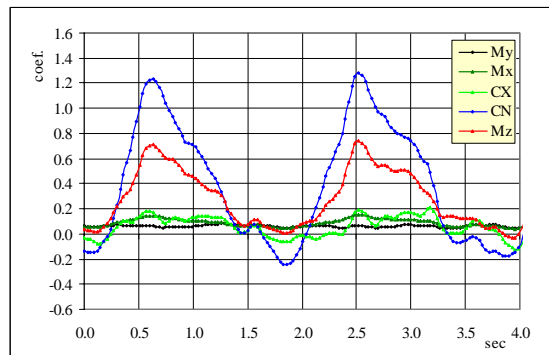


Fig. 14b Measured aerodynamic coefficients

Fig. 14 One-degree-of-freedom motion and corresponding loads

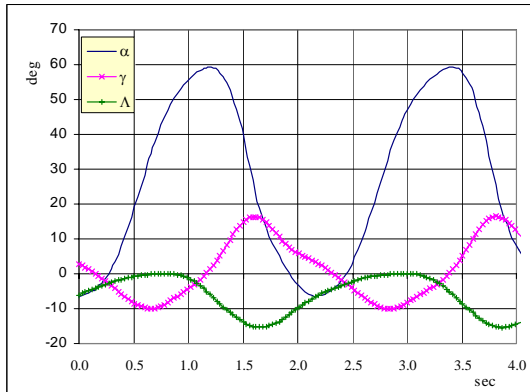


Fig. 15a 3D motion history

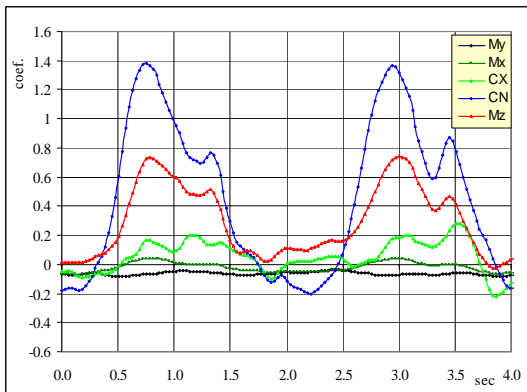


Fig. 15b measured aerodynamic coefficients

Fig. 15 Three-degree-of-freedom motion and corresponding loads

This page intentionally left blank.

Annex 6 – Experimental research on flapping wing aerodynamics; April 2007

This page intentionally left blank.



NRC-CNRC
NRCaerospace.com


***Experimental Research on
Flapping Wing Aerodynamics (TIF Project)***

X. Huang and T. Brown
Aerodynamics Laboratory
Institute for Aerospace Research
National Research Council of Canada

TTCP WPN-2
Ottawa, April 3, 2007

 **National Research
Council Canada** **Conseil national
de recherches Canada**

Canada



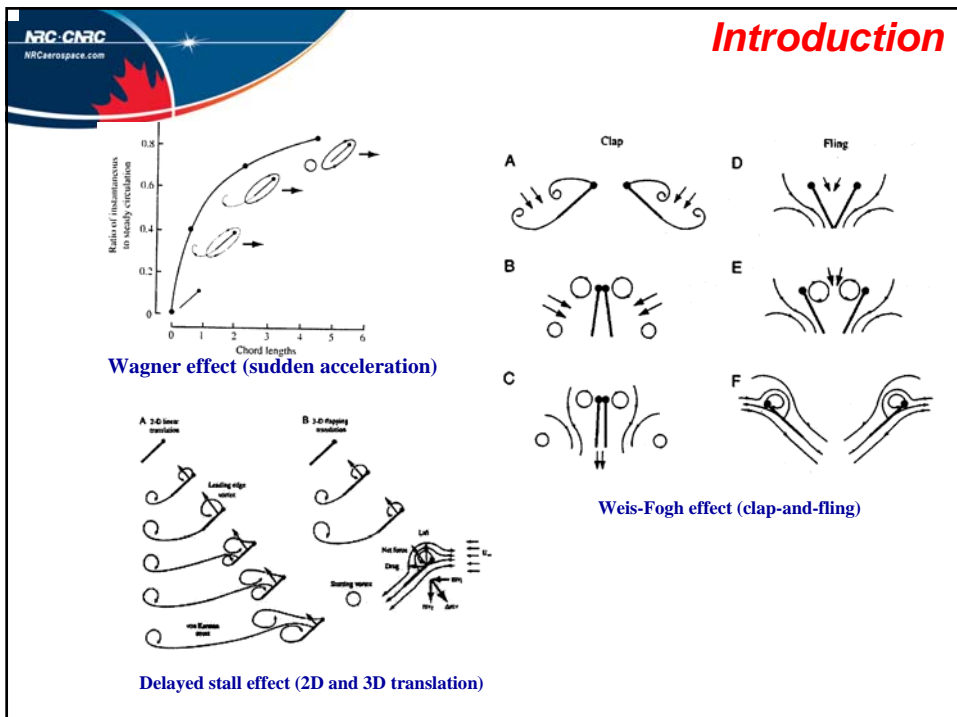
Content


- ❖ **Introduction**
- ❖ **Major Tasks**
- ❖ **Preliminary Experimental Results**
- ❖ **2-D test concept**
- ❖ **3-D test concept**

Introduction

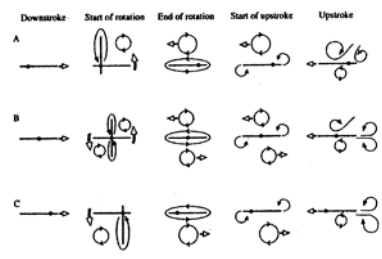
Different aerodynamic principles used by different insect's flapping wings

- 1) Wagner effect
- 2) Weis-Fogh effect (clap-and-fling)
- 3) Delayed stall effect
- 4) Kramer effect (rotational forces)
- 5) Wake capture effect
- 6) Added mass effect
- 7) Thrust-indicative vortex sheet

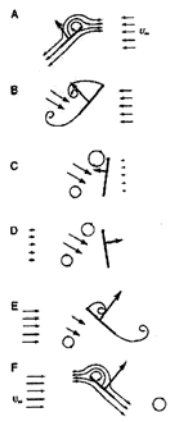





Introduction



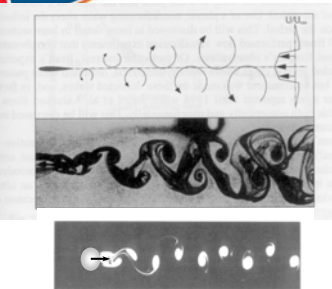
Kramer effect (rotational forces)



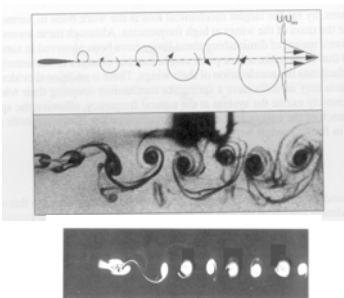
Wake capture effect



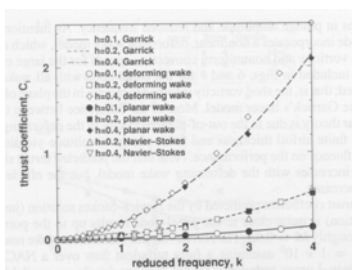
Introduction

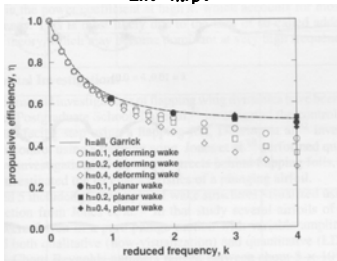


Drag

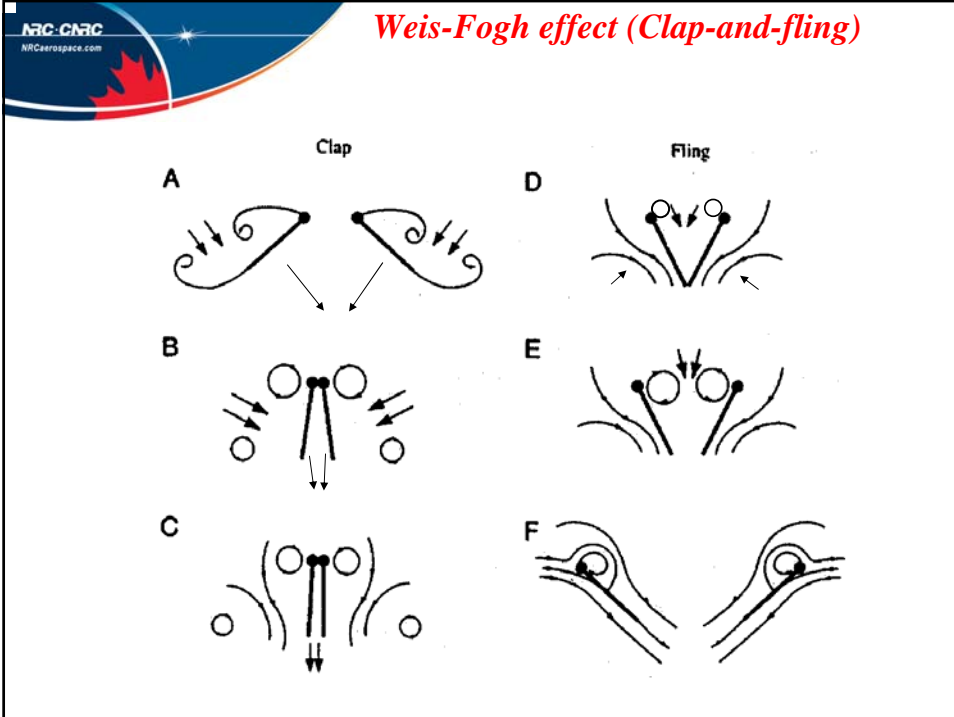


Lift= $4\pi\rho V^2$





Thrust/drag indicative vortex sheet



NRC-CNRC
NRCaerospace.com

Major Tasks

- Long-range micro-scale PIV technology
- Manipulation of mini-scale LE flap
- Preliminary experimental study on 3D motion system with one insect wing
- Developing 2D wing airfoil experiment
- Developing Clap-Fling motion system



NRC-CNRC
NRCaerospace.com

Long-range Micro-Scale PIV set-up in Wall-Bounded Flow Experiments

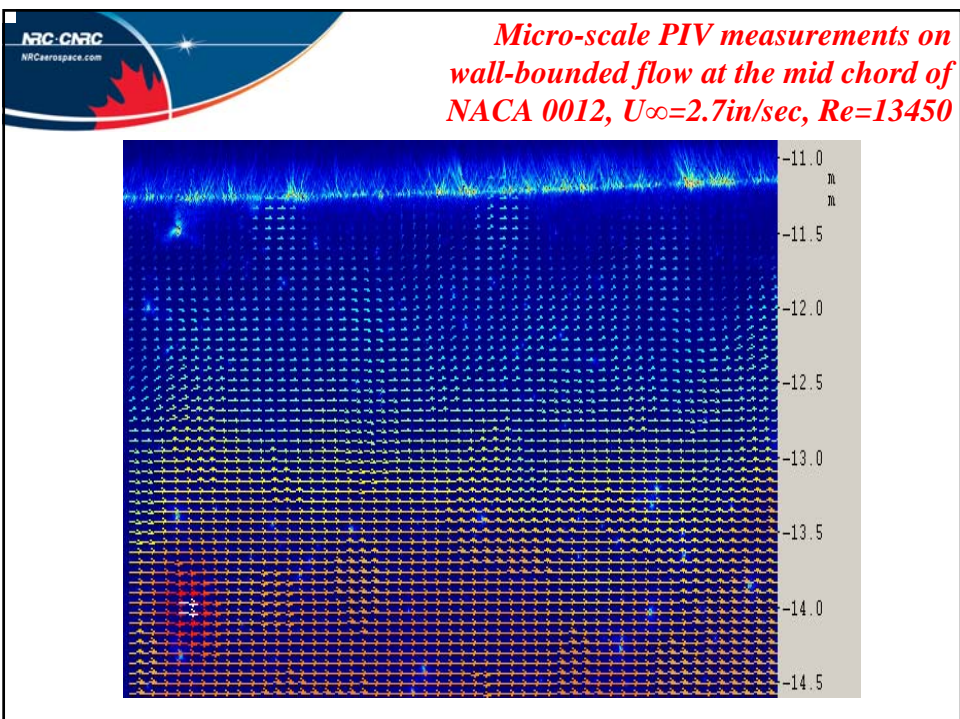


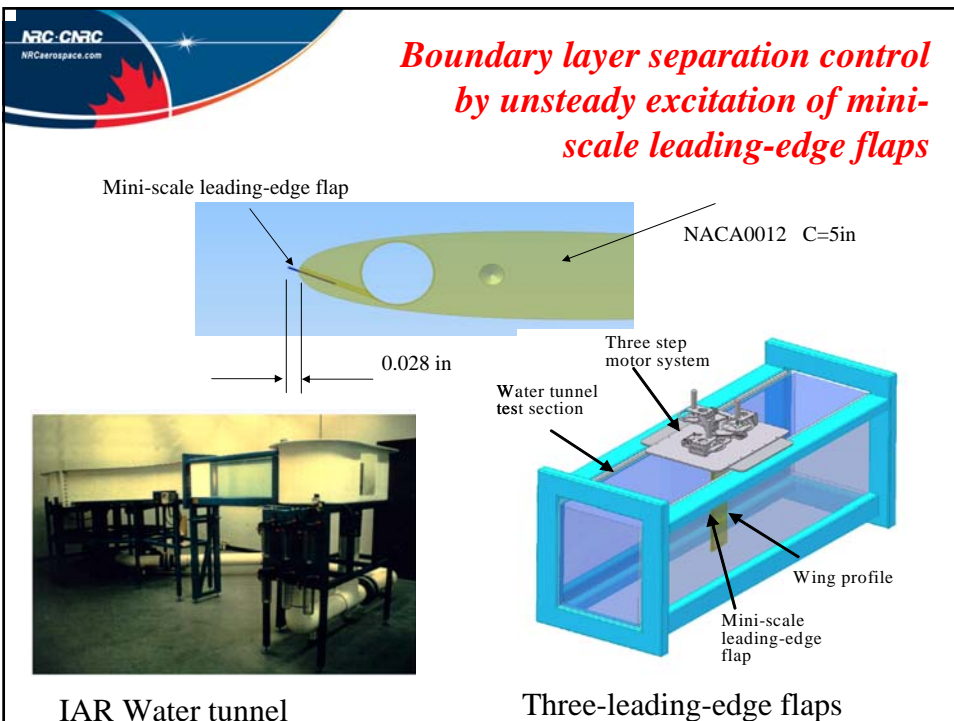
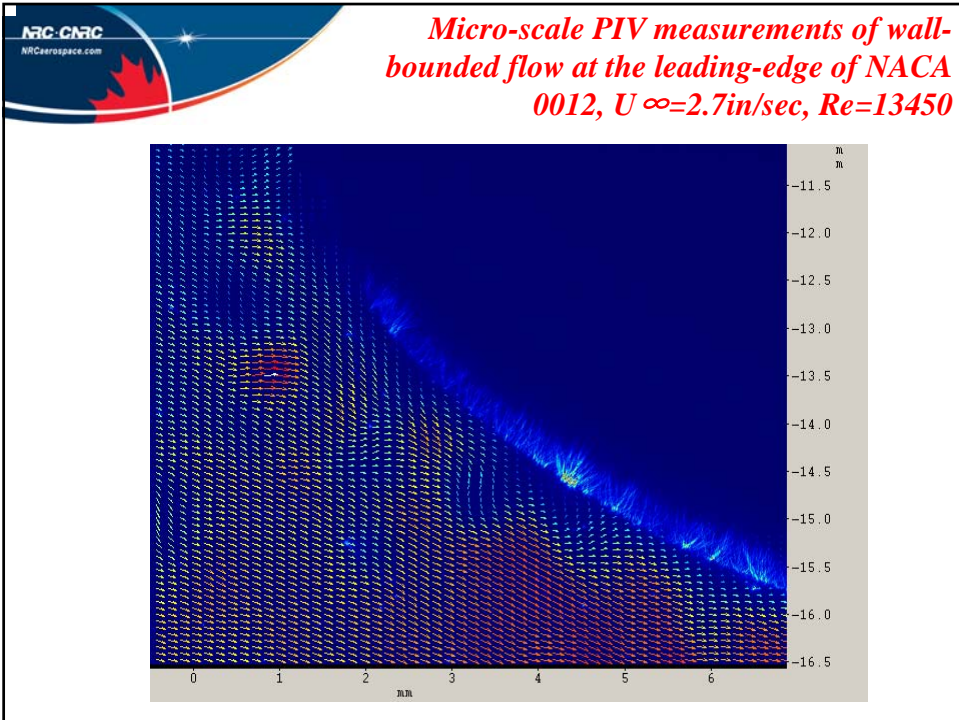
IAR Water tunnel

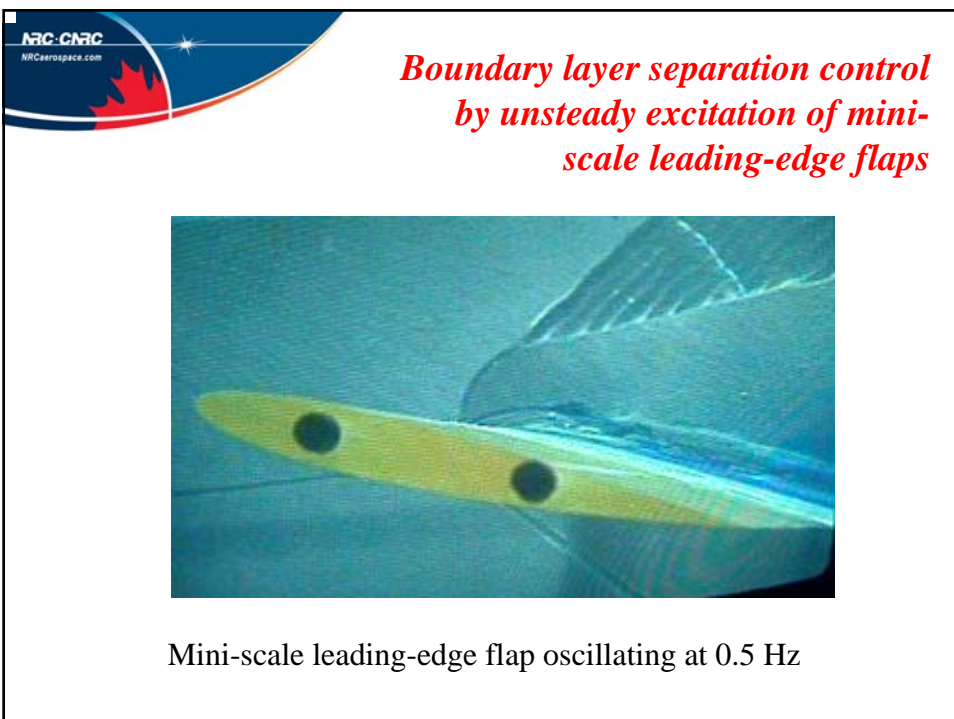
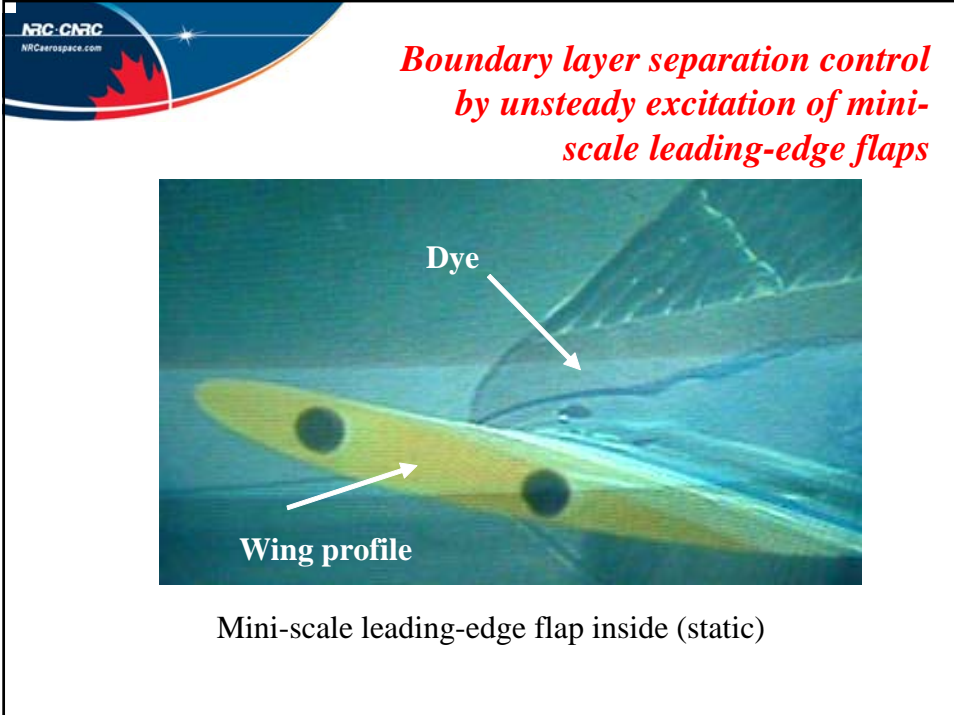


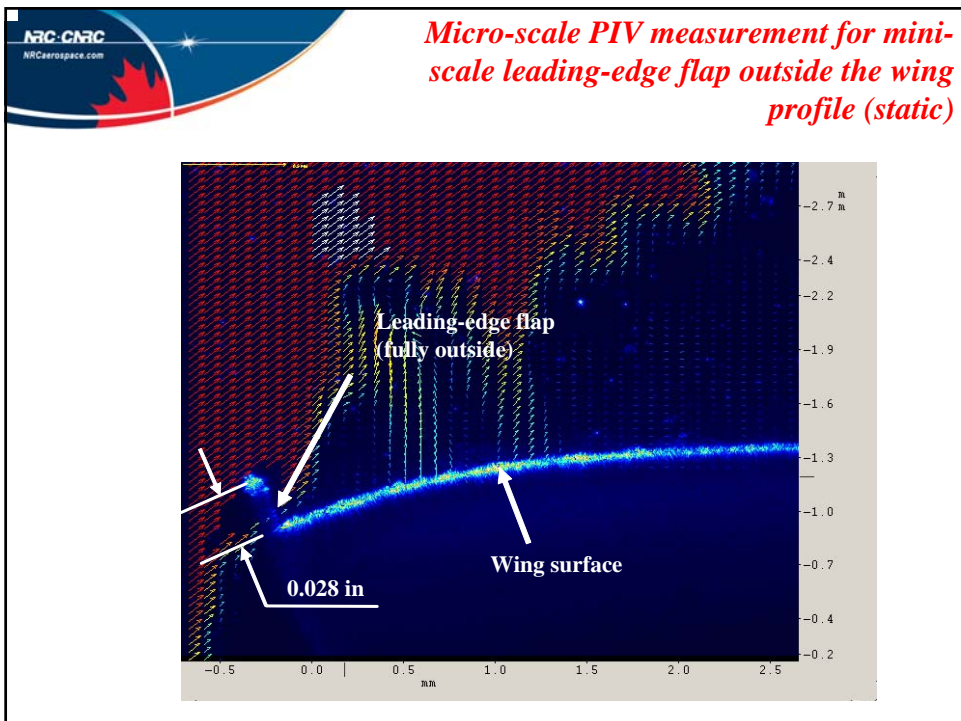
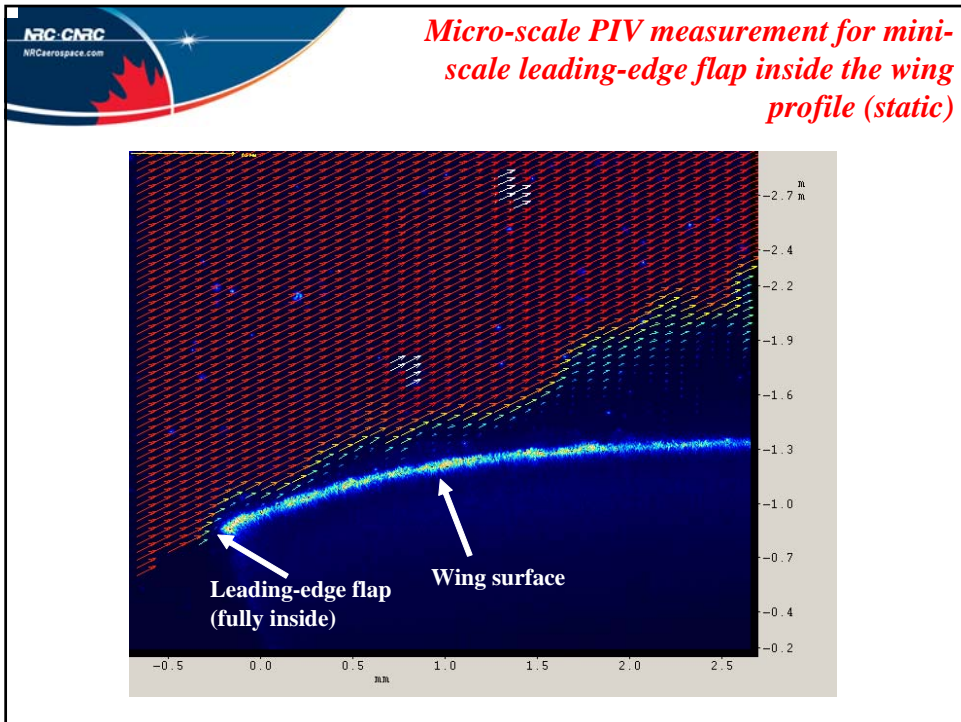
Long-range micro-scale PIV system

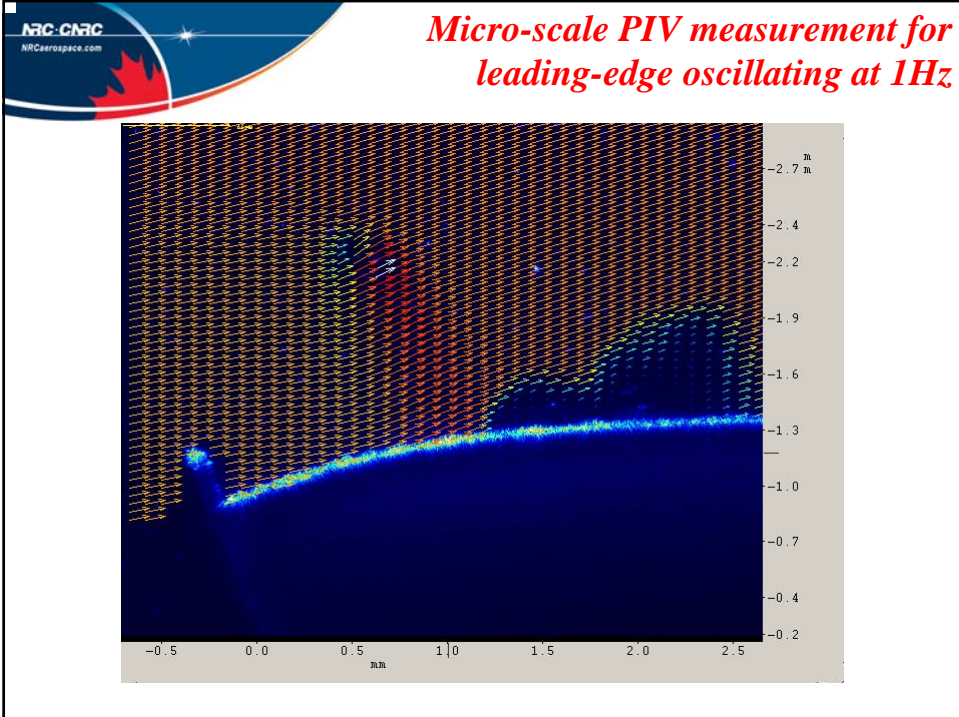
1.5 m range 1~5 μ m resolution, 10mm view area











NRC-CNRC
NRCaerospace.com

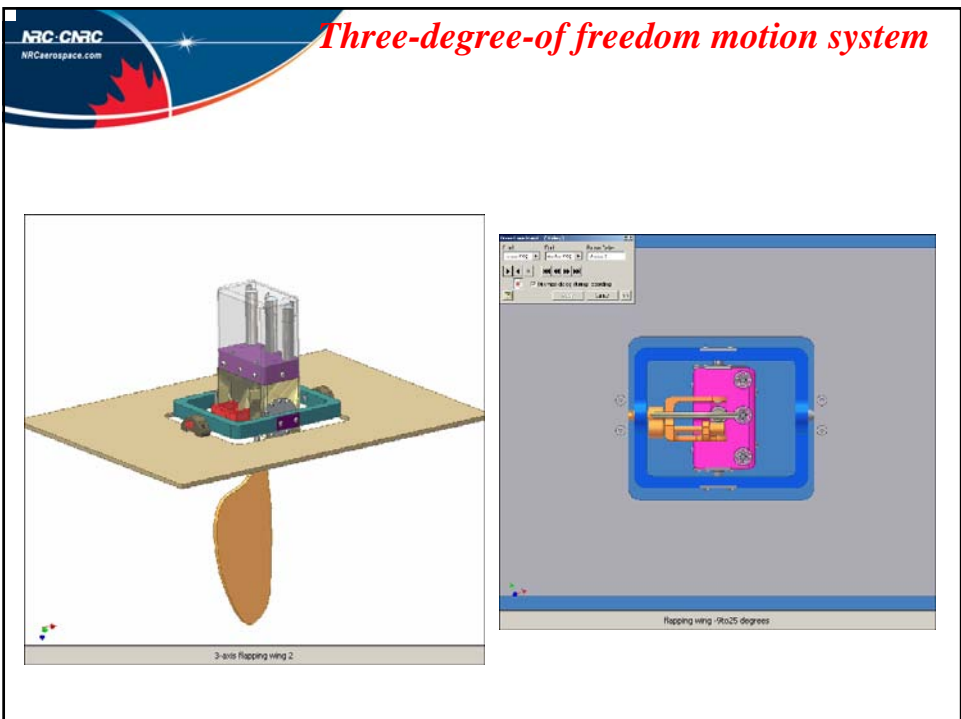
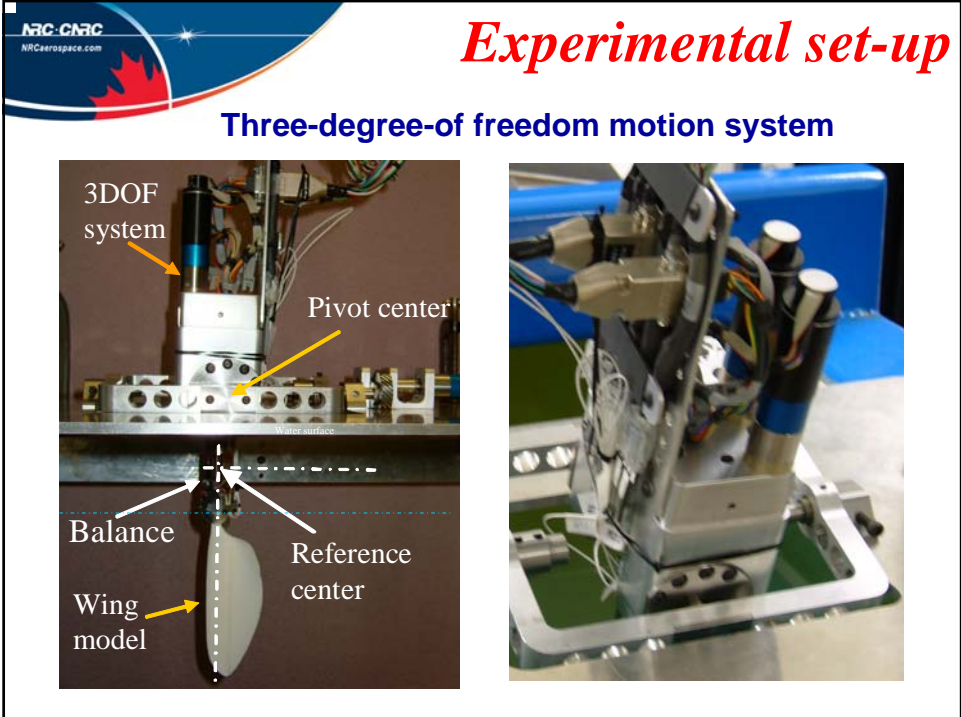
Preliminary Experiments

1. IAR 15x20 Water tunnel
2. Three-degree-of-freedom motion system
3. Five-component balance
4. Flapping wing model
5. 3D Motion and control system

The photograph shows the interior of the IAR 15x20 water tunnel. It features a large open test section with a vertical return circuit, supported by a complex metal frame. Various pipes, valves, and structural elements are visible within the facility.

IAR 15x20 water tunnel

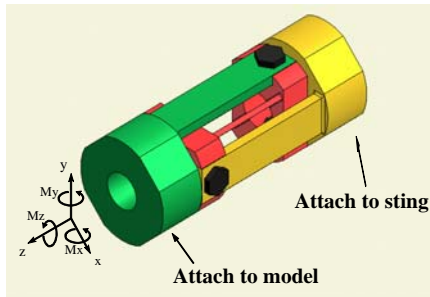
1. Open test section with vertical return circuit
2. Turbulence level $< 0.1\%$
3. $Re_{co}: 600 \sim 2 \times 10^4$
4. Coning motion, pitching and yawing motions,
5. Force, micro PIV and Dye measurement



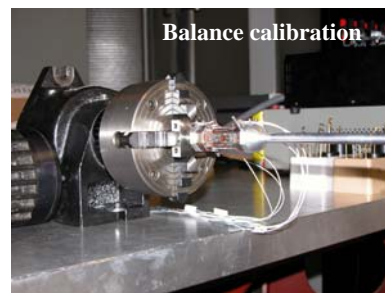
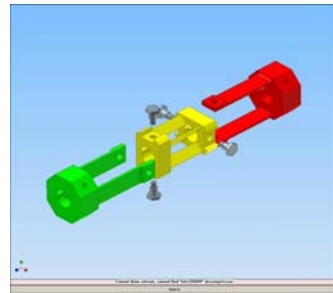
Five-component balance

Five-component Bi-fold balance

- short length
- 5 components
- easy to machine and gauge

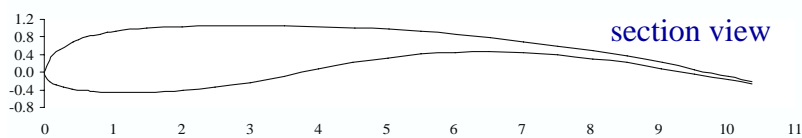


Schematic of 5-component balance



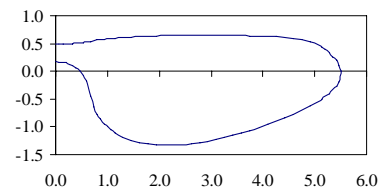
Balance calibration

Bird's wing model

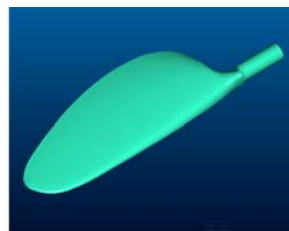


section view

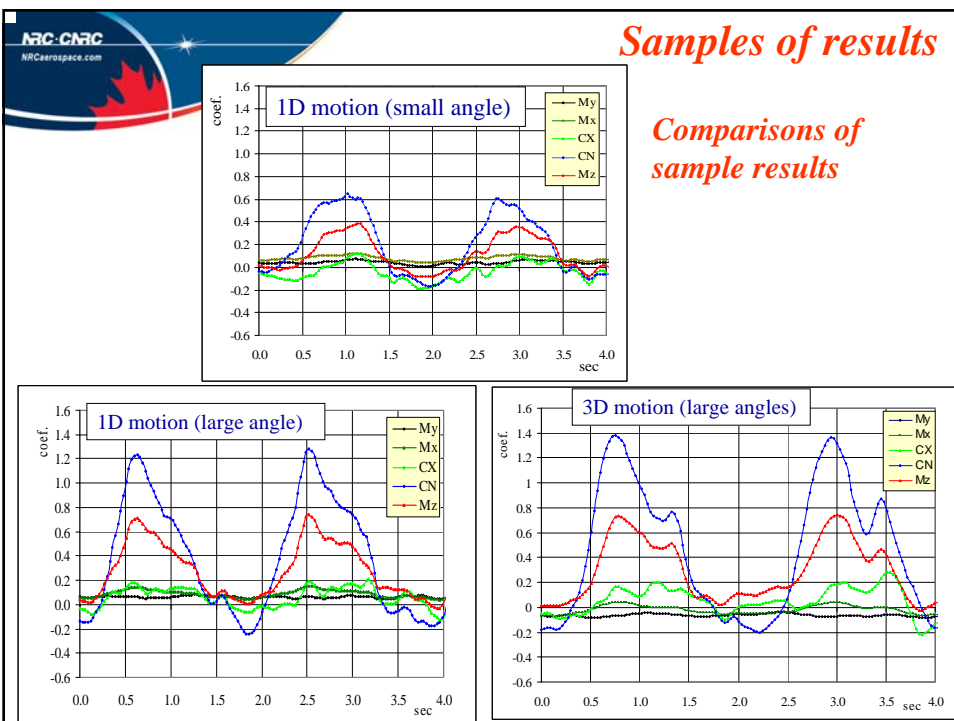
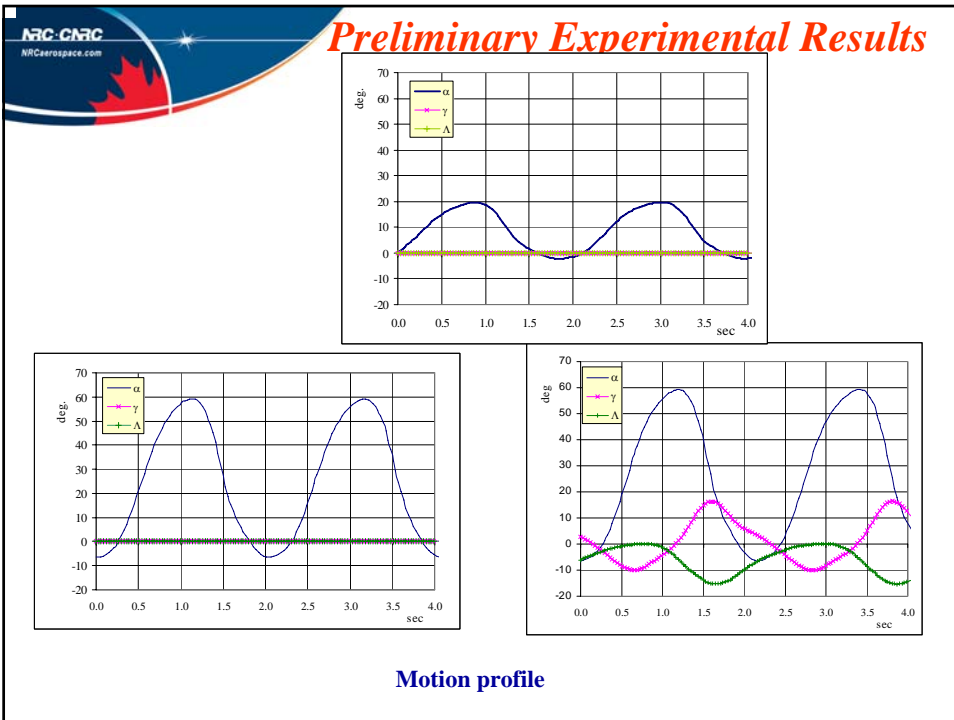
2D view

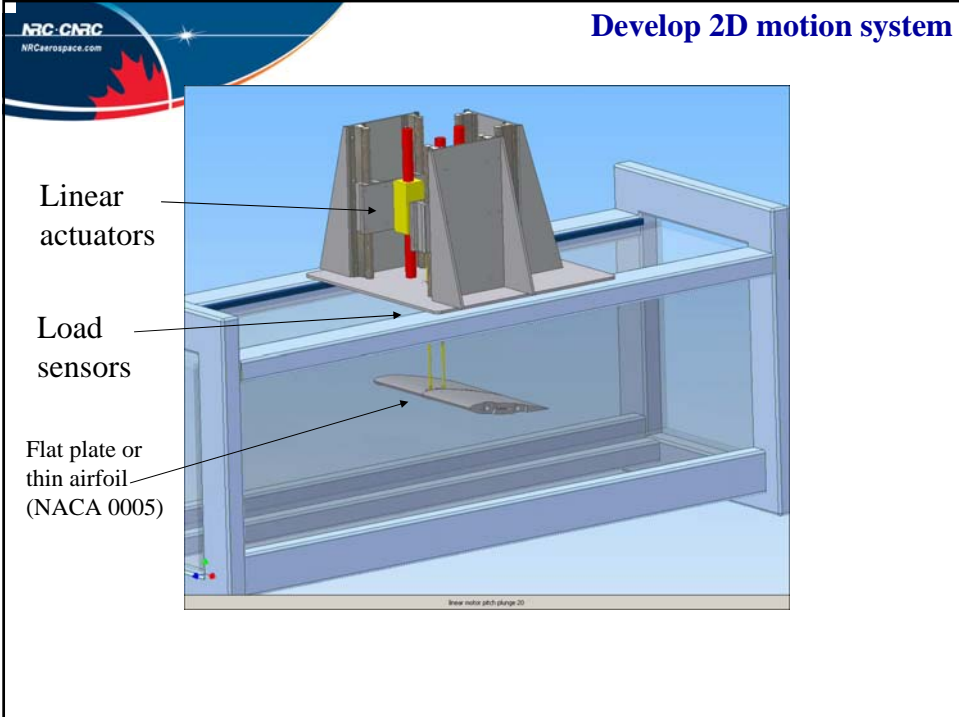


3D view



model made from rigid solidified photopolymer
surface details resolved to $3\mu\text{m}$





Develop 2D motion system for thin airfoil

Commonly used in thin airfoil experiment

$$C_L = C_N \cos \alpha - C_A \sin \alpha$$

$$C_D = C_N |\sin \alpha| + C_A \cos \alpha$$

C_A is axial force from surface shear stress (or $\approx C_D$ at $\alpha=0$) which is much smaller than C_N ($\approx 0.1\%$)

As an approximation, C_A can be taken from any handbook or simply ignored,

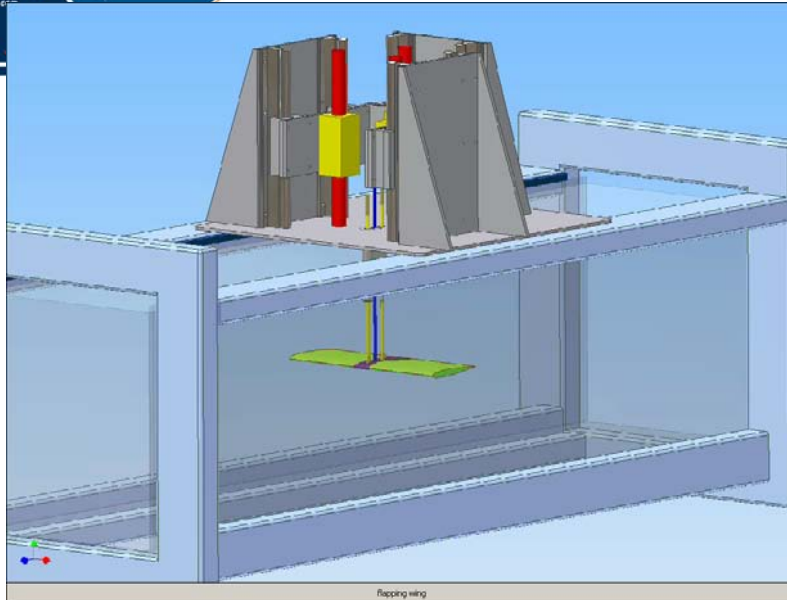
Thus,

$$C_N = C_L \sec \alpha = (C_{L_1} + C_{L_2}) \sec \alpha$$

$$C_D = C_L |\tan \alpha|$$

$$C_m = C_{L_2} \cdot x_2 - C_{L_1} \cdot x_1$$

For thick airfoil or deformed wing the load cell (C_N and C_A) has to and can be installed inside the model



List of symbols/abbreviations/acronyms/initialisms

2D	Two dimensional
3D	Three dimensional
b	Wing span
c	Chord
C4ISR	Command, control, communication, computers, intelligence, surveillance and reconnaissance
CFD	Computational fluid dynamics
d	Maximum thickness
DARPA	Defence Advanced Research Project Agency
DES	Detached eddy simulation
DND	Department of National Defence
DOF	Degree of freedom
f	Frequency
H	Plunge amplitude
h	Linear plunge displacement
IAR	Institute for Aerospace Research
k	Reduced frequency
LES	Large eddy simulation
MAV	Micro air vehicle
NAV	Nano air vehicle
NRC	National Research Council

PID	Proportional-plus-Integral-plus-Derivative Control
PIV	Particle image velocimetry
Re	Reynolds number
RMS	Root mean square
SGS	Subgrid-Scale
SST	Shear Stress Transport
t	Time
TIS	Technology investment strategy
UAV	Unmanned air vehicle
V	Velocity
VLM	Vortex lattice method
Γ	Flap angle amplitude
Θ	Twist amplitude
δ	Phase angle between pitching and plunging
ν	Kinematic viscosity
θ	Pitch angle of airfoil
ω	Circular frequency

Distribution list

DRDC Valcartier TM 2007-550

List Part 1: Internal Distribution by Centre:

- 1- Director General
 - 1- H/Precision Weapons Section
 - 3- Document Library
 - 1- F. Lesage (author)
 - 1- N. Hamel (author)
 - 1- R. Pimentel
 - 1- F. Wong
-

9 - TOTAL LIST PART 1

List Part 2: External Distribution by DRDKIM

- 1- Director Research and Development Knowledge and Information Management
(PDF file)
- 1- Library and Archives Canada (PDF file)
- 1- Director Science and Technology Air
Defence R&D Canada
305 Rideau Street
Ottawa, Ontario
K1A 0K2
- 1- Director Science and Technology Air 6
Defence R&D Canada
305 Rideau Street
Ottawa, Ontario
K1A 0K2
- 1- Director Science and Technology Land 6
Defence R&D Canada
305 Rideau Street
Ottawa, Ontario
K1A 0K2

1- Director Land Requirements 2
NDHQ
101 Col. By Drive
Ottawa, Ontario
K1A 0K2

1- Dominique Poirer, CD, PhD, PEng
Associate Professor
Department of Mechanical Engineering
Royal Military College of Canada
PO Box 17000, Stn Forces
Kingston, Ontario, Canada, K7K7B4
E-mail: poirer-d@rmc.ca

1- Guy Dumas, Ph.D., ing.
Professeur titulaire
Département de Génie Mécanique
Université Laval
Québec, QC
Canada G1K 7P4
email: gdumas@gmc.ulaval.ca

1- Dr. Michael V. OL
AFRL/VAAA
2130 8th St., Bldg 45
Wright-Patterson AFB, OH 45433-7542
Michael.OL@wpafb.af.mil

1- Marie-Josée Potvin, Ph.D.
Structural Dynamics Engineer, Space Technologies
Canadian Space Agency
6767, Route de l'Aéroport, Longueuil (St-Hubert), QC, Canada,
J3Y 8Y9
E-mail : Marie-Josée.Potvin@espace.gc.ca

1- Jean-Sébastien Plante
Département de génie mécanique - Université de Sherbrooke,
Sherbrooke (Québec), Canada,
J1K 2R1
jean-sebastien.plante@USherbrooke.ca

1- Prof. James DeLaurier
University of Toronto Institute for Aerospace Studies
University of Toronto
4925 Dufferin Street
Toronto, Ontario, Canada
M3H 5T6
james.delaurier@rogers.com

1- Jeff Dawson, Ph.D.
Assistant Professor
Department of Biology
Carleton University
1125 Colonel By Drive
Ottawa, Ontario, Canada, K1S 5B6
E-mail: jeff_dawson@carleton.ca

1- Gregg Abate
USAF - Air Force Research Lab (Munitions Directorate)
AFRL/MNAV
101 W Eglin Blvd, Ste 332
Eglin AFB, FL 32542, USA
gregg.abate@eglin.af.mil

1- Harris Edge
Team Leader, Unmanned Vehicles Technology Division
U.S. Army Research Laboratory
Attn: AMSRD-ARL-WM-BF
Aberdeen Proving Ground, MD 21005
United States
Email: edge@arl.army.mil

1- Chris Jones
Air Vehicle Technology Team
Dstl – Farnborough
Ively Road, Farnborough
Hampshire GU14 OLX. UK
cdjones@mail.dstl.gov.uk

1- Ron Schultz
Aeromechanics & Thermal Analysis Branch
NAWCWD
China Lake, CA 93555, USA
ronald.schultz@navy.mil

1- Dr Xing-Zhong Huang
National Research Council Canada
Fixed-Wing Aerodynamics
U-66 - Room: 221
1200 Montreal Road
Ottawa, Ontario
Canada
K1A 0R6
Xing-Zhong.Huang@nrc-cnrc.gc.ca

1- Dr Weixing Yuan
National Research Council Canada
Fixed-Wing Aerodynamics
U-66 - Room: 229
1200 Montreal Road
Ottawa, Ontario
Canada
K1A 0R6
Weixing.Yuan@nrc-cnrc.gc.ca

1- Dr Mahmood Khalid
National Research Council Canada
Fixed-Wing Aerodynamics
U-66 - Room: 229
1200 Montreal Road
Ottawa, Ontario
Canada
K1A 0R6
Mahmood.Khalid@nrc-cnrc.gc.ca

1- Mr. Patrick Zdunich
Advanced Subsonics Inc.
193 Jardin Drive
Vaughan, ON, Canada
L4K 1X5
patrick@advancedsubsonics.com

21 TOTAL LIST PART 2

30- TOTAL COPIES REQUIRED

UNCLASSIFIED

DOCUMENT CONTROL DATA (Security classification of the title, body of abstract and indexing annotation must be entered when the overall document is classified)		
1. ORIGINATOR (The name and address of the organization preparing the document, Organizations for whom the document was prepared, e.g. Centre sponsoring a contractor's document, or tasking agency, are entered in section 8.) Publishing: DRDC Valcartier Performing: DRDC Valcartier Monitoring: Contracting:		2. SECURITY CLASSIFICATION (Overall security classification of the document including special warning terms if applicable.) UNCLASSIFIED
3. TITLE (The complete document title as indicated on the title page. Its classification is indicated by the appropriate abbreviation (S, C, R, or U) in parenthesis at the end of the title) Initial investigation on the aerodynamic performance of flapping wings for nano air vehicles (U) (U)		
4. AUTHORS (First name, middle initial and last name. If military, show rank, e.g. Maj. John E. Doe.) F. Lesage; N. Hamel; X. Huang; W. Yuan; M. Khalid; P. Zdunich		
5. DATE OF PUBLICATION (Month and year of publication of document.) February 2008	6a NO. OF PAGES (Total containing information, including Annexes, Appendices, etc.) 159	6b. NO. OF REFS (Total cited in document.) 38
7. DESCRIPTIVE NOTES (The category of the document, e.g. technical report, technical note or memorandum. If appropriate, enter the type of document, e.g. interim, progress, summary, annual or final. Give the inclusive dates when a specific reporting period is covered.) Technical Memorandum		
8. SPONSORING ACTIVITY (The names of the department project office or laboratory sponsoring the research and development – include address.) Sponsoring: Tasking:		
9a. PROJECT OR GRANT NO. (If appropriate, the applicable research and development project or grant under which the document was written. Please specify whether project or grant.)		9b. CONTRACT NO. (If appropriate, the applicable number under which the document was written.)
10a. ORIGINATOR'S DOCUMENT NUMBER (The official document number by which the document is identified by the originating activity. This number must be unique to this document) DRDC Valcartier TM 2007–550		10b. OTHER DOCUMENT NO(s). (Any other numbers under which may be assigned this document either by the originator or by the sponsor.)
11. DOCUMENT AVAILABILITY (Any limitations on the dissemination of the document, other than those imposed by security classification.) Unlimited distribution		
12. DOCUMENT ANNOUNCEMENT (Any limitation to the bibliographic announcement of this document. This will normally correspond to the Document Availability (11). However, when further distribution (beyond the audience specified in (11) is possible, a wider announcement audience may be selected.)) Unlimited announcement		

UNCLASSIFIED

UNCLASSIFIED

DOCUMENT CONTROL DATA

(Security classification of the title, body of abstract and indexing annotation must be entered when the overall document is classified)

13. **ABSTRACT** (A brief and factual summary of the document. It may also appear elsewhere in the body of the document itself. It is highly desirable that the abstract of classified documents be unclassified. Each paragraph of the abstract shall begin with an indication of the security classification of the information in the paragraph (unless the document itself is unclassified) represented as (S), (C), (R), or (U). It is not necessary to include here abstracts in both official languages unless the text is bilingual.)

(U) A four-year project was approved with the purpose of increasing our understanding of the issues concerning the flight of very small air vehicles using flapping wings. This technical memorandum presents the progress made during the first year of the project. The potential impact of this technology on military operations and R&D is first described. The project plan, as revised during the first year, is presented. It combines the development of an ability to capture detailed flow physics using both a highly accurate Computational Fluid Dynamics (CFD) solution and a tailored experimental facility with an engineering-type method. The general characteristics of the target Nano Air Vehicle (NAV) to be studied, such as size, mass and wing motion, were established based on system considerations. Standard test cases in 2D and 3D for simulation and experimentation were set up by applying simplifications and scaling arguments to the target NAV. CFD simulations were initiated with the standard two-dimensional test case previously defined. The in-house INSflow code and the commercially-available Fluent code were both used to solve this unsteady incompressible flow. Motion rigs in 2D and in 3D for the NRC-IAR water tunnel were designed and are being fabricated. A micro-PIV method was also developed. The required equipment, mainly a high-frequency laser, was purchased. The system is being implemented.

(U) Un projet de quatre ans a été approuvé et a pour but d'accroître notre compréhension des enjeux du vol de très petits véhicules aériens (nanodrones) utilisant des ailes battantes. On présente dans ce mémorandum technique les progrès faits pendant la première année du projet. On décrit d'abord l'impact potentiel de cette technologie sur les opérations militaires et sur la R et D. On présente ensuite le plan du projet tel que révisé pendant la première année. Celui-ci combine le développement d'une habilité à capturer la physique détaillée de l'écoulement utilisant la grande précision d'une solution de calcul de fluide numérique (CFD) et une installation expérimentale sur mesure, avec une méthode de type engineering. On a établi les caractéristiques du nanodrone ciblé pour l'étude, telles que ses dimensions, sa masse et le mouvement des ses ailes, en se basant sur des considérations de systèmes. On a créé des cas tests standard en 2D et 3D pour la simulation et l'expérimentation en appliquant des simplifications et des lois d'échelle au véhicule ciblé. On a entrepris des simulations de CFD avec le cas test en 2D défini précédemment. On a utilisé le code maison INSflow et le code commercial Fluent pour résoudre cet écoulement incompressible instationnaire. On a conçu le dispositif de mouvement en 2D et 3D du tunnel hydrodynamique du CNRC-IAR et celui-ci est en fabrication. On a aussi développé une méthode de micro-PIV. On a acheté l'équipement requis, principalement un laser haute fréquence. On est à implanter le système.

14. **KEYWORDS, DESCRIPTORS or IDENTIFIERS** (Technically meaningful terms or short phrases that characterize a document and could be helpful in cataloguing the document. They should be selected so that no security classification is required. Identifiers, such as equipment model designation, trade name, military project code name, geographic location may also be included. If possible keywords should be selected from a published thesaurus, e.g. Thesaurus of Engineering and Scientific Terms (TEST) and that thesaurus identified. If it is not possible to select indexing terms which are Unclassified, the classification of each should be indicated as with the title.)

(U) flapping wing; aerodynamics; water tunnel; nano air vehicle; micro air vehicle; NAV; MAV; computational fluid dynamics; CFD; flight; military; vortex lattice; Fluent; unsteady; micro-PIV

Defence R&D Canada

Canada's Leader in Defence
and National Security
Science and Technology

R & D pour la défense Canada

Chef de file au Canada en matière
de science et de technologie pour
la défense et la sécurité nationale



www.drdc-rddc.gc.ca

